The Dynamics of Steady Supersonic

Dense Gas Flows

by

Andrew B. Crickenberger

Thesis submitted to the Faculty of the

Virginia Polytechnic Institute and State University

in partial fulfillment of the requirements for the degree of

Master of Science

in

Engineering Mechanics

APPROVED:

Mark S. Cramer, Chairman	George W. Swift
Ronald W. Landgraf	Layne T. Watson

April, 1991

Blacksburg, Virginia

The Dynamics of Steady Supersonic

Dense Gas Flows

by

Andrew B. Crickenberger

Mark S. Cramer, Chairman

Engineering Mechanics

(ABSTRACT)

A weak shock theory is developed which allows for dense gas effects when the fundamental derivative of gasdynamics, Γ, becomes small and possibly negative. The nonclassical behavior in these negative Γ regions has potential applications in turbomachinery design. The weak shock development results in a Burgers equation which is then solved numerically using the well-known MacCormack scheme. The results include the demonstration of many non-classical results such as expansion shocks, compression fans, shock-splitting and shock-fan combinations. Results are shown which could help improve turbine efficiency.

Acknowledgements

I would like to thank my advisor, Dr. Mark Cramer, for all his help and support throughout my graduate career. I could not have made it through without his help. I also thank Dr. Layne Watson for working with Dr. Cramer to be sure I always had the financial support I needed, and for his help solving some troubling numerical problems. My thanks go to the other members of my committee, Dr. Swift and Dr. Landgraf for their help in the preparation of this thesis. Much thanks to Lucinda Willis for helping with all the little everyday problems.

Special thanks to the National Science Foundation for supporting research in this area. This work was supported by the National Science Foundation grant number CTS-8913198.

Table of Contents

List of Illustrations

Chapter 1: Introduction

In the design of supersonic aircraft and turbomachinery, shock waves play a critical role. In the standard gasdynamics theory, which assumes perfect gases, the only types of shock waves possible are compression shocks, that is, shocks in which the pressure of a fluid increases as it passes through the shock. If the pressure decreases, the theory states that such an expansion wave will not form a shock, instead it will spread out to form an expansion fan.[1] If we extend gasdynamics to include non-perfect gas effects we find that other types of phenomena are possible. The type of shocks possible in a fluid depends upon the fundamental derivative, Γ, which is a thermodynamic property defined as

$$\Gamma \equiv \frac{V^4}{2a} \frac{\partial^2 p}{\partial V^2} \Big|_{\eta}, \qquad [1.1]$$

where $p = p(V, \eta)$ is the pressure, $V \equiv \frac{1}{\rho}$ is the specific volume, η is the entropy, and

$$a \equiv \left(- V^2 \frac{\partial p}{\partial V} \Big|_{\eta} \right)^{\frac{1}{2}} \qquad [1.2]$$

is the thermodynamic sound speed.[2] It is the sign of Γ that determines the behavior of a particular fluid. In the ideal gas theory, Γ is always positive, and indeed this is the case for many fluids. If $\Gamma < 0$, however, the standard thermodynamic inequalities are reversed and compression shocks become impossible. Instead, spreading compression fans are formed, and "negative" or expansion shocks become possible; these form instead of the expansion fans. The case where $\Gamma < 0$ is referred to as negative nonlinearity and $\Gamma > 0$ as positive nonlinearity.

The behavior of flows with totally negative nonlinearities are similar to those with positive nonlinearity, providing the various sign changes are taken into account. However, when the sign of Γ changes in the flow, the situation can become very complicated. Some examples of the phenomena encountered include shock-splitting, collisions of expansion and compression shocks, partial shock disintegration and sonic shocks, i.e., shocks which have a Mach number equal to one just upstream or downstream of the shock.[4,5] Cases such as these are referred to as mixed nonlinearity.

Fluids which exhibit this behavior are referred to as Bethe-Zel'dovich-Thompson (BZT) fluids, after H.A. Bethe [6], Y.B. Zel'dovich[7,8], and P.A. Thompson, [2,3] who performed pioneering work on these fluids. Although we will be using these non-classical BZT fluids, we will still be using the same assumptions of classical gasdynamics, that is, the fluids will be taken to be single phase gases in which relaxation, chemical reactions, dissociation, ionization, etc., play no role.

The motivation behind this work is partially to develop a more complete understanding of classical fluids and the behavior of BZT fluids. Another important motivation comes from the possible applications of the non-classical effects, especially in the area of turbine dynamics for Rankine cycle power systems where BZT fluids may be able to increase the efficiency and life of the turbines. In these turbines, a major cause of inefficiency is the very large pressure gradient caused by compression shocks striking adjacent blades.[9] Figure 1.1a shows the problem with shock waves in a turbine cascade. As these shocks collide with a second blade, they can cause the boundary layer to detach, causing a large increase in drag. In BZT fluids, operating conditions can be set so that these compression shocks will not exist and will instead become compression fans, as sketched in Figure 1.1b, spreading the pressure change over a much larger area causing the effect on the boundary layer to be minimal, thereby reducing drag.

We will keep these applications in mind as we set up our problem. We will solve a boundary value problem with a uniform upstream flow and a uniform downstream flow, as seen in Figure 1.2. The downstream conditions will be determined by the dynamics of the flow, but by the time the downstream boundary is reached the flow will be uniform once again. The lower boundary of our domain will be the shape we choose for the wing. We will look at both expansion and compression wedges, and a wing-shape defined as a sine wave. A sine wave wing with a small amplitude is a good approximation of a turbine blade.

Chapter 2: Theoretical Background

2.1 General Equations

We will limit our work to fluids which are governed by the standard Navier-Stokes equations. In addition we will assume the flows to be steady, supersonic, single-phase, inviscid, and two-dimensional. The Navier-Stokes equations for this case can be reduced to,

$$\nabla \cdot \rho \underline{v} = 0 \tag{2.1}$$

$$\rho \underline{v} \cdot \nabla \underline{v} + \nabla p = 0 \tag{2.2}$$

$$\underline{v} \cdot \nabla \eta = 0 \tag{2.3}$$

where ρ is the fluid density, T is the temperature, $p = p(\rho, T)$ is the pressure, $\eta = \eta(\rho, T)$ is the entropy and $\underline{v}$ is the particle velocity. These reduced equations are often referred to as the Euler equations, and are the equations most often used for supersonic flow calculations.

2.2 Shock-Jump Conditions

If we assume that shock waves are a discontinuity in the flow, we must have expressions which relate the properties on either side of this discontinuity. This is done through the Rankine-Hugoniot jump conditions [10, 11, 12], which all shocks must satisfy, and which can be written as

$$[\rho v_n] = 0 \qquad [2.4]$$

$$[v_t] = 0 \qquad [2.5]$$

$$\frac{[p]}{[V]} = -m^2 \qquad [2.6]$$

$$[h] = [p]\frac{V_2 + V_1}{2}, \qquad [2.7]$$

where $V \equiv \frac{1}{\rho}$ is the specific volume, v_n is the normal component of the relative velocity, v_t is the component of velocity parallel to the shock, m is the mass flux through the shock, and h is the enthalpy, defined as

$$h = h(\rho, T) \equiv e + \frac{p}{\rho}. \qquad [2.8]$$

In this case e is the internal energy and the square brackets denote the jump in a quantity, for example,

$$[A] = A_2 - A_1,$$

where A is any quantity and the subscripts denote conditions on either side of the shock. Using [2.4] we can write m as

$$m = \rho_2 v_{n2} = \rho_1 v_{n1}. \qquad [2.9]$$

Equation [2.4] or [2.9] represents conservation of mass, [2.5] and [2.6] represent the tangential and normal components of conservation of momentum, and equation [2.7] is the Hugoniot relationship for conservation of energy.

The direction of the jumps can be determined by examining these shock-jump equations. It is well-known that the sign of the jump of the density, enthalpy, and the internal energy is the same as that of the pressure.[10] The change in the normal component of the flow velocity is however, opposite the pressure. For example in a compression shock, where the pressure increases, the flow is decelerated through the shock, and in an expansion shock the flow is accelerated. In an oblique shock such as that shown in Figure 2.1, the change in direction of the velocity through the shock can also easily be determined. In a compression shock the flow is turned away from the normal, while in an expansion shock it is turned toward the normal. The temperature jump is more complicated, however it can be shown that with the assumption made in this case the temperature jump for all acceptable shocks will have the same sign as the pressure jump. Therefore compression shocks will heat the fluid, while expansion shocks will cool the fluid.

Chapter 3: Derivation

3.1 Foundations

To simplify the calculations, we will use a coordinate system aligned with the freestream as shown in Figure 3.1. The quantity θ is the flow deflection angle, s is the distance along the streamline in the direction of the flow, and n is the distance locally perpendicular to the streamline. Using these coordinates, the Euler equations, [2.1] - [2.3] can be rewritten as [5]

$$d\theta \pm C dp = \mp C \frac{p_\eta}{a^2} d\eta \qquad [3.1]$$

on the Mach lines

$$\frac{dn}{ds} = \pm \frac{1}{\sqrt{M^2 - 1}} \qquad [3.2]$$

and

$$\eta = constant \qquad [3.3]$$

$$h + \frac{a^2M^2}{2} = constant \qquad [3.4]$$

on the streamlines, i.e., where dn = 0. Here $p_\eta \equiv \frac{\partial p}{\partial \eta}|_\rho$ and

$$C \equiv \frac{\sqrt{M^2 - 1}}{M^2}\frac{1}{\rho}. \qquad [3.5]$$

Equations [3.1] are referred to as the compatibility conditions. They give the relation between the flow deflection angle θ and either M or ρ in our transformed coordinate system.

Equations [3.2] give the slopes of the Mach lines in the n-s plane as shown in Figure 3.2, where, by definition, μ is the local Mach angle such that

$$\sin\mu \equiv \frac{1}{M}. \qquad [3.6]$$

Using standard trigonometric identities we can also derive the following expressions

$$\cos\mu = \frac{\sqrt{M^2 - 1}}{M} \quad \text{and} \quad \tan\mu = \frac{1}{\sqrt{M^2 - 1}}. \qquad [3.7]$$

Equation [3.3] sets the entropy constant along the particle path, i.e. along the streamline, and equation [3.4] is a form of the Bernoulli equation. Another, more useful, form of [3.4] can be obtained by differentiating [3.4] and using [3.3] to get [5]

$$\frac{dM}{d\rho} = \frac{M}{\rho}\left(1 - \frac{\rho\Gamma}{a} - \frac{1}{M^2}\right), \qquad [3.8]$$

with Γ being the fundamental derivative given in equation [1.1]. Equation [1.1] can also be written in the alternate form

$$\Gamma = \frac{\partial a}{\partial \rho}|_\eta + \frac{a}{\rho}. \qquad [3.9]$$

3.2 Assumptions

The Assumptions introduced in Section 2, Two-dimensional, steady, inviscid, supersonic flow will still be used, in addition we assume that all disturbances, $\frac{\rho - \rho_\infty}{\rho_\infty}$, and θ are small. In particular,

$$\frac{\rho - \rho_\infty}{\rho_\infty} = O(\theta) = o(1), \quad [3.10]$$

where O(θ) means the same order of magnitude as θ, and o(1) means much less than 1. We will also only be considering fundamental derivatives which are small, so that

$$\overline{\Gamma} \equiv \frac{\rho\Gamma}{a} = O(\frac{\rho - \rho_\infty}{\rho_\infty}) = O(\theta) = o(1), \quad [3.11]$$

which implies that $\frac{\rho\Gamma}{a}$ is the same order of magnitude as the change in density. The last assumption assures disturbances caused by the wing, which will be of the order $\frac{\rho - \rho_\infty}{\rho_\infty}$, will be capable of moving the flow into or out of the negative Γ region.

3.3 Preliminary Calculations

The Hugoniot equation [2.7] may be expanded to show that when $[\rho]$ is small [6]

$$[\eta] = O(\overline{\Gamma}_1 [\rho]^3). \quad [3.12]$$

That is, the entropy jump is three orders of magnitude smaller than the density jump and is proportional to $\overline{\Gamma}$. Because of equations [3.3] and [3.11], the entropy change can be written

$$\eta - \eta_\infty = O([\rho]^4) = O(\theta^4) \quad [3.13]$$

everywhere in the flow. We can therefore substitute this into the right hand side of [3.1] to get

$$d\theta \pm C d\rho = O(\theta^4). \qquad [3.14]$$

In order to make a further approximation of [3.1], $C(\rho, M)$ can be expanded in a Taylor series around the upstream value $C(\rho_1, M_1)$ as follows

$$C(\rho, M) = C_1 + \frac{\partial C}{\partial \rho} |_M(\rho_1, M_1)(\rho - \rho_1) + \frac{\partial C}{\partial M} |_\rho(\rho_1, M_1)(M - M_1) + O(\rho - \rho_1)^2, \qquad [3.15]$$

where, from [3.5],

$$C_1 \equiv \frac{\sqrt{M_1^2 - 1}}{M_1^2} \frac{1}{\rho_1} \qquad [3.16]$$

$$\frac{\partial C}{\partial \rho} |_M(\rho_1, M_1) = -\frac{1}{\rho_1^2} \frac{\sqrt{M_1^2 - 1}}{M_1^2} \qquad [3.17]$$

$$\frac{\partial C}{\partial M} |_\rho(\rho_1, M_1) = \frac{2 - M_1^2}{\rho_1 M_1^3 \sqrt{M_1^2 - 1}}. \qquad [3.18]$$

In order to get an expression between M and ρ, [3.8] can also be expanded around M_1, ρ_1 to get

$$M - M_1 = (\rho - \rho_1)\frac{M_1}{\rho_1}(1 - \overline{\Gamma}_1 - \frac{1}{M^2}) + O(\rho - \rho_1)^2. \qquad [3.19]$$

Any errors due to the entropy variations, according to [3.12], are clearly an order of magnitude smaller than the error $O(\rho - \rho_1)^2$ already shown. Rewriting and rearranging [3.15]

$$C \simeq C_1 + B\frac{\rho - \rho_1}{\rho_1^2} + O(\rho - \rho_1)^2, \qquad [3.20]$$

where C_1 is given by [3.16] and

$$B \equiv -\rho_1 C_1 + \frac{\sqrt{M_1^2 - 1}\,(2 - M_1^2)}{M_1^4}. \qquad [3.21]$$

There are now two equations for the characteristic lines, one that represents upstream pointing waves, and one that represents downstream pointing waves. We will concentrate for the moment on the second equation in [3.14], i.e., that associated with the negative sign. Substituting [3.20] into this equation and integrating, assuming that $\theta = \theta_1$ when $\rho = \rho_1$ we find that

$$R^- \equiv \theta - \theta_1 - \rho_1 C_1 \left(\frac{\rho - \rho_1}{\rho_1}\right) - \frac{B}{2}\left(\frac{\rho - \rho_1}{\rho_1}\right)^2 + O(\rho - \rho_1)^3 = constant \qquad [3.22]$$

on the upstream pointing Mach lines defined by

$$\frac{dn}{ds} = -\frac{1}{\sqrt{M^2 - 1}}. \qquad [3.23]$$

Figure 3.3 shows graphically what [3.22] and [3.23] represent, that the upstream pointing Mach lines are constant, even when shocks are present. If we can say that $[R^-] \equiv R_2^- - R_1^- \simeq 0$ then we can assume that the reflected waves, i.e. waves which propagate upstream, can be neglected. This will be shown in later sections.

3.4 Derivation of Shock Angle

The physical definition of the shock angle σ is shown in Figure 3.4. Using trigonometry to relate the velocity to the shock angle, the following equations are developed

$$v_{ni} = v_i \sin(\sigma - \theta_i) \qquad [3.24]$$

$$v_{ti} = v_i \cos(\sigma - \theta_i) \qquad [3.25]$$

$$v_{ni} = v_{ti} \tan(\sigma - \theta_i), \qquad [3.26]$$

where i = 1,2 represents the values on either side of the shock. We can use the above equations with the shock jump relations [2.4] and [2.6] to get

$$M_1^2 a_1^2 \sin^2(\sigma - \theta_1) = \frac{\rho_2}{\rho_1} \frac{[p]}{[\rho]} \,. \qquad [3.27]$$

Expanding $p(\rho, \eta)$ in a Taylor series about the point $p_1 = p(\rho_1, \eta_1)$ and rearranging,

$$\frac{[p]}{[\rho]} = a_1^2 \{1 - \frac{[\rho]}{\rho_1} + \overline{\Gamma}_1 \frac{[\rho]}{\rho_1} + (1 + \frac{\Lambda}{3})(\frac{[\rho]}{\rho_1})^2 + O(\frac{[\rho]}{\rho_1})^3 \} \qquad [3.28]$$

where

$$\Lambda \equiv \frac{\rho_1^2}{a_1} \frac{\partial \Gamma}{\partial \rho} \,|_{\eta}(\rho_1, \eta_1). \qquad [3.29]$$

We can now substitute [3.28] into the our shock jump relation [3.27]. A new variable, ε, is now introduced

$$\varepsilon_1 \equiv \sigma - \mu_1 - \theta_1. \qquad [3.30]$$

Using ε_1 with [3.27] and [3.28] and combining these expressions, the sine function can be expanded in a Taylor series about μ_1 to get

$$\varepsilon_1 \equiv \sigma - \mu_1 - \theta_1 = \frac{\tan(\mu_1)}{2} \{\overline{\Gamma}_1 \frac{[\rho]}{\rho_1} + \frac{\Lambda}{3} \left(\frac{[\rho]}{\rho_1} \right)^2 \} + O\left(\frac{[\rho]}{\rho_1} \right)^3 . \qquad [3.31]$$

This gives an approximation for σ in terms of the Mach angle μ_1, and the shock strength $\frac{[\rho]}{\rho_1}$. If we set θ_1 and the shock strength equal to zero we get that $\sigma \rightarrow \mu_1$, that is, the shock angle is equal to the Mach angle. This is the correct result for a freestream steady flow.

3.5 Derivation of [ρ] vs [θ] Relation

We will now need to get an expression which will give us ρ as a function of θ. We will start with [3.24] - [3.26] and use the shock-jump relations [2.4] and [2.5] to get

$$\frac{\rho_2}{\rho_1} = 1 + \frac{[\rho]}{\rho_1} = \frac{\tan(\mu_1 + \varepsilon_1)}{\tan(\mu_1 + \varepsilon_2)}, \tag{3.32}$$

where

$$\varepsilon_2 \equiv \sigma - \mu_1 - \theta_2 = \varepsilon_1 - [\theta]. \tag{3.33}$$

The expression $\tan(\mu_1 + \varepsilon_i)$ can be expanded in a Taylor series about μ_1 and rearranged to get

$$\frac{[\rho]}{\rho_1} = \frac{[\theta]}{\cos^2\mu_1 \tan\mu_1} + \frac{[\theta]^2}{\sin^2\mu_1} + O([\theta]^3). \tag{3.34}$$

Going back to our definition of μ, [3.6], μ can be replaced with the Mach number,

$$\frac{[\rho]}{\rho_1} = \frac{[\theta]M_1^2}{\sqrt{M_1^2 - 1}} + M_1^2[\theta]^2 + O([\theta]^3). \tag{3.35}$$

Returning to our expression for R^-, [3.22], and observing that $R_1^- = R^-(\theta_1, \rho_1) = 0$, we find that

$$[R^-] = R_2^- = [\theta] - \rho_1 C_1 \frac{[\rho]}{\rho_1} - \frac{B}{2}\left(\frac{[\rho]}{\rho_1}\right)^2 + O\left(\frac{[\rho]}{\rho_1}\right)^3. \tag{3.36}$$

where B and C are defined in [3.21] and [3.20]. Substituting for B, C, and $\frac{[\rho]}{\rho_1}$ it is easily shown that $[R^-] = O([\theta]^3)$. We may now conclude that R^- is constant on all upstream pointing Mach lines, even when shock waves are present, that is,

$$R^- = R_\infty^- + O([\theta]^3). \tag{3.37}$$

Substituting into [3.22] and solving for θ we find that

$$\theta = \rho_1 C_1 \frac{\rho - \rho_\infty}{\rho_1} + \frac{B}{2}\{(\frac{\rho - \rho_1}{\rho_1})^2 - (\frac{\rho_\infty - \rho_1}{\rho_1})^2\} + O([\theta^3]) \qquad [3.38]$$

which is valid at every point in the flow. The definitions of C and B, [3.20] and [3.21], can be used to get

$$C_1 \simeq C_\infty - B\frac{\rho_\infty - \rho_1}{\rho_1^2} + O([\theta]^2)$$

$$B \simeq B_\infty + O(\frac{\rho_1 - \rho_\infty}{\rho_\infty}).$$

Substitute back into [3.38] we get the final expression

$$\theta = \frac{\sqrt{M_\infty^2 - 1}}{M_\infty^2}\frac{\rho - \rho_\infty}{\rho_\infty} - \frac{(M_\infty^2 - 1)^{\frac{3}{2}}}{M_\infty^4}\left(\frac{\rho - \rho_\infty}{\rho_\infty}\right)^2 + O\left(\frac{\rho - \rho_\infty}{\rho_\infty}\right)^3, \qquad [3.39]$$

which is valid at every point in the flow, even if shocks are present. Another form of [3.39] can be obtained by solving for $\frac{\rho - \rho_\infty}{\rho_\infty}$ which yielding

$$\frac{\rho - \rho_\infty}{\rho_\infty} \simeq \frac{M_\infty^2}{\sqrt{M_\infty^2 - 1}}\theta + M_\infty^2\theta^2 + O(\theta^3). \qquad [3.40]$$

We now have an expression for the density change in terms of the flow deflection angle. This expression will be important in the next section.

3.6 Mach Number and Mach angle

We must now get a usable expression for the Mach number. Assume that $M = M(\rho)$, we can expand M in a Taylor series around ρ_∞, and use [3.8], to get

$$M \simeq M_\infty\{1 + \frac{M_\infty^2 - 1}{M_\infty^2}\frac{\rho - \rho_\infty}{\rho_\infty} + \frac{1}{2}\frac{M_\infty^2 - 1}{M_\infty^3}(\frac{\rho - \rho_\infty}{\rho_\infty})^2 \tag{3.41}$$

$$- (\bar{\Gamma}_\infty + \frac{1}{2}\Lambda_\infty\frac{\rho - \rho_\infty}{\rho_\infty})\frac{\rho - \rho_\infty}{\rho_\infty}\} + O(\frac{\rho - \rho_\infty}{\rho_\infty})^3,$$

where

$$\bar{\Gamma}_\infty = \frac{\rho_\infty \Gamma_\infty}{a_\infty} \tag{3.42}$$

$$\Lambda_\infty = \frac{\rho_\infty^2}{a_\infty}\frac{\partial \Gamma}{\partial \rho}|_\eta(\rho_\infty, \eta_\infty).$$

Now [3.40] and [3.41] can be combined to get

$$M \simeq = M_\infty\{1 + \sqrt{M_\infty^2 - 1}\,\theta + (2M_\infty^2 - 1)\frac{\theta^2}{2} - \tag{3.43}$$

$$(\bar{\Gamma}_\infty + \frac{\Lambda_\infty}{2}\frac{M_\infty^2}{\sqrt{M_\infty^2 - 1}}\theta)\frac{M_\infty^2}{\sqrt{M_\infty^2 - 1}}\theta\} + O(\theta^3).$$

Note that this expression gives the Mach number in terms of the upstream conditions and θ, which is a function of the upstream conditions and ρ only.

The same calculation can be performed to get an expression for the Mach angle $\mu = \mu(M)$. After carrying out an expansion similar to [3.41] and substituting [3.40],

$$\mu \simeq \mu_{\infty} - \theta + \frac{M_{\infty}^2}{M_{\infty}^2 - 1}\theta(\overline{\Gamma}_{\infty} + \frac{\Lambda_{\infty}}{2}\frac{M_{\infty}^2}{\sqrt{M_{\infty}^2 - 1}}\theta) + O(\theta^3). \qquad [3.44]$$

Thus given the conditions upstream, the Mach number and the Mach angle at any point can be determined.

The slope of the Mach line, as shown in Figure 3.2, is equal to

$$\frac{dy}{dx} = \tan(\mu + \theta) = \tan(\mu_{\infty} + \mu - \mu_{\infty} + \theta). \qquad [3.45]$$

Expanding this expression in a Taylor series, assuming θ is small, and substituting [3.42]

$$\frac{dy}{dx} \simeq \frac{1}{\sqrt{M_{\infty}^2 - 1}} + \frac{M_{\infty}^2}{(M_{\infty}^2 - 1)^{\frac{3}{2}}}(\overline{\Gamma}_{\infty} + \frac{\Lambda_{\infty}}{2}\frac{\rho - \rho_{\infty}}{\rho_{\infty}})\frac{\rho - \rho_{\infty}}{\rho_{\infty}} + O(\frac{\rho - \rho_{\infty}}{\rho_{\infty}})^3. \qquad [3.46]$$

This equation will be used to show that the Mach lines are straight lines, i.e. $\frac{dy}{dx} = constant$. From [3.14]

$$R^+ = \theta + C_{\infty}(\rho - \rho_{\infty}) + O(\theta^3) \simeq constant \qquad [3.47]$$

on the Mach lines [3.45]. But from [3.39], a lowest order expression for θ in terms of ρ can be formed. Substituting this into [3.47]

$$\frac{2\sqrt{M_{\infty}^2 - 1}}{M_{\infty}^2}\frac{\rho - \rho_{\infty}}{\rho_{\infty}} \simeq constant. \qquad [3.48]$$

From this, it is seen that $\frac{\rho - \rho_{\infty}}{\rho_{\infty}}$ is to the lowest approximation equal to a constant. Therefore along the Mach line [3.45], ρ is a constant. Since $\theta = \theta(\rho)$, θ is also a constant along these Mach lines. Thus, $\frac{dy}{dx}$ is also a constant and we may conclude that the Mach lines are straight.

3.7 Derivation of Shock Slope

Another expression which we must have is the slope of the shock wave, which is given by the tangent of the shock angle, σ. We can use [3.31], and solve for σ to get

$$\sigma \simeq \mu_\infty + \frac{1}{\sqrt{M_\infty^2 - 1}} \{ \frac{\overline{\Gamma}_\infty}{2} (\frac{\theta_2 + \theta_1}{2} + \frac{\Lambda_\infty}{6} \frac{M_\infty^2}{\sqrt{M_\infty^2 - 1}} (\theta_1^2 + \theta_1\theta_2 + \theta_2^2)\} + O(\theta^3). \quad [3.49]$$

The actual shock slope will be determined by the tangent of the shock angle

$$\frac{dy}{dx}\Big|_{shock} \equiv \tan\sigma = \tan(\mu_\infty + \sigma - \mu_\infty) = \tan\mu_\infty + \frac{\sigma - \mu_\infty}{\cos^2\mu_\infty} + O(\sigma - \mu_\infty)^2. \quad [3.50]$$

The above expansion is possible by observing from [3.49] that the quantity $\sigma - \mu_\infty = O(\theta^2)$. This allows us to expand the tangent around μ_∞. The final expression for the shock slope is obtained by substituting [3.49] and [3.39] into [3.50]

$$\frac{dy}{dx}\Big|_{shock} \simeq \frac{1}{\sqrt{M_\infty^2 - 1}} + \frac{M_\infty^2}{(M_\infty^2 - 1)^{\frac{3}{2}}} \{ \frac{\overline{\Gamma}_\infty}{2} \left(\frac{\rho_2 - \rho_\infty}{\rho_\infty} + \frac{\rho_1 - \rho_\infty}{\rho_\infty} \right) \quad [3.51]$$

$$+ \frac{\Lambda_\infty}{6} \left(\left(\frac{\rho_2 - \rho_\infty}{\rho_\infty} \right)^2 + \left(\frac{\rho_2 - \rho_\infty}{\rho_\infty} \right)\left(\frac{\rho_1 - \rho_\infty}{\rho_\infty} \right) + \left(\frac{\rho_1 - \rho_\infty}{\rho_\infty} \right)^2 \right) \} + o\left(\frac{\rho - \rho_\infty}{\rho_\infty} \right)^3.$$

3.8 Formation of a Burgers Equation

To simplify our equations a non-dimensional u is defined to be

$$u = \frac{\rho - \rho_\infty}{\varepsilon \rho_\infty}. \qquad [3.52]$$

If we take u = u(x,y), the change in u can be written

$$du = \frac{\partial u}{\partial y} dy + \frac{\partial u}{\partial x} dx. \qquad [3.53]$$

We can see from equation [3.48] that ρ, and therefore u, is necessarily a constant on the Mach lines. We may therefore set du = 0 and rearrange [3.53] to get an equation whose form matches the standard Burgers equation

$$\frac{\partial u}{\partial y} + \frac{dx}{dy}\frac{\partial u}{\partial x} = 0. \qquad [3.54]$$

Upon substituting [3.52] into the θ equation [3.38] it is seen that

$$\theta = \frac{\sqrt{M_\infty^2 - 1}}{M_\infty^2} \varepsilon u \qquad [3.55]$$

when we ignore higher order terms. Converting the Mach lines [3.45] to this new variable we find

$$\frac{dx}{dy} = \frac{1}{\frac{dy}{dx}} = \sqrt{M_\infty^2 - 1} - \varepsilon^2 \frac{M_\infty^2}{(M_\infty^2 - 1)^{\frac{3}{2}}} \{\hat{\Gamma}_\infty u + u^2 \frac{\Lambda_\infty}{2}\} \qquad [3.56]$$

where

$$\hat{\Gamma} = \frac{\overline{\Gamma}_\infty}{\varepsilon}. \qquad [3.57]$$

Now this expression is substituted into our Burgers equation, [3.54], and rearranged to get

$$\frac{\partial u}{\partial \bar{y}} + \{ -\hat{\Gamma} u - \frac{\Lambda}{2} u^2)\} \frac{\partial u}{\partial \bar{x}} = 0, \tag{3.58}$$

where

$$\bar{x} = \frac{x}{L} - \sqrt{M_\infty^2 - 1}\ \frac{y}{L} \qquad \bar{y} = \frac{y}{L} \frac{\varepsilon^2 M_\infty^2}{\sqrt{M_\infty^2 - 1}}. \tag{3.59}$$

From equation [3.55] our boundary condition at the wing can be written, to lowest order, as

$$u(\bar{x}, 0) = \frac{M_\infty^2}{\sqrt{M_\infty^2 - 1}} F'(\bar{x}) \tag{3.60}$$

where θ has been approximated as a function, $F'(\frac{x}{L})$, which is valid for small values of θ. The function F' is a mathematical description of the shape of the wing. Simplifying, our differential equation can be written

$$\frac{\partial u}{\partial \bar{y}} + \frac{\partial Q}{\partial \bar{x}} = 0 \tag{3.61}$$

where

$$Q \equiv -\hat{\Gamma} \frac{u^2}{2} - \Lambda_\infty \frac{u^3}{6}. \tag{3.62}$$

and $\hat{\Gamma}$ and Λ_∞ are properties which are dependent upon the fluid and the upstream thermodynamic state.

3.9 Heuristic Proof

In the previous few sections the expressions to determine the Burgers equation describing the flow were rigorously derived. If we now start with an isentropic flow with pure downstream pointing Mach lines, both of which have been shown to be true in the previous sections, it turns out that a heuristic approach can be used to achieve the same results. The local Mach angle Ψ is defined to be the Mach angle plus the flow deflection angle, i.e. $\Psi \equiv \mu + \theta$. If we differentiate this equation with respect to θ, and use the chain rule we get:

$$\frac{d\Psi}{d\theta} = \frac{d\mu}{dM}\frac{dM}{d\rho}\frac{d\rho}{d\theta} + 1. \tag{3.63}$$

Using [3.6], [3.8], and [3.14] to determine the derivatives on the right hand side, [3.63] simplifies to

$$\frac{d\Psi}{d\theta} = \frac{M^2}{M^2 - 1}\overline{\Gamma} \tag{3.64}$$

where $\overline{\Gamma}$ is defined by the first of equations [3.11]. The slope of the Mach lines is defined as

$$\frac{dy}{dx} \equiv \tan\Psi \simeq \tan\Psi_\infty + \frac{1}{\cos^2\Psi_\infty}(\Psi - \Psi_\infty). \tag{3.65}$$

By definition, at the upstream condition, $\theta = 0$ so $\Psi_\infty = \mu_\infty$. Now equations [3.7] can be used in [3.65]. Ψ can be expanded in a Taylor series to get

$$\Psi - \Psi_\infty = \frac{d\Psi}{d\theta}\theta + \frac{d^2\Psi}{d\theta^2}\theta^2 + O(\theta^3). \tag{3.66}$$

This expression can be rewritten by substituting [3.63] and its derivative to get

$$\Psi - \Psi_\infty = \frac{M_\infty^2}{M_\infty^2 - 1}\overline{\Gamma}_\infty\theta + \frac{M_\infty^4}{(M_\infty^2 - 1)^{\frac{3}{2}}}\Lambda_\infty\theta^2 + O(\theta^3). \tag{3.67}$$

where Λ is defined in [3.29]. Equations [3.7], [3.39], and [3.67] can be used in equation [3.65] to get the final form of the expression

$$\frac{dy}{dx} = \frac{1}{\sqrt{M_\infty^2 - 1}} + \frac{M_\infty^2}{(M_\infty^2 - 1)^{\frac{3}{2}}}(\overline{\Gamma}_\infty + \frac{\Lambda_\infty}{2}\frac{\rho - \rho_\infty}{\rho_\infty})\frac{\rho - \rho_\infty}{\rho_\infty} + O(\frac{\rho - \rho_\infty}{\rho_\infty})^3, \quad [3.68]$$

which is the same as [3.46]. So we have derived the same expression with much less work, once it was known that the flow was isentropic and was comprised of simple right running waves.

A final quantity that must be found is the slope of the shock waves. The shock slope, in terms of our Q, defined in equation [3.62], is [18]

$$\frac{d\overline{y}}{d\overline{x}}\Big|_{shock} = \frac{[Q]}{[u]} = \frac{Q_2 - Q_1}{u_2 - u_1}. \quad [3.69]$$

If we substitute [3.62] for the Q's an expression for the shock is formed

$$\frac{d\overline{y}}{d\overline{x}}\Big|_{shock} = -\frac{\hat{\Gamma}_\infty}{2}(u_2 + u_1) - \frac{\hat{\Lambda}}{6}(u_2^2 + u_1 u_2 + u_1^2), \quad [3.70]$$

which is, when the definition of u [3.52] is remembered, identical to our derived version [3.51].

3.10 Extension to Higher Order

In order to capture the phenomenon of shock splitting, it has been shown that the approximation in the previous sections must be extended to a higher order.[13] We will use our simple derivation of the previous section to extend the theory to a higher order by replacing assumption [3.11] with

$$\overline{\Gamma} \equiv \frac{\rho\Gamma}{a} = O(\frac{\rho - \rho_\infty}{\rho_\infty})^2 = O(\theta^2) = o(1) \quad [3.71]$$

$$\Lambda = \frac{\rho^2}{a}\frac{\partial \Gamma}{\partial \rho}\Big|_\eta = O(\frac{\rho - \rho_\infty}{\rho_\infty}) = O(\theta) = o(1).$$

Following the same steps outlined in Section 3.9, the Taylor series expansions can all be expanded one step further, to derive a final expression for

$$\frac{dy}{dx} \simeq \frac{1}{\sqrt{M_\infty^2 - 1}} + \frac{M_\infty^2}{(M_\infty^2 - 1)^{\frac{3}{2}}}(\overline{\Gamma}_\infty + \frac{\Lambda_\infty}{2}\frac{\rho - \rho_\infty}{\rho_\infty} \qquad [3.72]$$

$$+ \frac{\Xi_\infty}{6}(\frac{\rho - \rho_\infty}{\rho_\infty})^2)\frac{\rho - \rho_\infty}{\rho_\infty} + O(\frac{\rho - \rho_\infty}{\rho_\infty})^4,$$

where

$$\Xi_\infty = \frac{\rho_\infty^3}{a_\infty}\frac{\partial^2 \Gamma}{\partial \rho^2}\Big|_\eta(\rho_\infty, \eta_\infty) = O(1), \qquad [3.73]$$

and $\overline{\Gamma}_\infty$ and Λ_∞ are defined in [3.57] and [3.42]. The technique described in Section 3.7 can now be used to create our Burgers equation [3.61], except that now our Q [3.62] is replaced by a higher order expression

$$Q \equiv -\frac{u^2}{2}\hat{\Gamma}_\infty - \frac{u^3}{6}\hat{\Lambda}_\infty - \frac{u^4}{24}\Xi_\infty. \qquad [3.74]$$

Now

$$\hat{\Gamma}_\infty = \frac{\overline{\Gamma}_\infty}{\varepsilon^2} \qquad \hat{\Lambda}_\infty = \frac{\Lambda_\infty}{\varepsilon} \qquad [3.75]$$

and Ξ_∞ is defined in [3.73]. We can use our higher order Q in the shock slope equation, [3.70], to get an expression for the slope of the shock wave

$$\frac{d\overline{y}}{dx}\Big|_{shock} = -\frac{\hat{\Gamma}_\infty}{2}(u_2 + u_1) - \frac{\hat{\Lambda}_\infty}{6}(u_2^2 + u_1u_2 + u_1^2) - \frac{\Xi_\infty}{24}(u_2^3 + u_1u_2^2 + u_1^2u_2 + u_1^3). \qquad [3.76]$$

3.11 Existence Conditions

A shock wave can satisfy the shock-jump relations and still not exist in actual physical flows. We must therefore impose some existence conditions to determine if a shock wave will exist. One of the most important of these conditions is found by analysis of the shock adiabat. The shock adiabat is a graphical representation of the Hugoniot equation [2.7]. The curve produced is a plot of all the thermodynamic states which can be connected by a shock wave. Since our problem has been transformed into different quantities than the p and V used in [2.7], and because it is nearly isentropic, we will use a "Q-curve", [3.74] as a direct analog to the adiabat. If we draw a line between the upstream and downstream conditions, called the Rayleigh line, we have a valuable tool to see if the shock with these end conditions can exist. There are two things, in general, which can be shown by looking at the Rayleigh line. The most important for our work is that this Rayleigh line must lie either totally above or totally below the Q-curve for a shock to exist between the two points. If it intersects anywhere between the proposed upstream and downstream points, the shock will only go the to nearest tangency point and the flow will follow the adiabat to the downstream conditions. For example, in Figure 3.5 a shock from 1 to 2 and from 3 to 4 is possible but a shock from 2 to 4 is not, since the Rayleigh line crosses the adiabat. If 2 and 4 are the upstream and downstream conditions, the flow will follow the adiabat in the form of a fan from 2 to point 5 where a shock will form to the final condition 4.

If we have a Rayleigh line which lies totally above or below the Q-curve, we must have a second condition to determine which direction the shock will jump. For example, in Figure 3.5, which shock exists, the one from 3 to 4 or the one from 4 to 3? It can be shown that this second condition is the upstream normal Mach number must be supersonic, i.e. greater than 1, and the downstream normal Mach number must be subsonic, i.e. less than 1 [13]. We can tell the magnitude of the Mach number at the end conditions by comparing the slope of the Rayleigh line to the slope of the adiabat at the intersection point. If the slope of the Rayleigh line is greater than that of the Q-curve, the flow is supersonic, i.e., the normal Mach number is greater than one. If the slope of the Rayleigh line is less, the flow is subsonic. If the Rayleigh line is tangent to the Q-curve at either the upstream or downstream condition, we have what is called a sonic shock, a shock with the normal Mach number exactly equal to one at the upstream or downstream condition. We can translate this Mach number relation into simple rules for determining if a shock can exist. If the shock is moving from right to left, i.e., from 1 to 2 in Figure 3.5, the Rayleigh line must lie below the Q-curve. If it is moving from left to right, i.e., from 3 to 4, the Rayleigh line must lie above the Q-curve. These, combined with the fact that the Rayleigh line must not cross the adiabat, gives us sufficient conditions to determine if a shock exists.

Chapter 4: Numerical Method

After much mathematical manipulation in the previous section, we have shown that the fluid is governed by a relatively simple Burgers equation, [3.61]. In effect, we have three different equations: One where only $\hat{\Gamma}_\infty$ is non-zero, one where both $\hat{\Gamma}_\infty$ and $\hat{\Lambda}_\infty$ are non-zero, and a third when all three constants $\hat{\Gamma}_\infty$, $\hat{\Lambda}_\infty$, and Ξ_∞ are non-zero. This is because for each case we have a different definition of $\hat{\Gamma}_\infty$, due to differences in order. We will need to write a general expression which can take these differences into account. We will accomplish this through our definition of $\bar{x}$ and $\bar{y}$. Equations [3.59] gave the definition for these quantities with only Ξ_∞ equal to zero. We can write the extension of [3.59] as follows

$$\bar{x} = \frac{x}{L} - \sqrt{M_\infty^2 - 1}\,\frac{y}{L} \qquad\qquad \bar{y} = \frac{y}{L}\frac{\varepsilon^n M_\infty^2}{\sqrt{M_\infty^2 - 1}} \tag{4.1}$$

where the exponent n is dependent upon the case we are running. If only $\hat{\Gamma}_\infty$ is non-zero, i.e. classical theory, n = 1 and $\hat{\Gamma}_\infty = \overline{\Gamma}_\infty$. If both $\hat{\Gamma}_\infty$ and $\hat{\Lambda}_\infty$ are non-zero, i.e. the theory derived in Chapter 3, then n = 2 and $\hat{\Gamma}_\infty$ and $\hat{\Lambda}_\infty$ are defined by [3.57] and [3.42] respectively. If all three constants are non-zero, i.e. the extended theory derived in Section 3.10, then n = 3 and $\hat{\Gamma}_\infty$, $\hat{\Lambda}_\infty$, and Ξ_∞ are defined by [3.75] and [3.73] respectively.

We will solve the Burgers equation using MacCormack's predictor-corrector scheme with artificial viscosity introduced to minimize oscillations [12]. This scheme is a very effective, and often used finite-difference technique for examining shock waves in supersonic inviscid flow. The first stage, the predictor, is

$$u_j^* = u_j^n - \frac{\Delta y}{\Delta x}(Q_{j+1}^n - Q_j^n), \tag{4.2}$$

where j is the node number in the x direction, and n is the node number in the y direction, Q is defined by [3.74]. We then use this value in the corrector stage

$$\hat{u}_j^* = \frac{(u_j^n + u_j^*)}{2} - \frac{\Delta y}{2\Delta x}(Q_j^* - Q_{j-1}^*). \tag{4.3}$$

We then apply the artificial viscosity, ν to get the final value of u at the next y value,

$$u_j^{n+1} = \hat{u}_j^* + \nu\frac{\Delta y}{\Delta x}\{|\hat{u}_{j+1}^* - \hat{u}_j^*|(\hat{u}_{j+1}^* - \hat{u}_j^*) - |\hat{u}_j^* - \hat{u}_{j-1}^*|(\hat{u}_j^* - \hat{u}_{j-1}^*)\}. \tag{4.4}$$

The artificial viscosity enters into the stability condition.[12] This condition is

$$|Q'|_{\max}\frac{\Delta y}{\Delta x} \le (1+\nu^2)^{\frac{1}{2}} - \nu \tag{4.5}$$

where

$$Q' = -\hat{\Gamma}_\infty u - \frac{\hat{\Lambda}_\infty}{2}u^2 - \frac{\Xi_\infty}{6}u^3. \tag{4.6}$$

In other words, the value of ν must remain small for the solution to be stable, and in our case this means we will never use a value of $\nu > 1$

The program is set up so that the values of the upstream Mach number, along with $\hat{\Gamma}_\infty$, $\hat{\Lambda}_\infty$, and Ξ_∞, must be input in order to define the upstream conditions. The program then uses

MacCormack's scheme to march in the $\bar{y}$-direction, outputting the values for $\bar{x}$ and u at specified $\bar{y}$ values. These values can then be plotted to give us the flow dynamics. If a physical picture is desired, the values of $\bar{x}$ and $\bar{y}$ must be converted to physical x and y coordinates using the following equations derived from [4.1]

$$\frac{x}{L} = \bar{x} + \frac{M_\infty^2 - 1}{M_\infty^2} \frac{1}{\varepsilon^n} \bar{y} \qquad [4.7]$$

$$\frac{y}{L} = \frac{\sqrt{M_\infty^2 - 1}}{M_\infty^2 \varepsilon^n} \bar{y}$$

where the values of ε are determined by the wedge or wing angle, and n is determined by the case we are running.

Chapter 5: Results

5.1 Comparison to Classical Flows

Our first goal will be to verify the program's accuracy by running two classical, well known cases. The first will be an ideal gas, such as air, over a wedge such as that in Figure 5.1. As shown in the figure, in such a configuration, with a gas such as air, ideal gas theory states that we will get a compression shock wave coming off the leading edge of the wedge, and a centered expansion fan off the rear shoulder. For a perfect gas, the equivalent flow in our system is $\hat{\Gamma}_\infty = 1.2$, $\hat{\Lambda}_\infty = \Xi_\infty = 0$, n = 1, a wedge angle ε = .176 (tan(10°)), and we will use an upstream Mach number, $M_\infty = 2$. Figure 5.2 shows the program's output from the solution of our Burgers equation. Most of the output from the program will be in the form of Figure 5.2, a density, u, versus x plot, with the y coordinate fixed. Figure 5.3 is a sketch of the way the output is presented. In this case the output will start with the upstream values, intersect the shock and then pass through the fan ending up back at the freestream condition. Looking again at Figure 5.2, we see that the density takes a sharp rise, i.e. a compression shock and then slowly falls back to the freestream value through an expansion fan. This is the correct qualitative result. If we take a larger y value we see that the expansion fan has collided with the shock and started to weaken it. Such a case has been plotted in Figure

5.4. The oscillations seen at the end of the shock are a common occurrence in MacCormack schemes when large shocks are encountered. The artificial viscosity keeps these oscillations small and confined to the region of the shock. In order to check the quantitative results, we will compare our results to an exact value for the shock slope obtained from equation [3.51]. If we substitute values into this equation, we see that for the 10 degree wedge used in this case, the x location of the shock will be 0.86 when $\frac{y}{L}$ = 0.74. Figure 5.2, taken at this $\frac{y}{L}$ value shows that, indeed, the center of the shock is around x = 0.86. Our artificial viscosity causes the shock to be a smooth profile rather than a discontinuity.

We can run a second case with an ideal gas flow over a standard expansion wedge as seen in Figure 5.5. In this case we first get an expansion fan followed by a compression shock at the trailing edge. In the program we will use the same values for $\hat{\Gamma}_\infty$, $\hat{\Lambda}_\infty$, Ξ_∞, and Mach number as we used above. Running the program we get the results shown in Figure 5.6. These are exactly reversed from our case in Figure 5.2. We can lay the plots on top of each other and verify that the results are identical, except for the sign.

5.2 *Non-Classical Cases*

We will now run several cases to show the results of mixed non-linearity. We will gradually progress into the more complicated flows by changing our values of $\hat{\Gamma}_\infty$, $\hat{\Lambda}_\infty$, and Ξ_∞. Our first non-classical case will be a purely negative Γ case. This type of situation was shown to exist in heavy heat transfer fluids such as PP10 and PP11 and 3-M's FC-70 and FC-71.[13] This type of flow results in the situation shown in Figure 5.7 and described in Section 1, a compression fan followed by an expansion shock. We will again set $\hat{\Lambda}_\infty = 0$, $\Xi_\infty = 0$, $\varepsilon = .176$, and the Mach number, $M_\infty = 2$, in our program and use $\hat{\Gamma}_\infty = -0.4$, the lowest value for Γ in FC-70. The results are shown in Figure 5.8 and 5.9. We see that the flow is qualitatively opposite that of Figure 5.2, a fan in front and a shock on the rear. Since the density increases in the front, the fan can only be a compression fan, and the shock, since the density drops, can only be an expansion shock. Although there is no experimental data to confirm the numerical results, negative Γ flows are a relatively new area of study, the qualitative results agree with our theoretical prediction. In Figure 5.9, the fan and shock have collided and are in the process of weakening each other.

Our next case will be a positive $\hat{\Gamma}_{\infty}$, but now we will use our second constant $\hat{\Lambda}_{\infty}$ to make the flow equivalent to flows very near the negative Γ range. Recall that since we now have $\hat{\Lambda}_{\infty}$ non-zero, we will be scaling $\hat{\Gamma}_{\infty}$ with our wedge angle ε. This will give us an effective $\overline{\Gamma}_{\infty}$ equal to a much smaller number. If we plot the Q-curve for this case, described in Section 3.11 and given by equation [3.74], we get Figure 5.10. We will take the upstream Mach number, $M_{\infty} = 2$ which will cause an initial disturbance, u, as defined by equation [3.60] to be approximately 2.3. If we look at Figure 5.10, condition A is the upstream, infinity, condition which is by definition always zero, and B is the initial disturbance at u = 2.3. If we draw the Rayleigh line connecting these two, we see that it lies totally below the curve. Since the flow starts at A, a shock wave will form from A to C and then the flow will form a compression fan connecting C to B, following the Q-curve. Once the flow gets to B it must return to A, it can do this by one shock since the Rayleigh line lies totally below the Q-curve. The output from the program is displayed in Figures 5.11 and 5.12. We see that indeed there is a small compression shock, followed by a compression fan and then, at the rear, a large expansion shock. The expansion shock and compression fan are possible in negative Γ flows only, so this flow started with a positive Γ and then moved into the negative Γ region. Note that the compression fan, as it collides with the expansion shock, in Figure 5.12, causes the expansion shock to weaken. Eventually, the expansion shock will collide with the forward compression shock and we will be left with a picture similar to the classical flow in Figure 5.4. Figure 5.13 is a sketch of how this flow would look from a stationary viewpoint.

In real flows, we can also get a flow where we start with positive Γ, dip into the negative Γ region for a small distance, then return to the positive Γ region. This can be accomplished using our third constant Ξ_{∞}. Once again, recall that for this case, with Ξ_{∞} not equal to zero, $\hat{\Gamma}_{\infty}$ is scaled with ε^2

and $\hat{\Lambda}_\infty$ is scaled with ε, this will result in a much smaller value for these quantities in the real flow. If we expand upon the above case, with $\hat{\Gamma}_\infty = 0.8$, $\hat{\Lambda}_\infty = -2.1$, and now set $\Xi_\infty = 1.6$ we get the Q-curve seen in Figure 5.14. We will run the two cases seen in Figure 5.14, a Mach number of 3.3 and then a Mach number of 3.7. Looking at our Q-curve in Figure 5.14 we see that the Rayleigh line connecting the first flow, at Mach number 3.3 crosses the curve twice. This is going to result in a very complex flow.

In Figure 5.15, the flow for M = 3.3 has been depicted. It will start at the upstream condition, u = 0, and shock to the tangency point 1, it will then follow the Q-curve, forming a fan until it hits a second tangency point 2, such that it can then form a sonic shock over to our final condition A. In order to return to the initial condition, the flow will follow the curve to a third tangency point, 3, and then form an expansion shock returning to u = 0. Figures 5.16-19 show the evolution of this flow as the y value increases. In 5.16, we see the initial compression shock, the small compression fan and then the second compression shock. This phenomena of two shocks forming from the same initial discontinuity is called shock-splitting and occurs only in BZT fluids, if the flow is single phase.[4] Once the flow reaches the final condition it then forms a small expansion fan and a larger expansion shock. Because both expansion and compression shocks are present, the flow must be dipping into the negative Γ region somewhere over the wedge. Figure 5.17 shows the flow at a higher y value. We see that the compression fan has become wider and the second compression shock is catching up to the rear expansion shock. Figure 5.18 shows that at an even greater y value, the second shock has collided with the rear expansion shock, weakening it considerably. Such a collision demonstrates the reason that expansion shocks are sometimes referred to as "negative" shock waves. A collision between a compression shock and an expansion shock results in the shocks canceling each other out, eliminating the weaker shock and weakening the stronger shock. Figure 5.18 looks very similar to the case where Ξ_∞ equals zero and the flow has clearly moved into this simpler region. Figure 5.19 shows what happens at an even greater y value, as the flow moves out of the negative Γ region the rear expansion shock starts to break up into an expansion fan. If we could run this case out far enough, we would eventually get a picture that looked similar to

Figure 5.4, a totally classical flow. The shock collisions are shown more vividly in Figure 5.20, which is a contour plot produced from the output of the program. It clearly shows the shock collision and the resulting weakening of the rear expansion shock. The contour plot is in our $\bar{x}, \bar{y}$ coordinates which is a system moving along with the Mach lines. Figure 5.21 is a sketch which shows how the flow would look from a stationary viewpoint.

We will now look at the second case shown in Figure 5.14, a Mach number of 3.7. We can see that initially the Rayleigh line lies totally above the Q-curve. This means that a compression shock will exist initially in the flow, and the rear flow will be the same, an expansion fan followed by an expansion shock. This is shown in Figure 5.22. However as the expansion shock or fan collides with the compression shock it will weaken it until the situation shown in Figure 5.23 exists. The Rayleigh line now crosses the Q-curve, which means the large compression shock is no longer possible. The flow has now developed into the case we talked about previously, i.e. the case of $M_\infty = 3.3$ in Figure 5.14.

In order to be sure that the phenomena demonstrated above are a result of our theory and not some type of numerical creation, an exact solution to the flow over an infinite wedge has been has been developed in Appendix A. The results of the exact solution can be superimposed over the data created by the program to demonstrate the accuracy of our numerical scheme. Looking at Figure 5.24 we can see that the agreement is good, and we can be confident that the program is producing results in agreement with our theory.

5.3 Flows Over Wing Shapes

All of the flows discussed in the previous section used a wedge as the disturbance shape. Obviously this is not a good representation of real turbine blades. We will use a sine wave to represent our turbine blade. This provides for the smooth curvature and the pointed leading edge, which must be present to keep the shocks from detaching. The flow over such a shape will be more complex because it has both a positive and negative slope along its length, thereby setting up both compressions and expansions. Once again we will first look at the classical flow of a perfect gas, such as air, where $\hat{\Gamma}_\infty = 1.2$, $\hat{\Lambda}_\infty = \Xi_\infty = 0$. Classical theory says we will get a compression shock at the leading edge, and a compression shock at the trailing edge, with a smooth expansion fan along the rest of the wing, as seen in Figure 5.25. Figure 5.26 shows the output from the program which is exactly as we expected, two compression shocks with an expansion wedge connecting them.

Looking at Figure 5.26 we once again see one of the major problems facing supersonic turbine designers, the compression shock from the leading edge of the wing will collide with a second blade above, it possibly causing losses to occur. If we run a case with purely negative Γ we will get the flows shown in Figures 5.27 and 5.28. The major difference we have in this flow is that the two compression shocks of the previous case have been replaced by a single expansion shock in the center of the wing and a compression fan at both the leading and trailing edges. These compression fans, upon striking the expansion shock, cause it to weaken quickly. This makes this type of flow much more efficient, the compression is spread out over a much larger area, and the expansion shock has no adverse effect on the upper wing. Indeed it thins the boundary layer and may even reduce drag. We will discuss this in more detail in the next section.

A more complex flow is encountered with a slightly positive $\hat{\Gamma}_\infty$ and a negative $\hat{\Lambda}_\infty$. We will use the same conditions used in Section 5.2, $\hat{\Gamma}_\infty = 0.8$, $\hat{\Lambda}_\infty = -2.1$, $\Xi_\infty = 0$, and $M_\infty = 2$. The output from the program run for this case is shown in Figures 5.29 and 5.30. We can use these plots to generate a sketch, 5.31, of how this flow will look. The front part of the flow is similar to the case of these conditions over a wedge, while the second part of the flow is a simple expansion fan and compression shock. As the flow progresses, the compression fan and expansion shock slowly eliminate each other. Eventually the expansion shock will collide with the compression shock and the flow will look like our classical case in Figure 5.26.

A final possibility is the case where all three of our constants are non-zero. We will use a similar case to the one we used in Section 5.2, $\hat{\Gamma}_\infty = 0.8$, $\hat{\Lambda}_\infty = -2.1$, $\Xi_\infty = 1.6$, and $M_\infty = 3.0$. The results are shown in Figures 5.32-5.35. We can then sketch how this flow will look in Figure 5.36. Again we see the shock splitting taking place off the leading edge. This happens for the same reason as over the wedge, the Rayleigh line is intersecting the Q-curve. Again the split compression shock is weakened by the expansion fan until it collides with the expansion shock, causing the expansion shock to be weakened considerably. We now have a picture, in Figure 5.35 which is similar to our previous case, i.e. the shock has traveled into the simpler region. Eventually, as in the case with the wedge, the expansion shock will collide with the compression shock and we will have a classical flow similar to that of Figure 5.26.

5.4 Application to Turbine Design

We will now see how we can use the phenomena discussed above to produce advantages over ideal gases in turbine design. Unfortunately, for the cases where Ξ_∞ was non-zero, when we transform them into real coordinates, the beneficial non-classical effects like shock disintegration, take place at distances much too far from the wing to be used in a turbine, where the blades are relatively close together. We can, however, still have a much more efficient flow by using a BZT fluid at a thermodynamic state with negative Γ. Figure 5.37 is a plot comparing two identical flows over a wing, the only difference being one case is an ideal gas, steam, with positive Γ, the other is a BZT fluid, PP24, with negative Γ. The output is given at a physical $\frac{y}{L}$ coordinate of 1 which is reasonable for a turbine design, i.e., the upper wing is one chord length away from the lower wing. Looking at the figure we see the n-shaped classical picture for steam, with the compression shocks at the leading and trailing edges, and the PP24 with its one expansion shock and two compression fans. The compression caused by the PP24 is a little larger than the steam, the compression shocks were slightly weakened by the expansion fan in the steam, but it is spread over an area of almost half a chord length, where the shock is spread over a very small area, theoretically, zero area. This means that the steam is much more likely to cause the boundary layer on the upper wing to separate. The PP24 also contains an expansion shock, which has the opposite effect on the boundary layer than a compression shock; it makes the boundary layer thinner, making it even less likely that the PP24 flow will have the excessive drag the steam flow has. Although, this simple picture is a strong demonstration of the potential for BZT fluids in this application, we can however have another situation which may even more desirable. If we take the same two fluids and reduce the Mach number to $M_\infty = 1.2$, we can produce a flow in the PP24 which has no shock waves at all. Figure 5.38 is a plot at $\frac{y}{L} = .75$, i.e., $\frac{3}{4}$ of a chord length away. The stream flow still contains large compression shocks. The PP24 however, contains only fans, two compression fans and a large expansion fan. Eventually the expansion fan would steepen to form an expansion shock, but, for these relatively short distances, this will not happen.

Chapter 6: Conclusions and Recommendations

In the previous section we have used our theory to show many types of non-classical behaviors in BZT fluids. Expansion shocks, compression fans, shock-splitting, shock-fan combinations, and collisions of expansion and compression shocks were all demonstrated. When we transformed our results into physical coordinates, we saw that most of the non-classical effects happened a very large distance from the wing. So when we looked at possible uses for BZT fluids in turbines, we had to discount most of the higher order effects and concentrate on the very simplest of non-classical flows, the $\Gamma < 0$ flow. By looking at the two cases in Section 5.4 we saw that a BZT fluid could dramatically reduce the likelihood of a compression shock causing the boundary layer of an adjacent blade to separate. Indeed, if our operating conditions are set right, it appears that a totally shock free flow can be produced in a turbine cascade.

This study has left much room for future study. One of the major drawbacks of our approach is that it ignores reflected waves. In order to incorporate reflected waves, we could solve the Euler equations, [2.1]-[2.3] directly. In this case we could have both the top and bottom blade present and look at how the reflected waves interact.

There is also much work to be done to experimentally verify the results and to determine effects of BZT fluid effects on boundary layers and exactly how boundary layers interact with non-classical flows such as expansion shocks and compression fans. As is the case with most new technologies there may be unforseen effects which can be found only through experiments. Although this study shows that BZT fluids are feasible and indeed, more desirable than classical fluids, there is much engineering work left to be done before a BZT turbine system can become reality.

References

1. Anderson, J.D. *Modern Compressible Flow* . New York: McGraw-Hill, 1982.

2. Thompson, P. A. "A Fundamental Derivative in Gasdynamics", *The Physics of Fluids* , Vol. 14, pp. 1843-1849, 1971.

3. Thompson, P. A. and Lambrakis, K. "Negative Shock Waves", *Journal of Fluid Mechanics*, Vol. 60, pp. 187-208, 1973.

4. Cramer, M.S. "Shock Splitting in Single Phase Gases." *Journal of Fluid Mechanics.*, Vol. 199, pp. 281-296, 1989.

5. Cramer, M.S. "Nonclassical Dynamics of Classical Gases. "Article in *Nonlinear Waves in Real Fluids* , ed. A. Kluwick, Springer-Verlag, 1991.

6. Bethe, H.A., "The theory of shock waves for an arbitrary equation of state", *Office of Scientific Research and Development* , Report #545, 1942.

7. Zel'dovich, Y.B., "On the possibility of rarefacation shock waves" *Zh. Eksp. Teor. Fiz.*, Vol. 4, pp.363-364, 1946.

8. Zel'dovich, Y.B., *Theory of Shock Waves and Introduction to Gas Dynamics* . Izadat. Akad. Nauk SSR, Moscow, 1946.

9. Graham, C.G. and Kost, F.H., "Shock Boundary Layer Interaction on High Turning Transonic Turbine Cascades," *ASME Paper 79-GT-37* , 1979.

10. Thompson, P.A., *Compressible-Fluid Dynamics* . McGraw-Hill: New York, 1972.

11. Anderson Jr., J.D., *Fundamentals of Aerodynamics* , McGraw-Hill: New York, 1984.

12. Bertin, J.J. and Smith, M.L., *:Aerodynamics for Engineers* , Prentice-Hall, 1979.

13. Cramer, M.S. and Crickenberger, A.B. "The dissipative structure of shock waves in dense gases." *Journal of Fluid Mechanics* Vol 223, pp.325-355, 1991.

14. Fletcher, C.A.J. *Computational Techniques for Fluid Dynamics, Volume II.* New York: Springer-Verlag, 1988.

15. Cramer, M.S., "Negative Nonlinearity in Selected Flurocarbons," *Physics of Fluids A* , Vol. 3, pp. 1894-1897, 1989.

16. Cramer, M.S., and Kluwick, A. "On the propagation of waves exhibiting both positive and negative nonlinearity." *The Journal of Fluid Mechanics.*, Vol. 142, pp. 9-37, 1984.

17. Cramer, M.S., and Crickenberger, A.B., "The Prandtl-Meyer Function for Dense Gases," Accepted for publication, *AIAA Journal* , April, 1991.

18. Lax, P.D., "Hyperbolic Systems of Conservation Laws and the Mathematical Theory of Shock Waves," *Regional Conference Series in Applied Mathematics.* Philadelphia: SIAM, 1973.

Figures

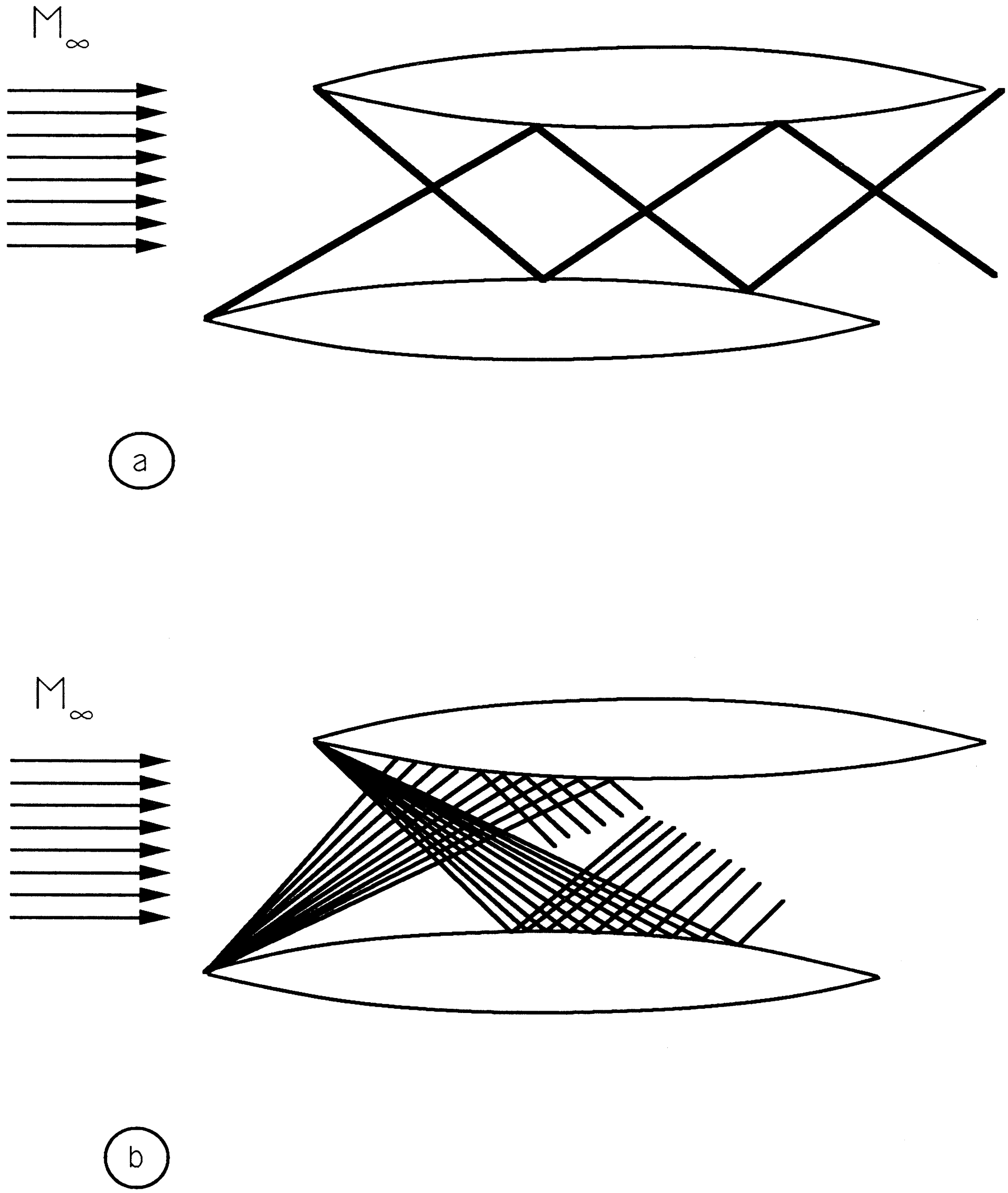

Figure 1.1. Comparison of the turbine cascade flow of a (a) classical fluid to a (b) BZT fluid.

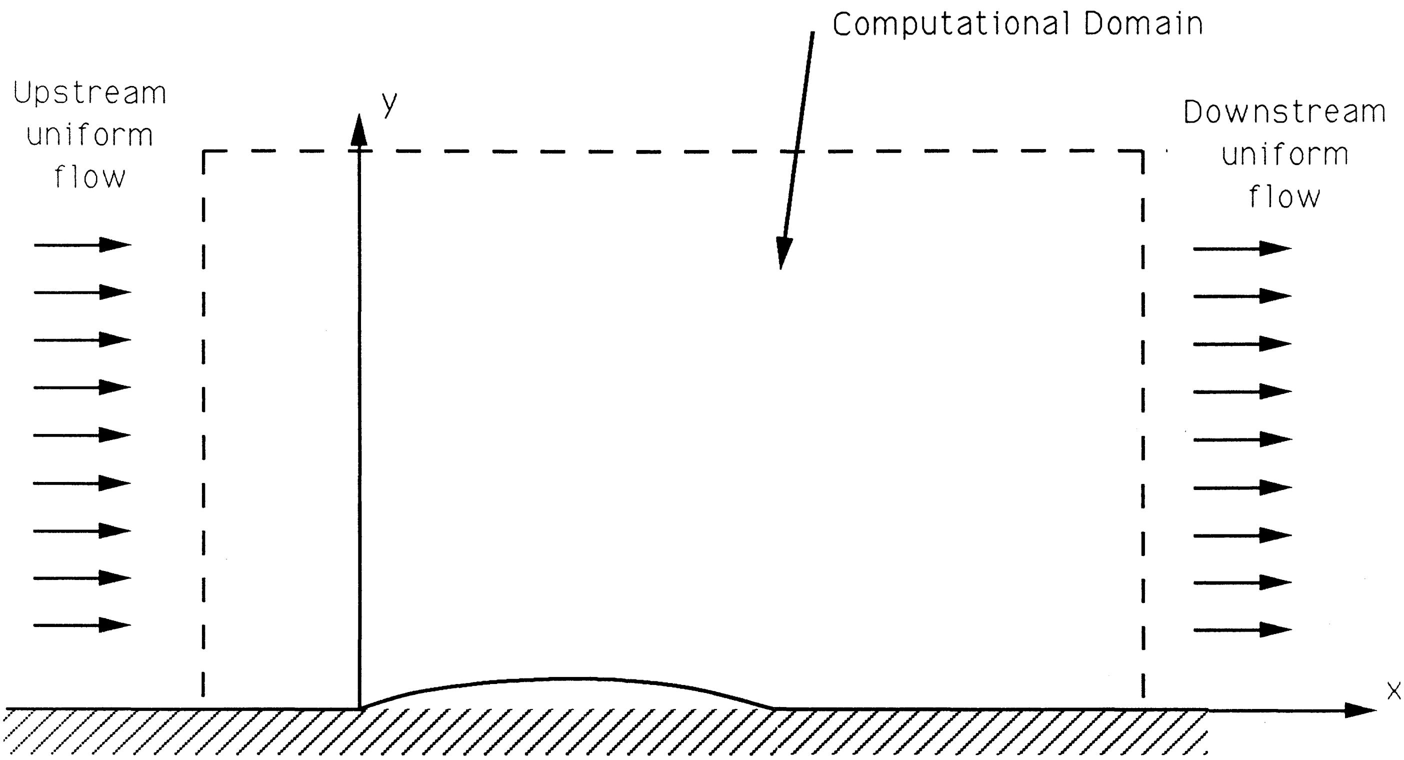

Figure 1.2. Solution domain for the numerical problem.

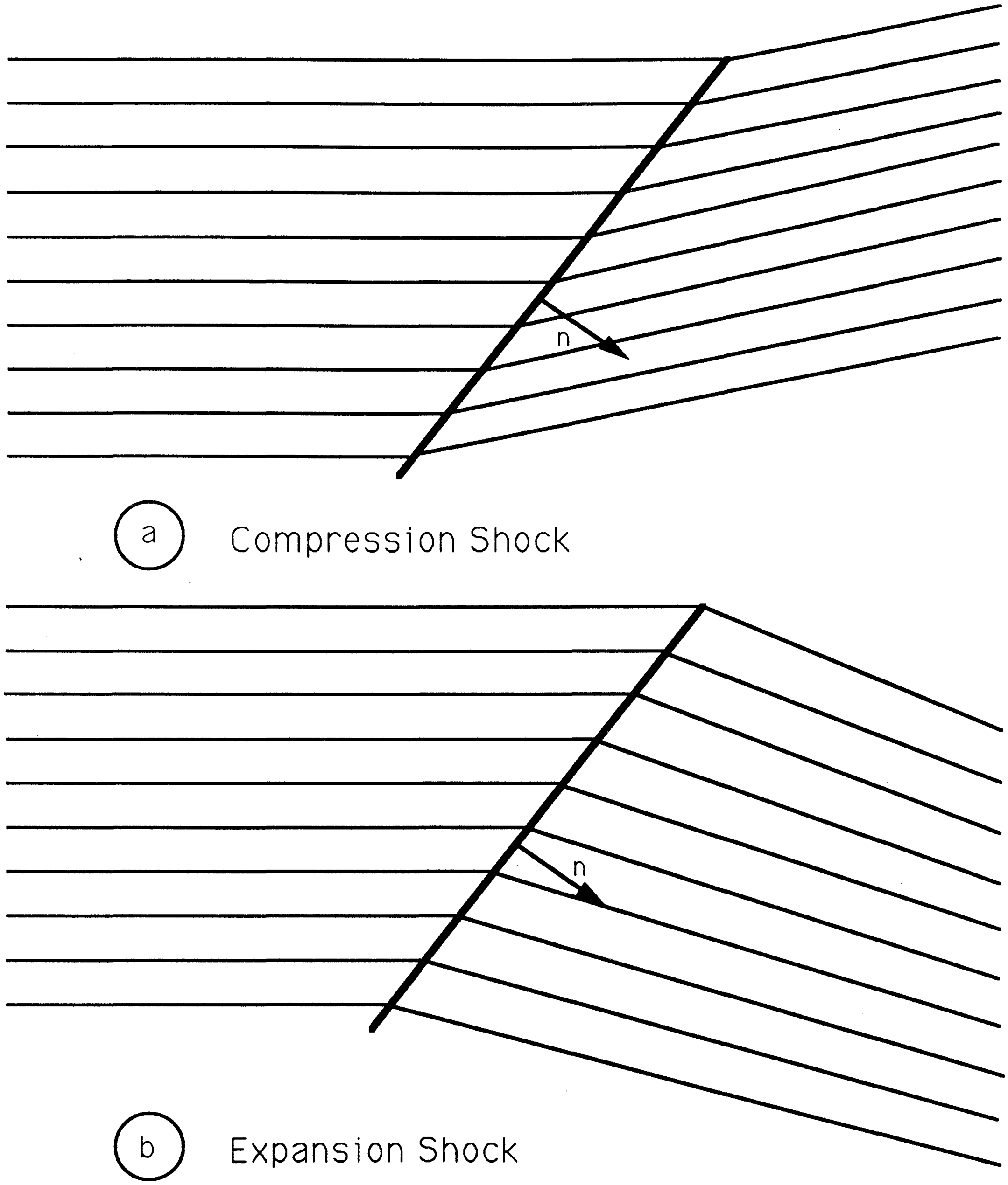

Figure 2.1. Comparison of an (a) oblique compression shock to an (b) oblique expansion shock

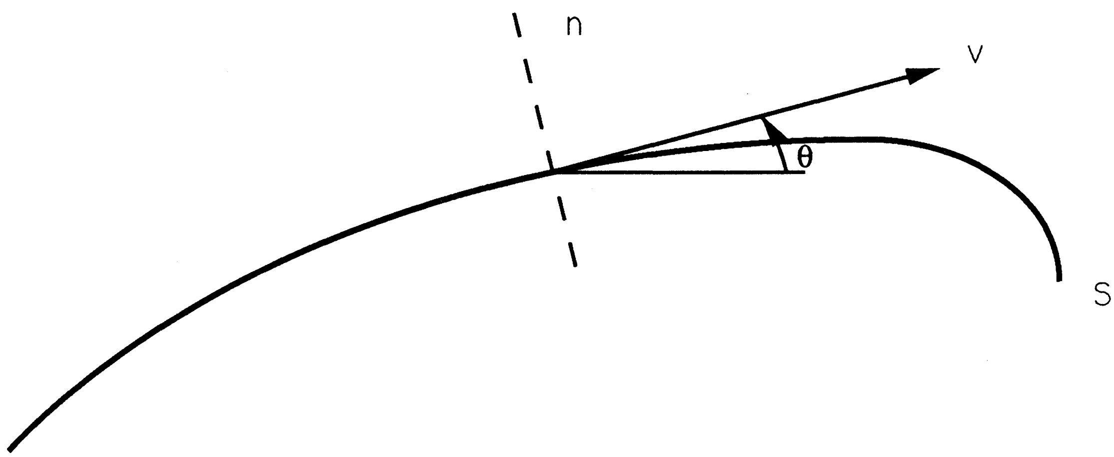

Figure 3.1. Coordinate system for the characteristic lines

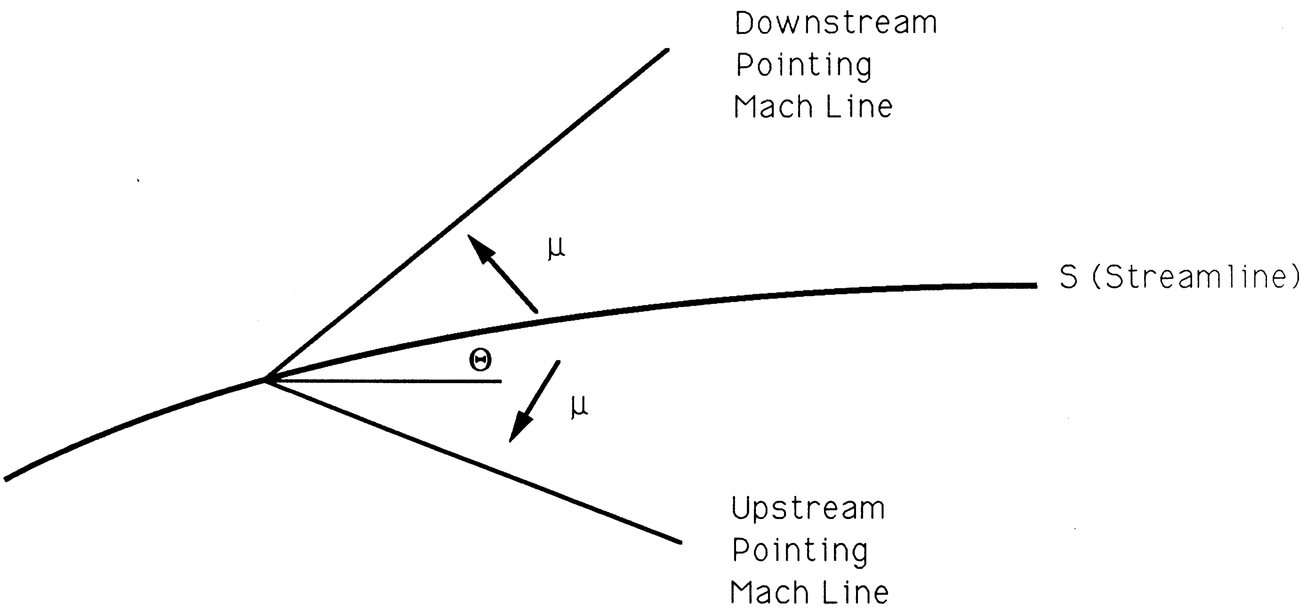

Figure 3.2. Slopes of the Mach lines in the n-s Plane

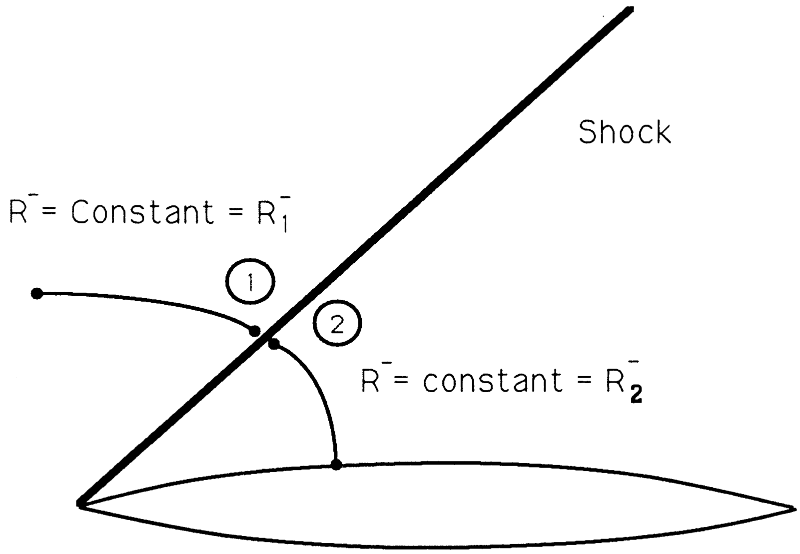

Figure 3.3. Graphical representation of R^-

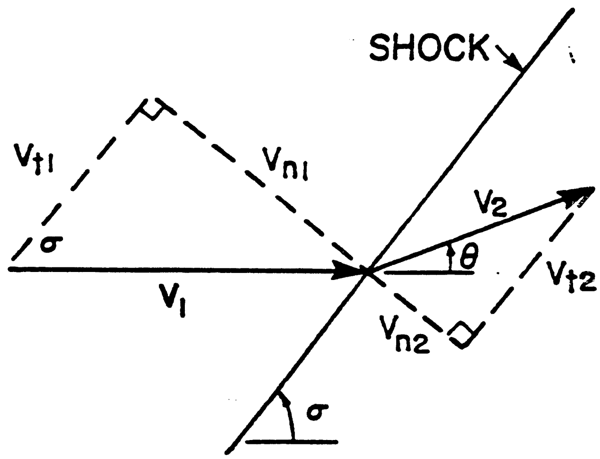

Figure 3.4. Breakdown of the components of velocity in an oblique shock.

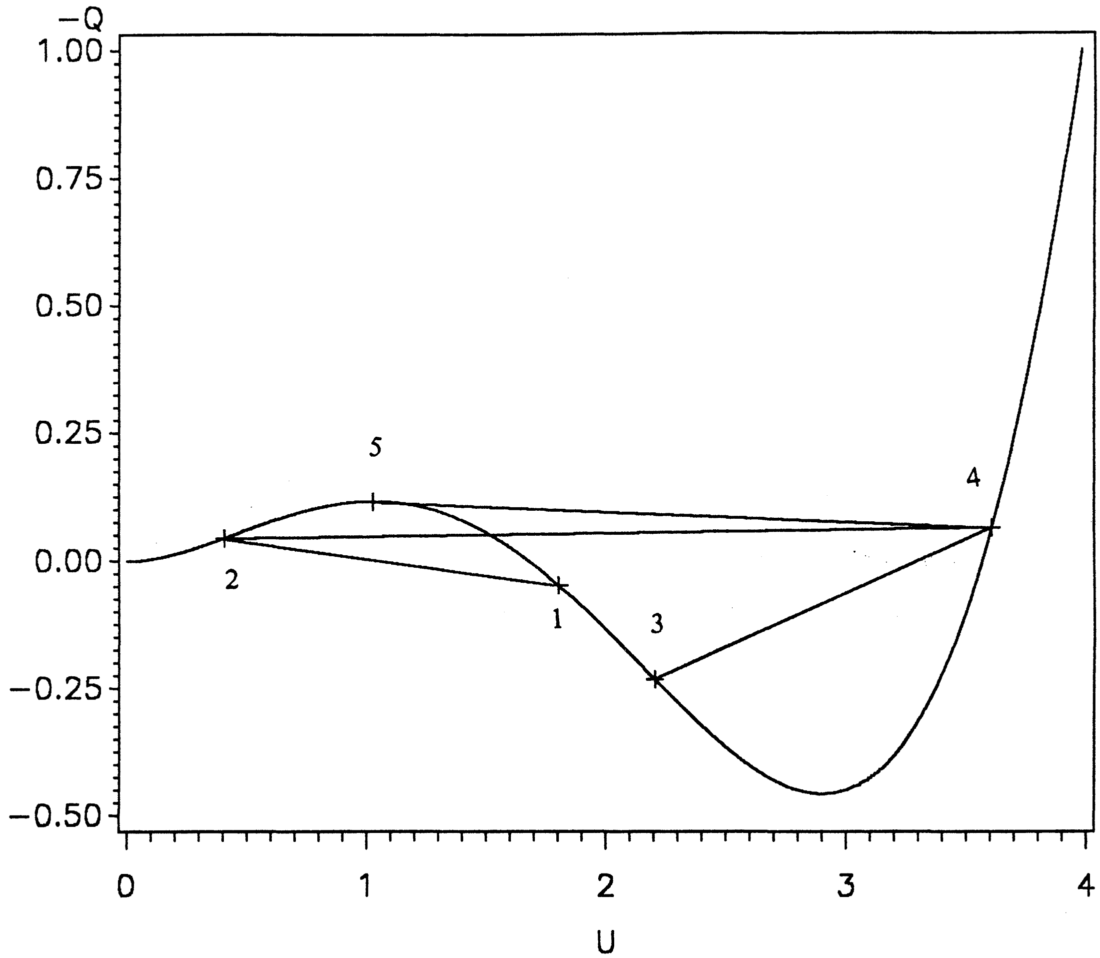

Figure 3.5. Existence conditions with a sample shock adiabat.

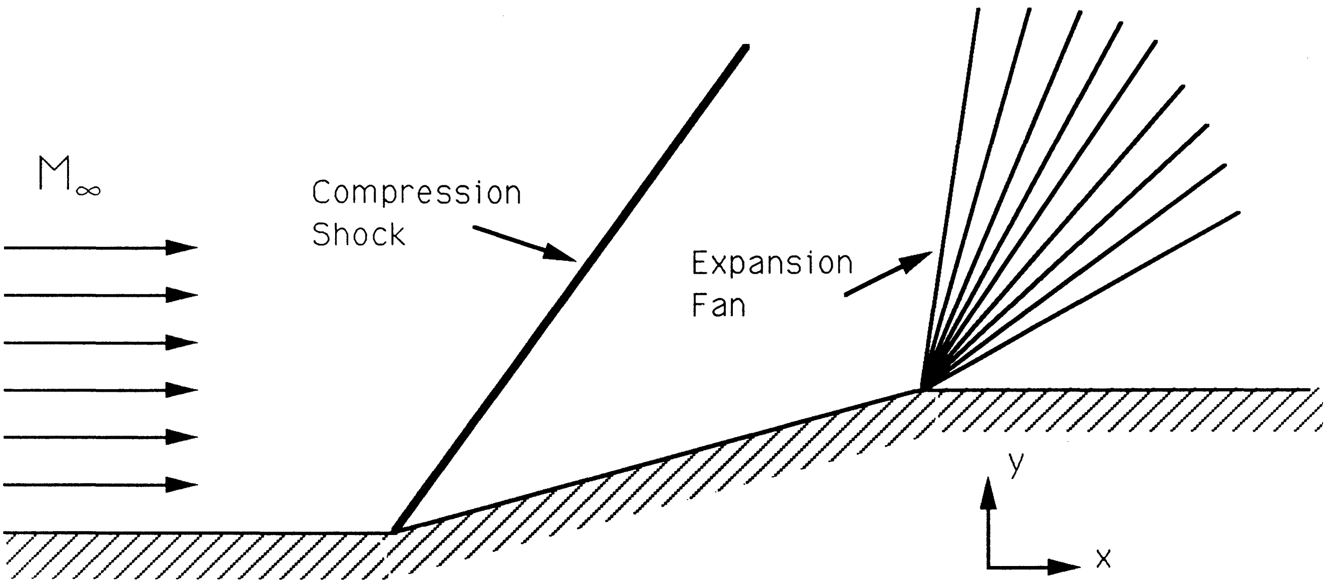

Figure 5.1. Sketch of classical flow over a compression wedge.

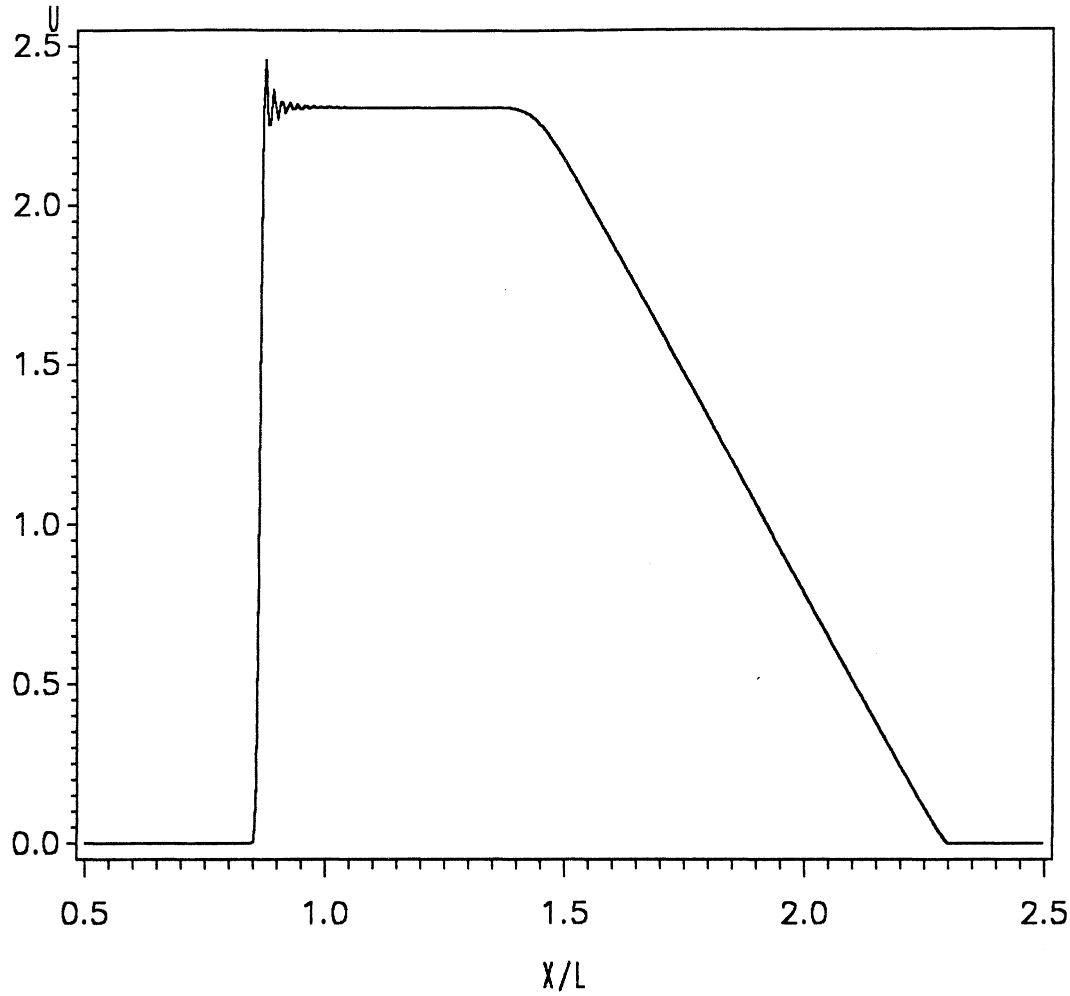

Figure 5.2. x-u plot for $\hat{\Gamma}_\infty = 1.2$, $\hat{\Lambda}_\infty = \Xi_\infty = 0$, $M_\infty = 2$ over a compression wedge at y/L = 0.74

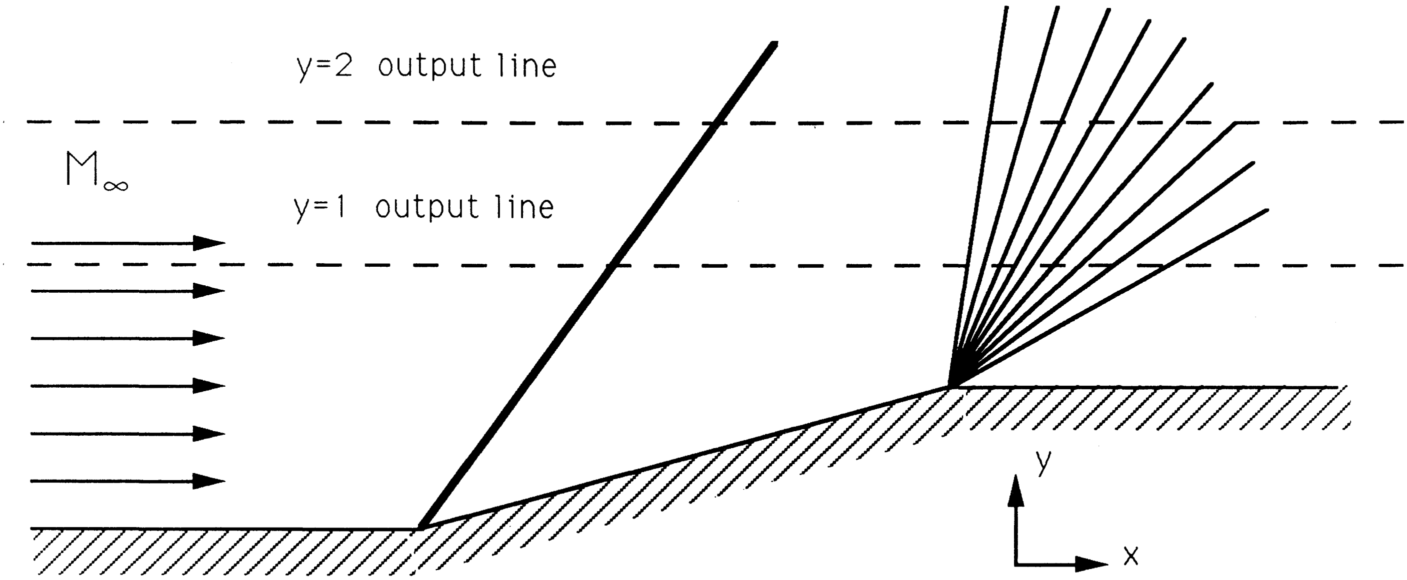

Figure 5.3. Form of output from the shock solver program.

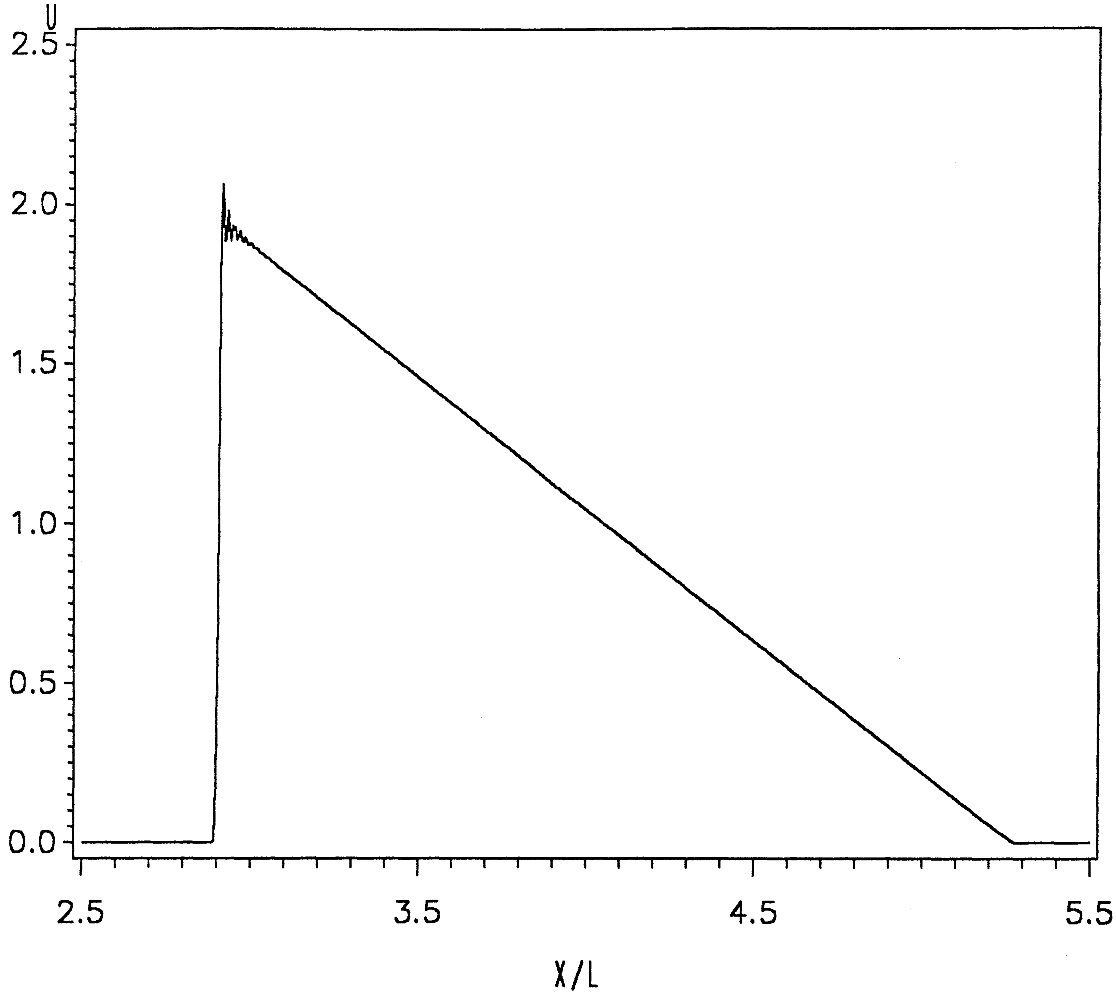

Figure 5.4. x-u plot for $\hat{\Gamma}_{\infty} = 1.2$, $\hat{\Lambda}_{\infty} = \Xi_{\infty} = 0$, $M_{\infty} = 2$ over a compression wedge at y/L = 2.46

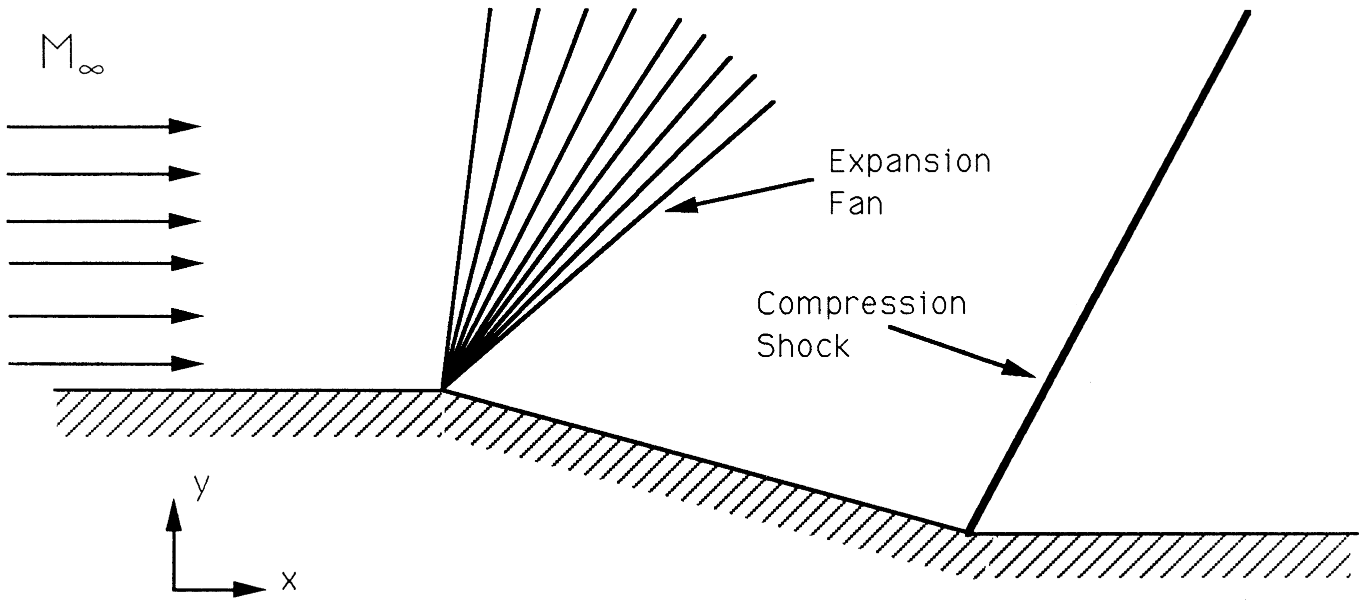

Figure 5.5. Sketch of classical flow over a expansion corner.

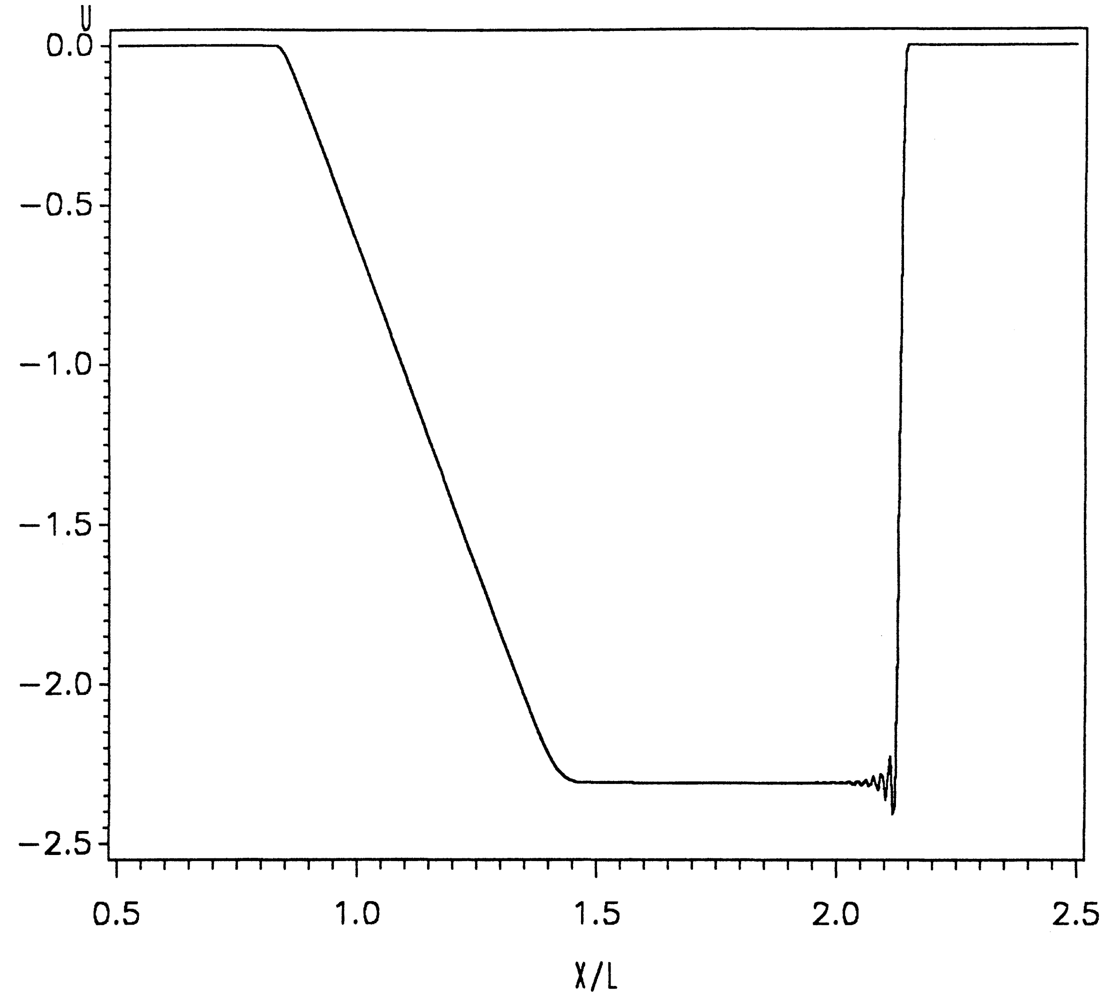

Figure 5.6. x-u plot for $\hat{\Gamma}_\infty = 1.2$, $\hat{\Lambda}_\infty = \Xi_\infty = 0$, $M_\infty = 2$ over an expansion corner at y/L = 0.49

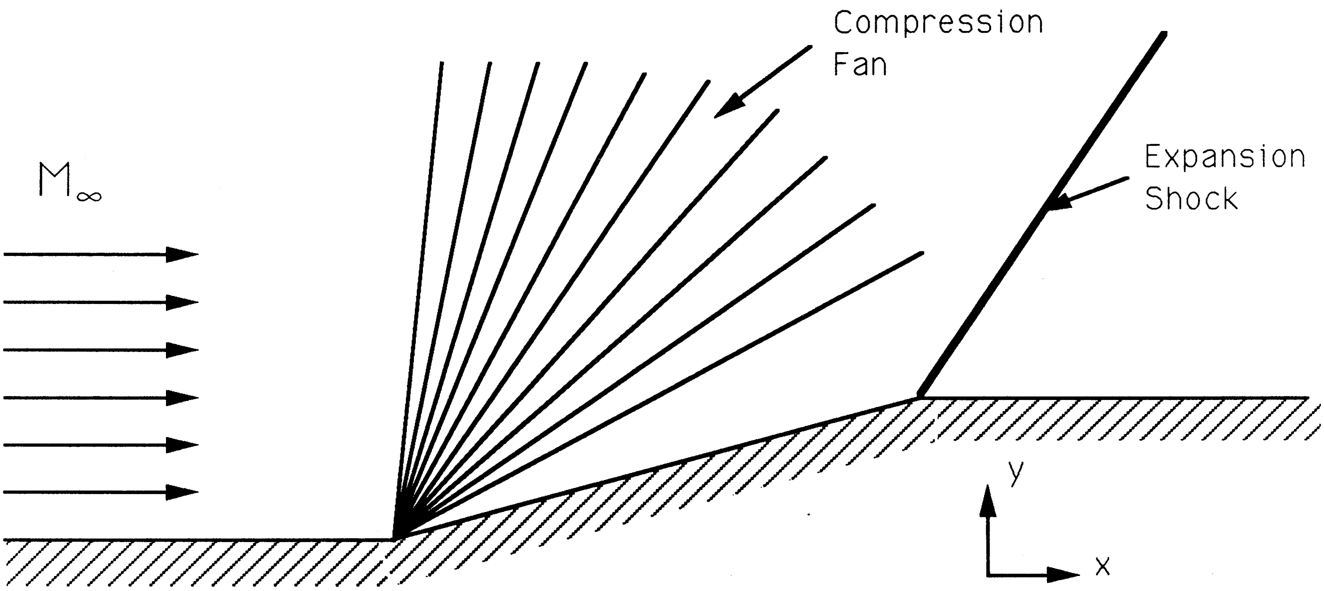

Figure 5.7. Sketch of purely $\Gamma < 0$ flow over a wedge.

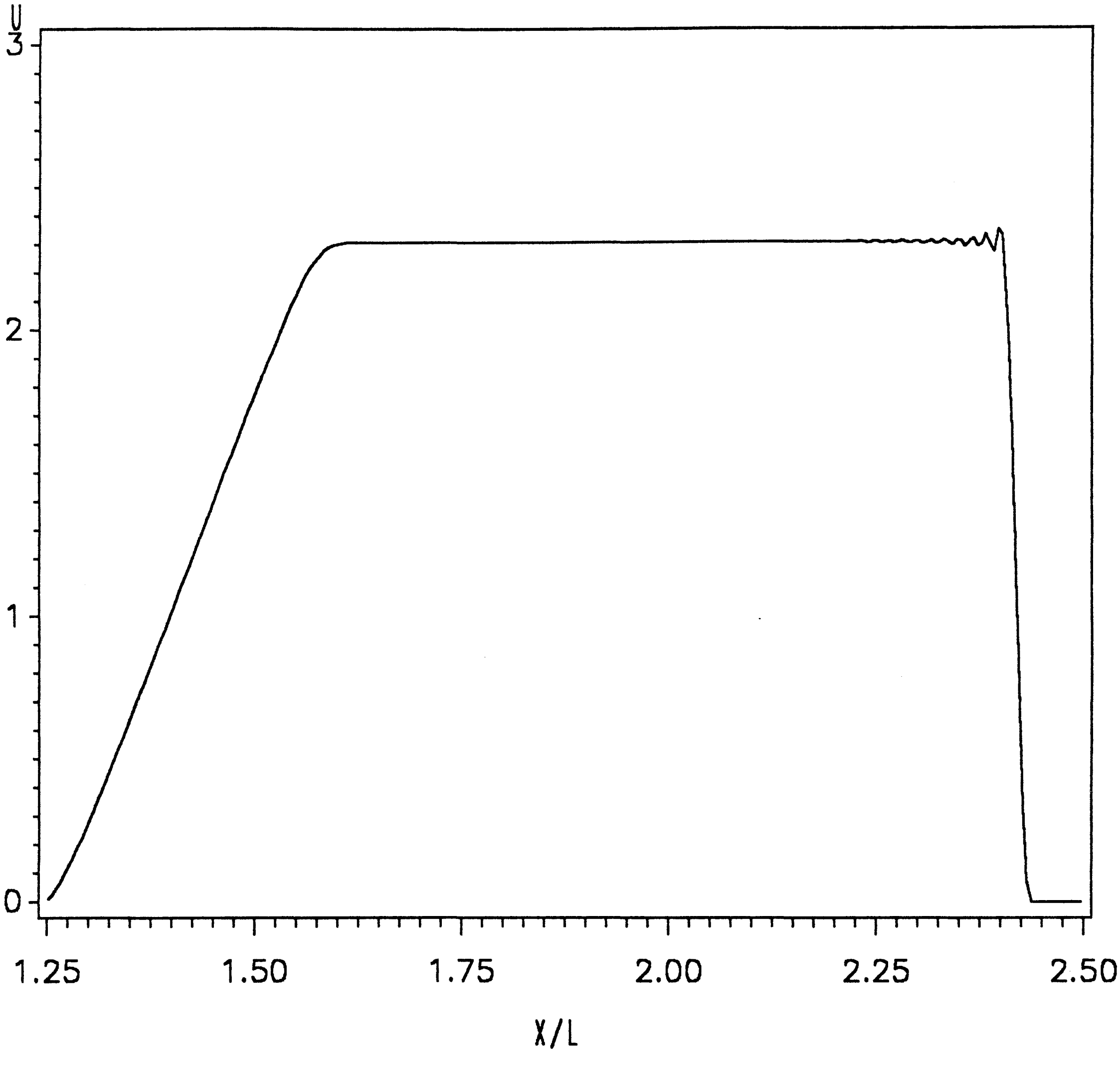

Figure 5.8. x-u plot for $\hat{\Gamma}_\infty$ = -0.4, $\hat{\Lambda}_\infty = \Xi_\infty$ = 0, M_∞ = 2 over a wedge at y/L = 0.74

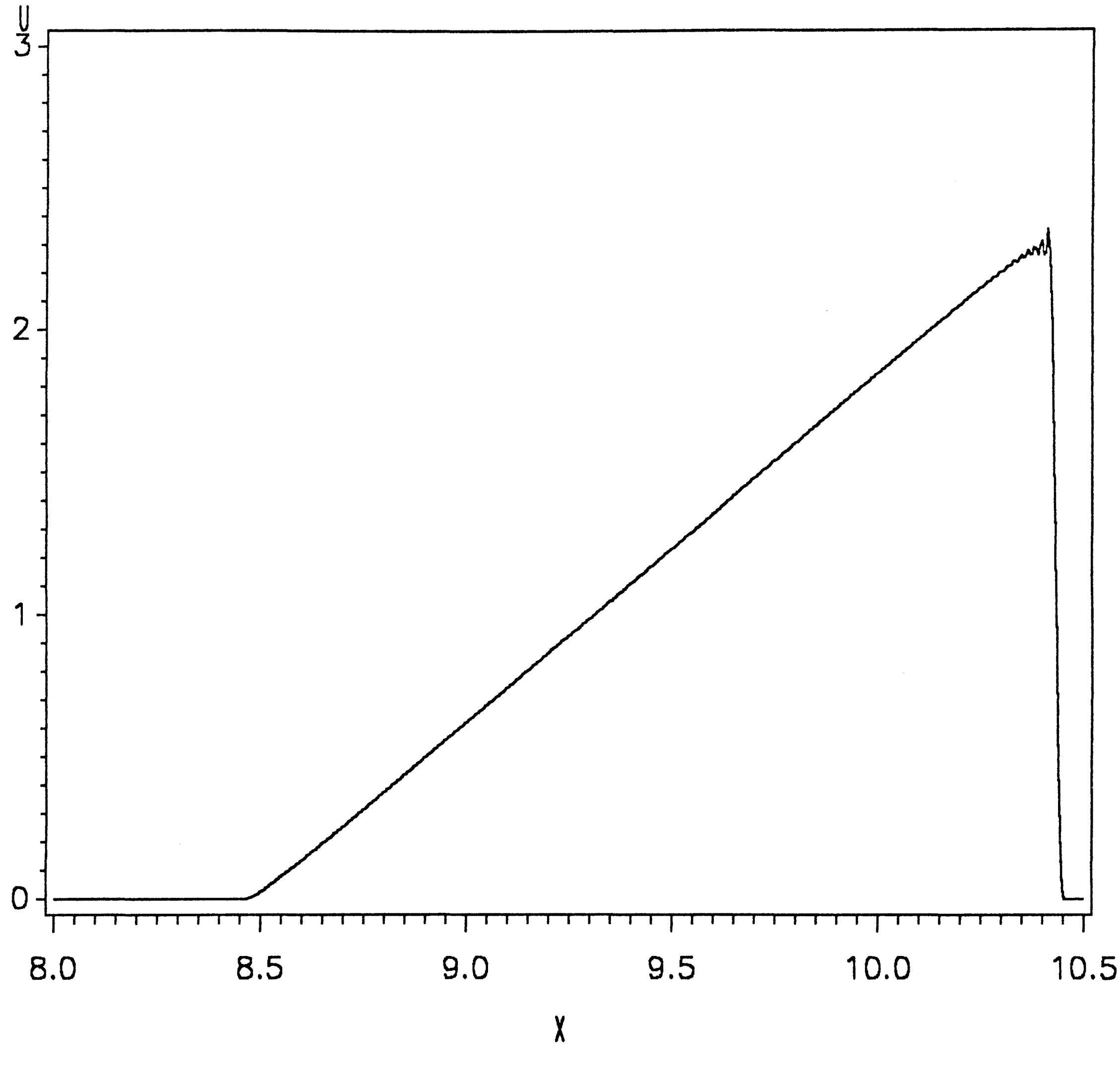

Figure 5.9. x-u plot for $\hat{\Gamma}_\infty = -0.4$, $\hat{\Lambda}_\infty = \Xi_\infty = 0$, $M_\infty = 2$ over a wedge at $y/L = 4.9$

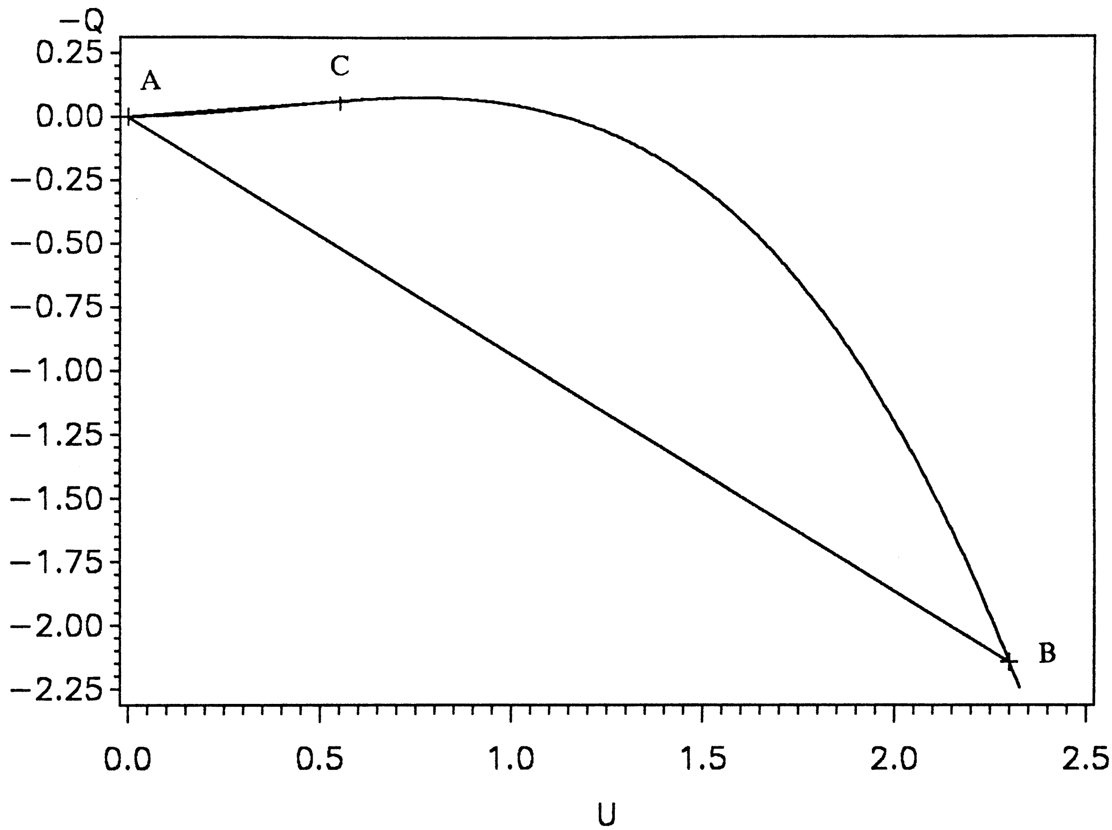

Figure 5.10. Q-curve for $\hat{\Gamma}_\infty = 0.8$, $\hat{\Lambda}_\infty = -2.1$, $\Xi_\infty = 0$

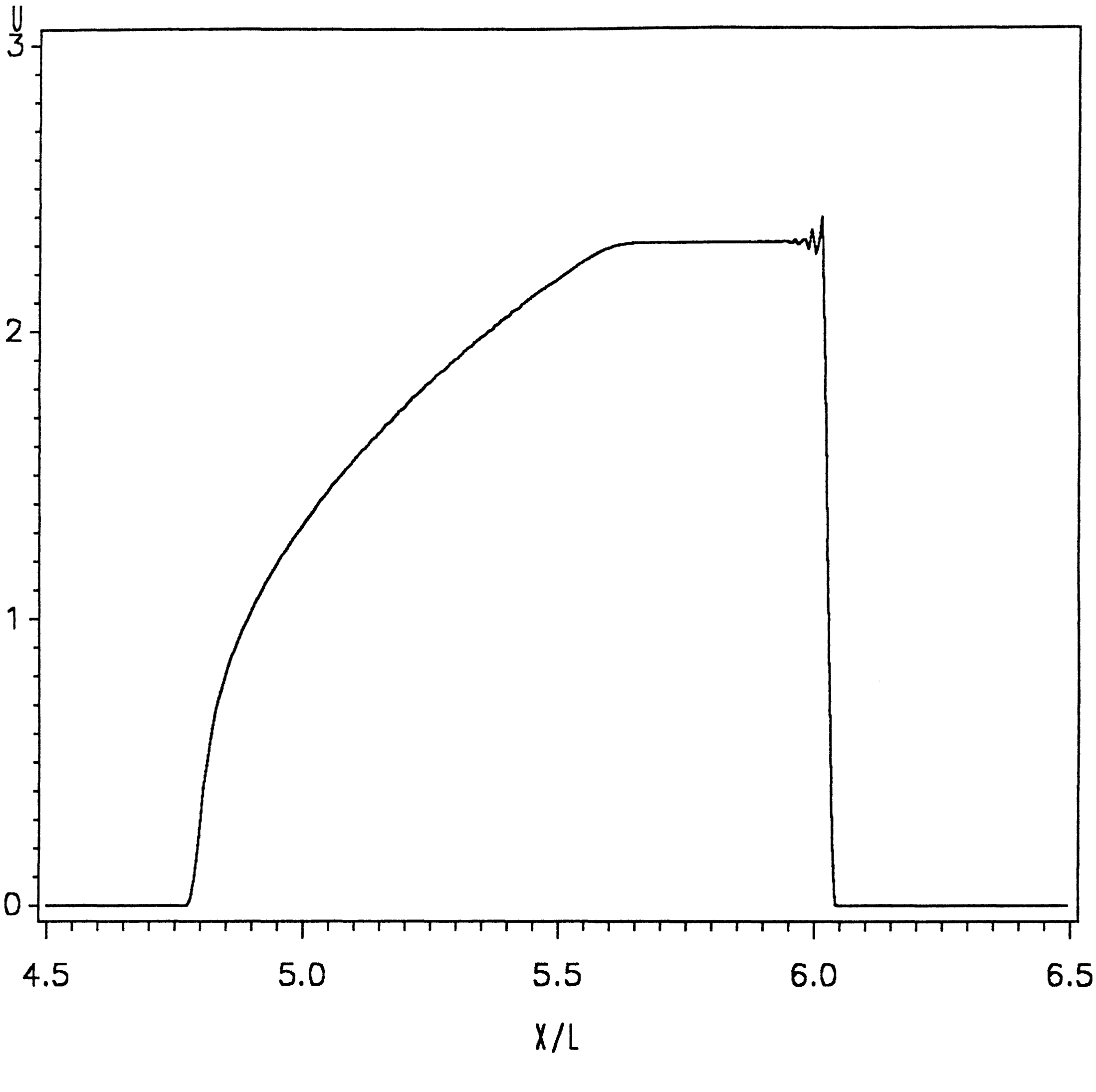

Figure 5.11. x-u plot for $\hat{\Gamma}_{\infty} = 0.8$, $\hat{\Lambda}_{\infty} = -2.1$, $\Xi_{\infty} = 0$, $M_{\infty} = 2$ over a wedge at $y/L = 2.79$

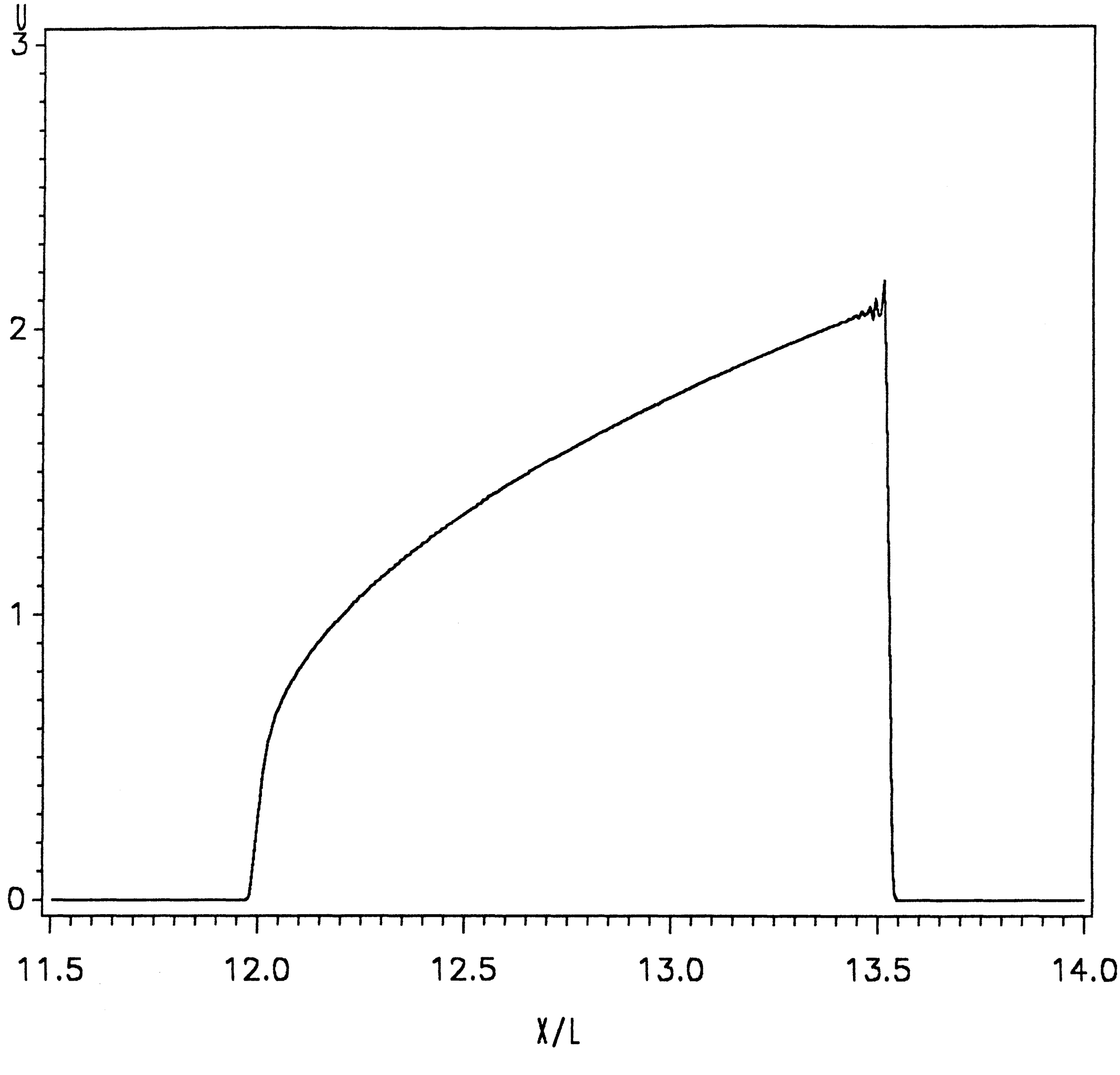

Figure 5.12. x-u plot for $\hat{\Gamma}_{\infty} = 0.8$, $\hat{\Lambda}_{\infty} = -2.1$, $\Xi_{\infty} = 0$, $M_{\infty} = 2$ over a wedge at y/L = 7.0

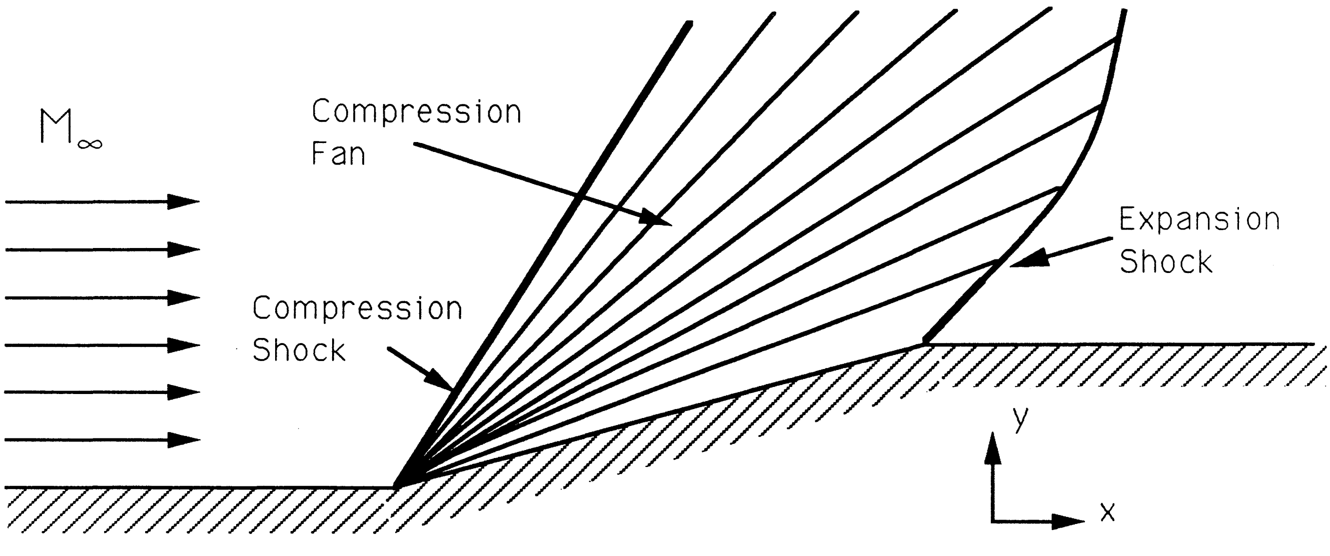

Figure 5.13. Sketch of the flow for $\hat{\Gamma}_\infty$ = 0.8, $\hat{\Lambda}_\infty$ = -2.1, Ξ_∞ = 0, M_∞ = 2 over a wedge

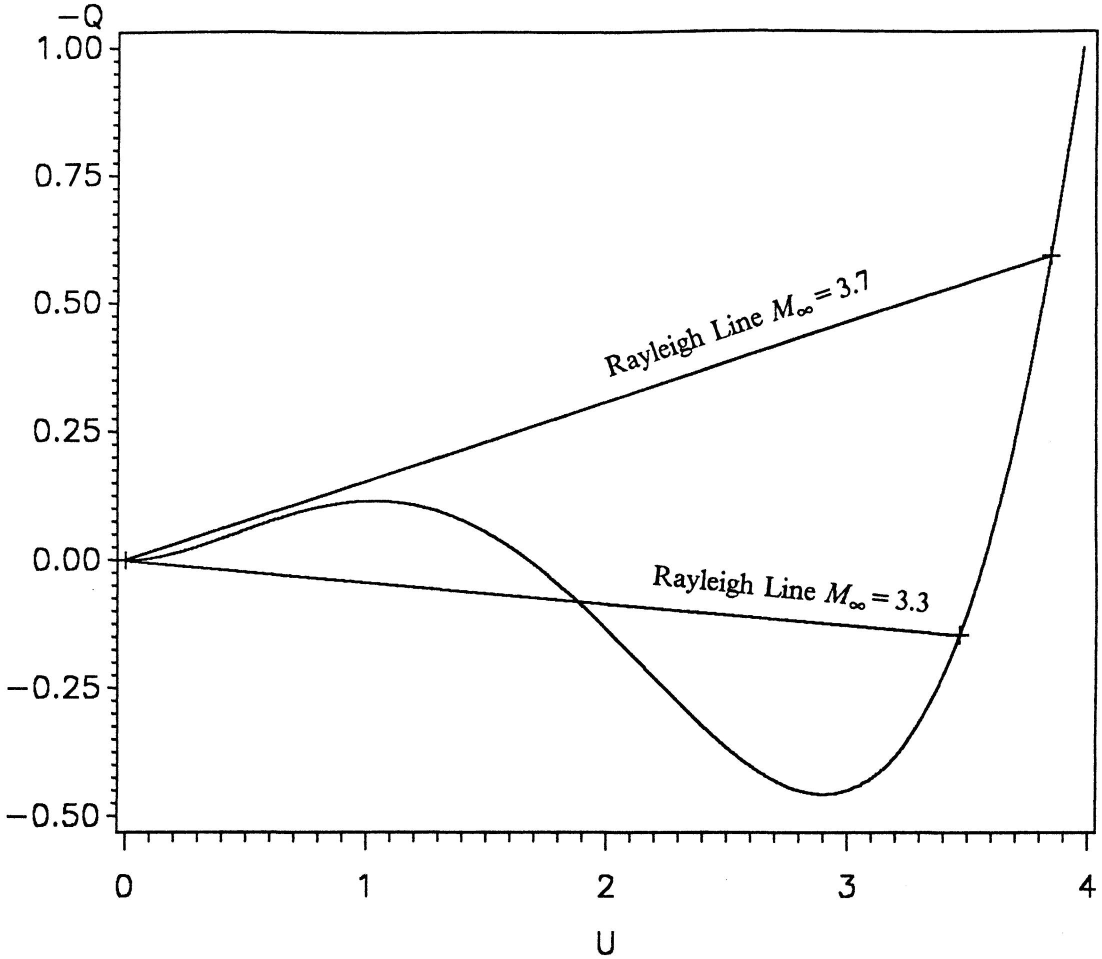

Figure 5.14. Q-curve for $\hat{\Gamma}_\infty$ = 0.8, $\hat{\Lambda}_\infty$ = -2.1, Ξ_∞ = 1.6 with Rayleigh line for M_∞ = 3.3 and M_∞ = 3.7

Attention Patron:

Page 63 omitted from numbering

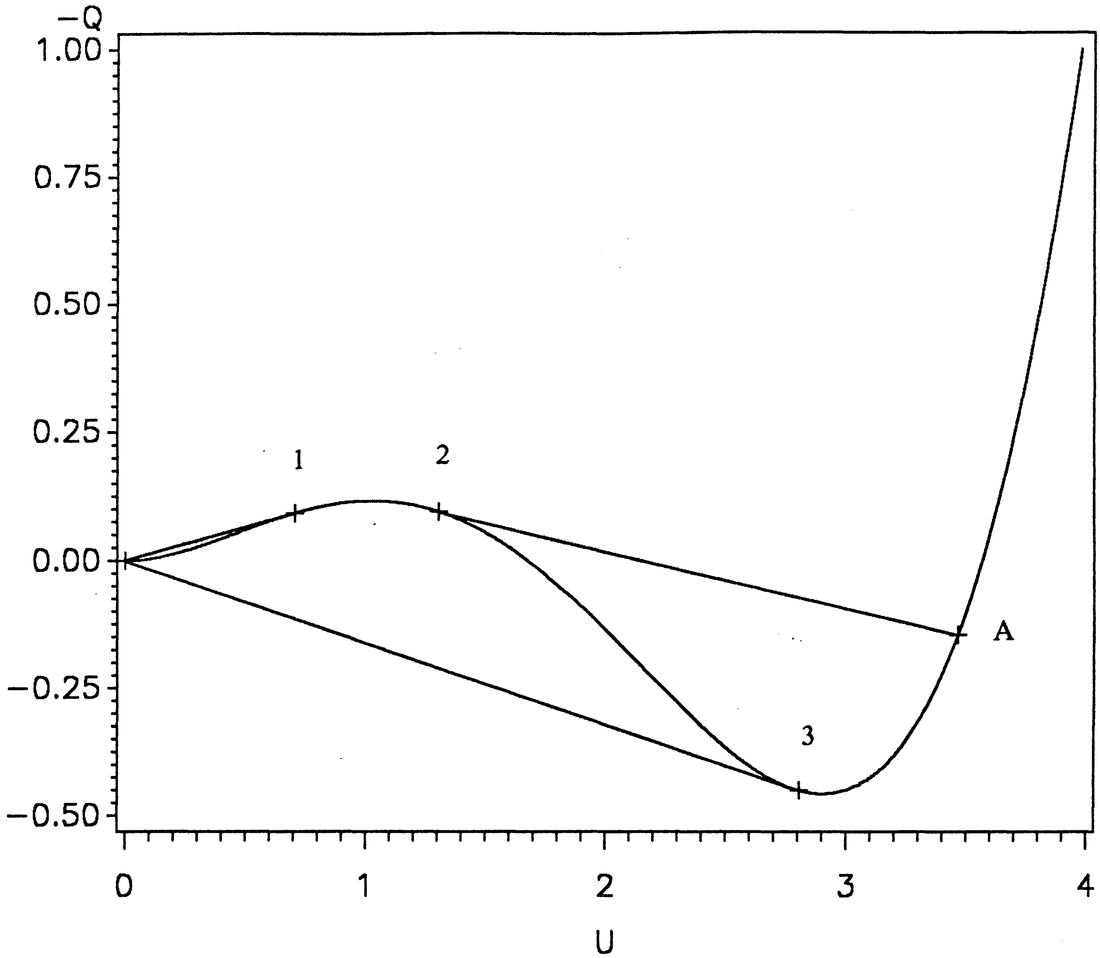

Figure 5.15. Q-curve for $\hat{\Gamma}_{\infty}$ = 0.8, $\hat{\Lambda}_{\infty}$ = -2.1, Ξ_{∞} = 1.6 with actual flow for M_{∞} = 3.3

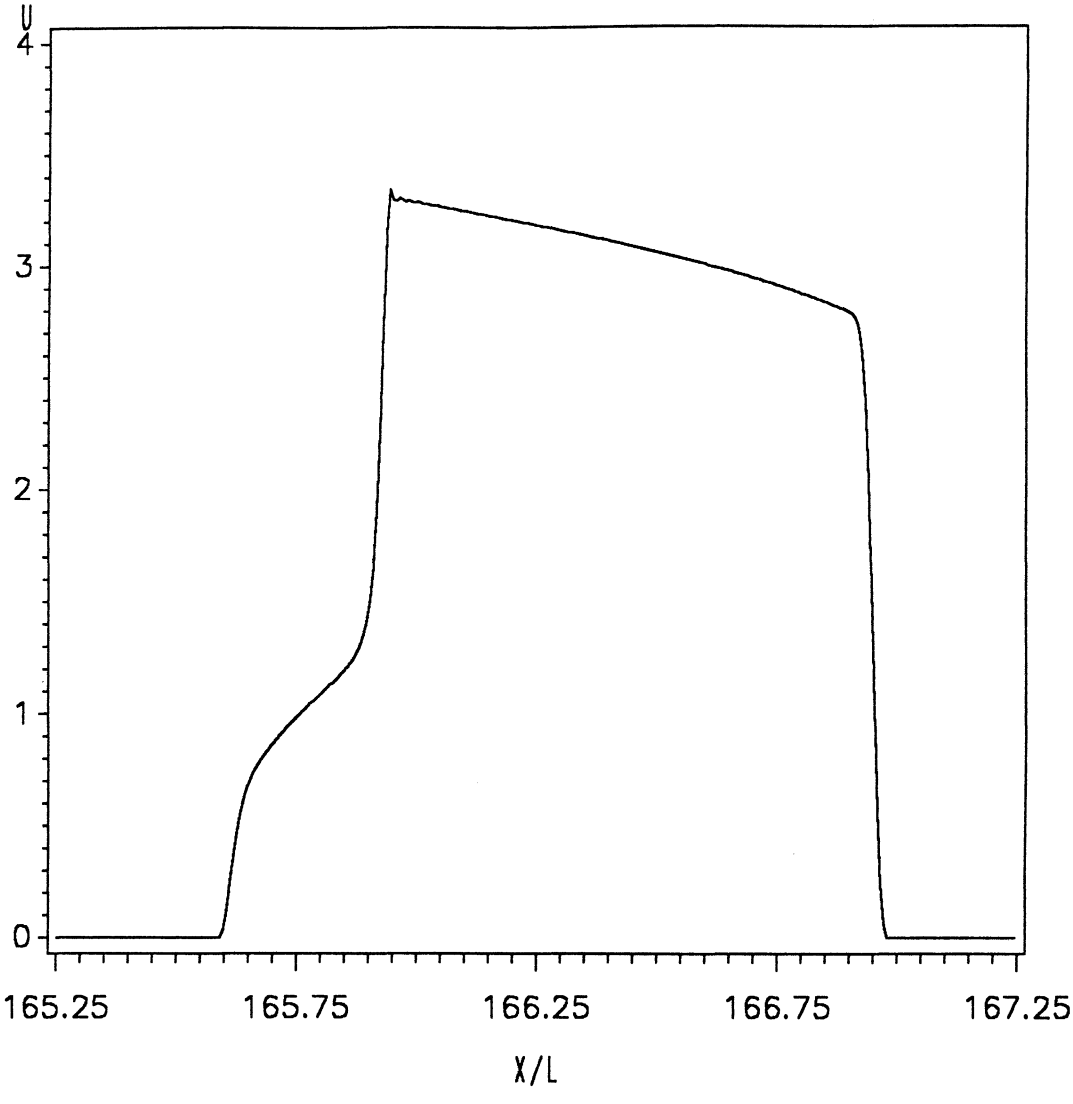

Figure 5.16. x-u plot for $\hat{\Gamma}_\infty$ = 0.8, $\hat{\Lambda}_\infty$ = -2.1, Ξ_∞ = 1.6, M_∞ = 3.3 , over a wedge at y/L = 52.7

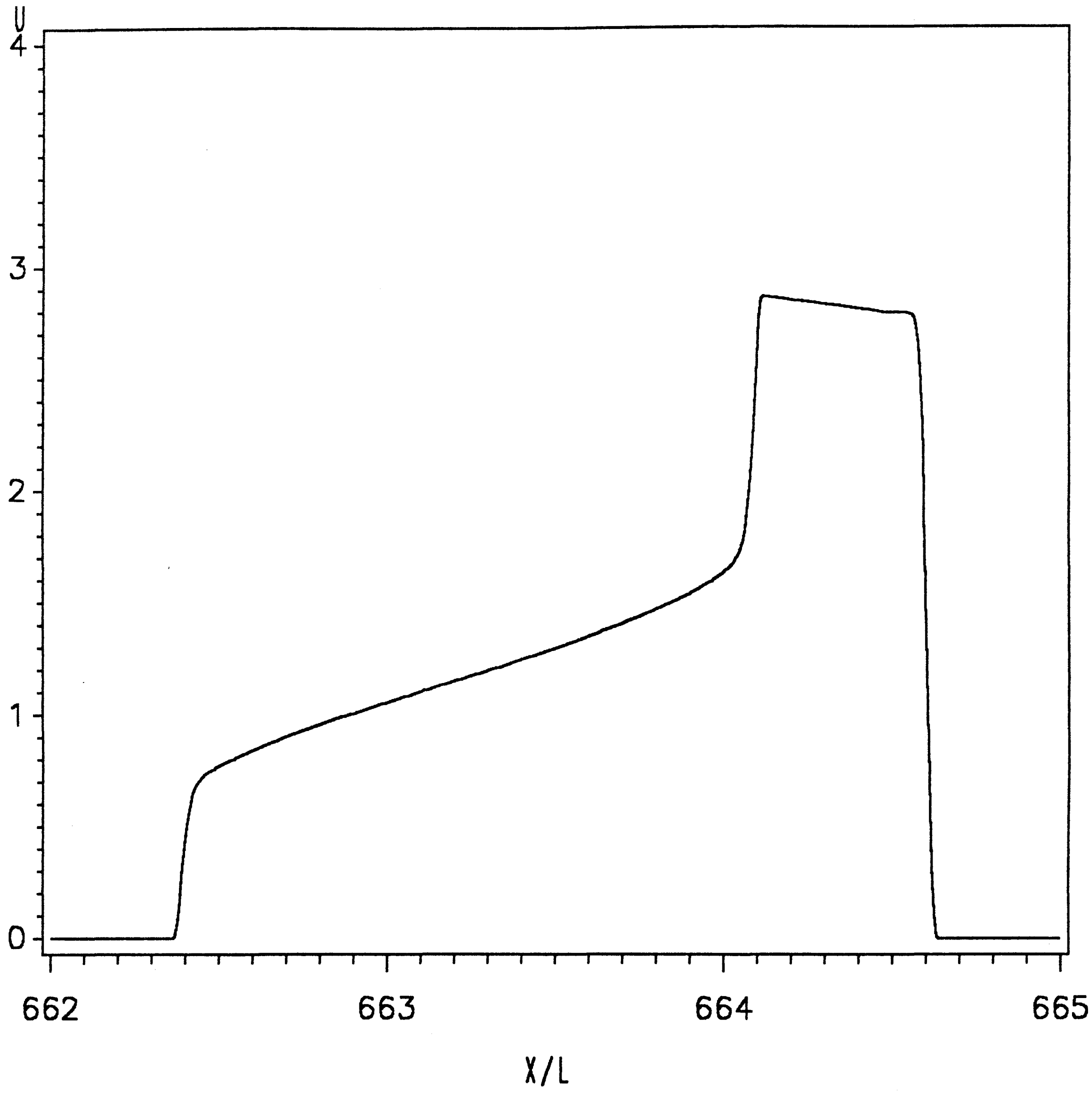

Figure 5.17. x-u plot for $\hat{\Gamma}_\infty = 0.8$, $\hat{\Lambda}_\infty = -2.1$, $\Xi_\infty = 1.6$, $M_\infty = 3.3$ over a wedge at y/L = 211

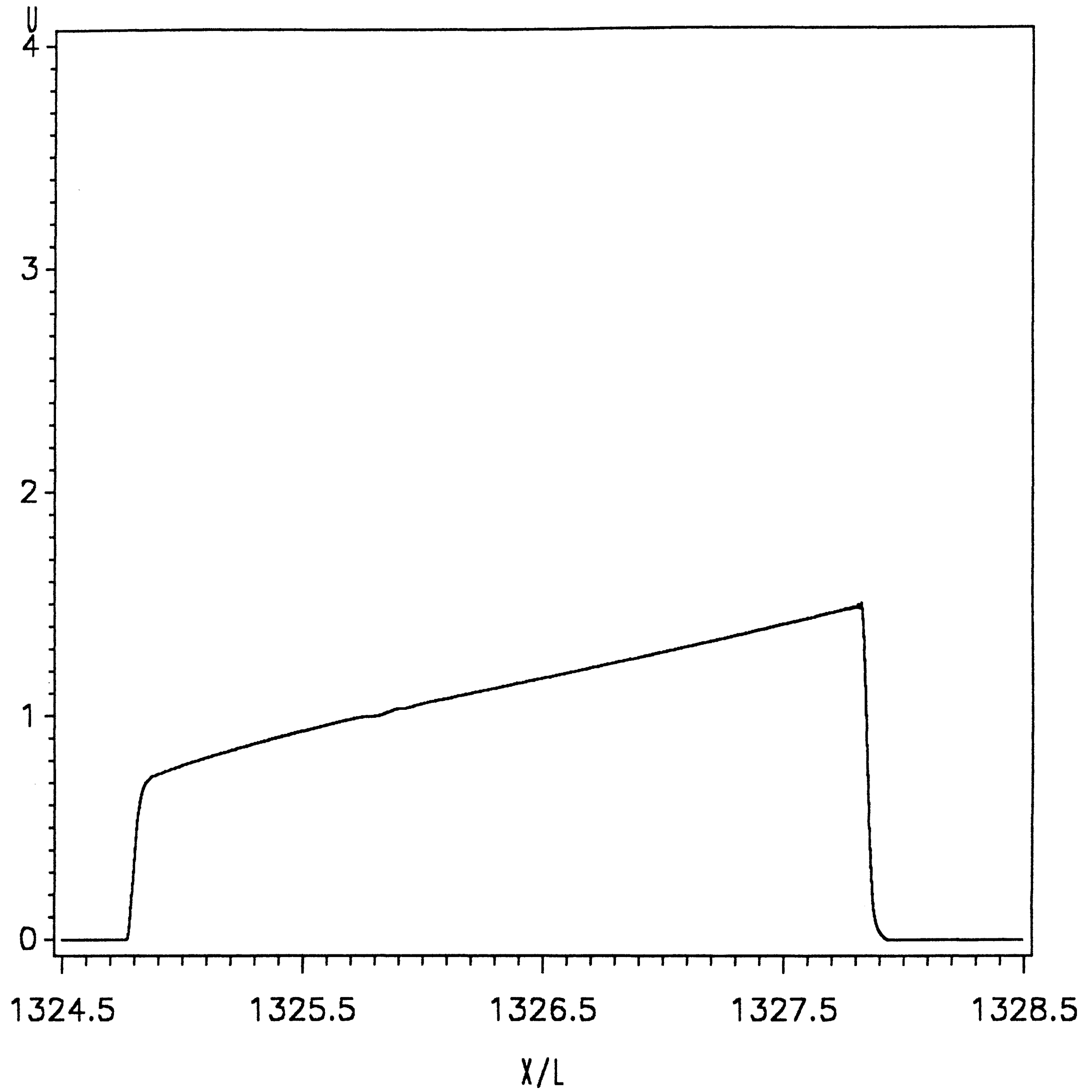

Figure 5.18. x-u plot for $\hat{\Gamma}_\infty = 0.8$, $\hat{\Lambda}_\infty = -2.1$, $\Xi_\infty = 1.6$, $M_\infty = 3.3$ over a wedge at y/L = 421

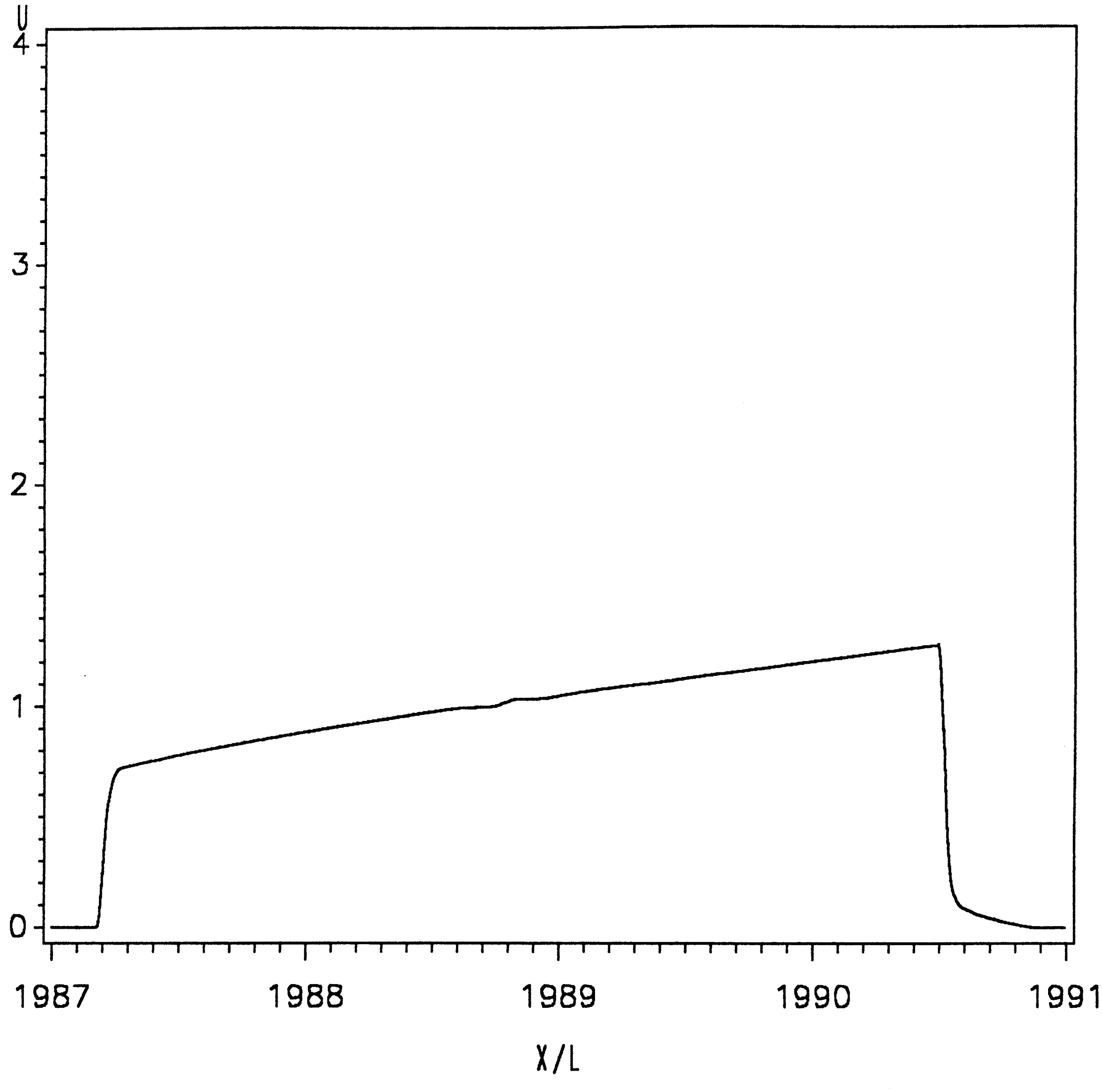

Figure 5.19. x-u plot for $\hat{\Gamma}_\infty = 0.8$, $\hat{\Lambda}_\infty = -2.1$, $\Xi_\infty = 1.6$, $M_\infty = 3.3$ over a wedge at y/L = 632

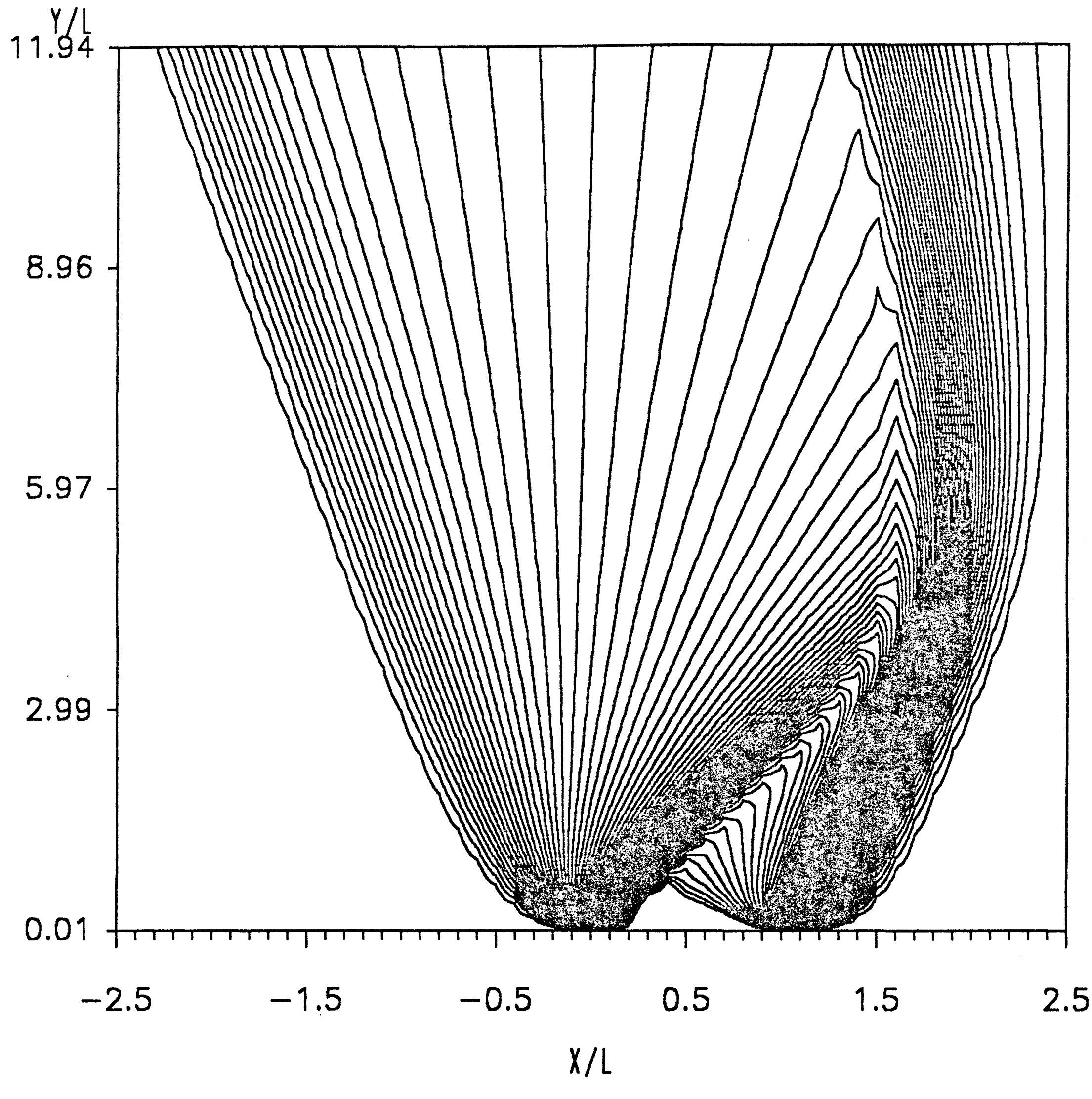

Figure 5.20. Contour plot for $\hat{\Gamma}_\infty$ = 0.8, $\hat{\Lambda}_\infty$ = -2.1, Ξ_∞ = 1.6. M_∞ = 3.3 over a wedge

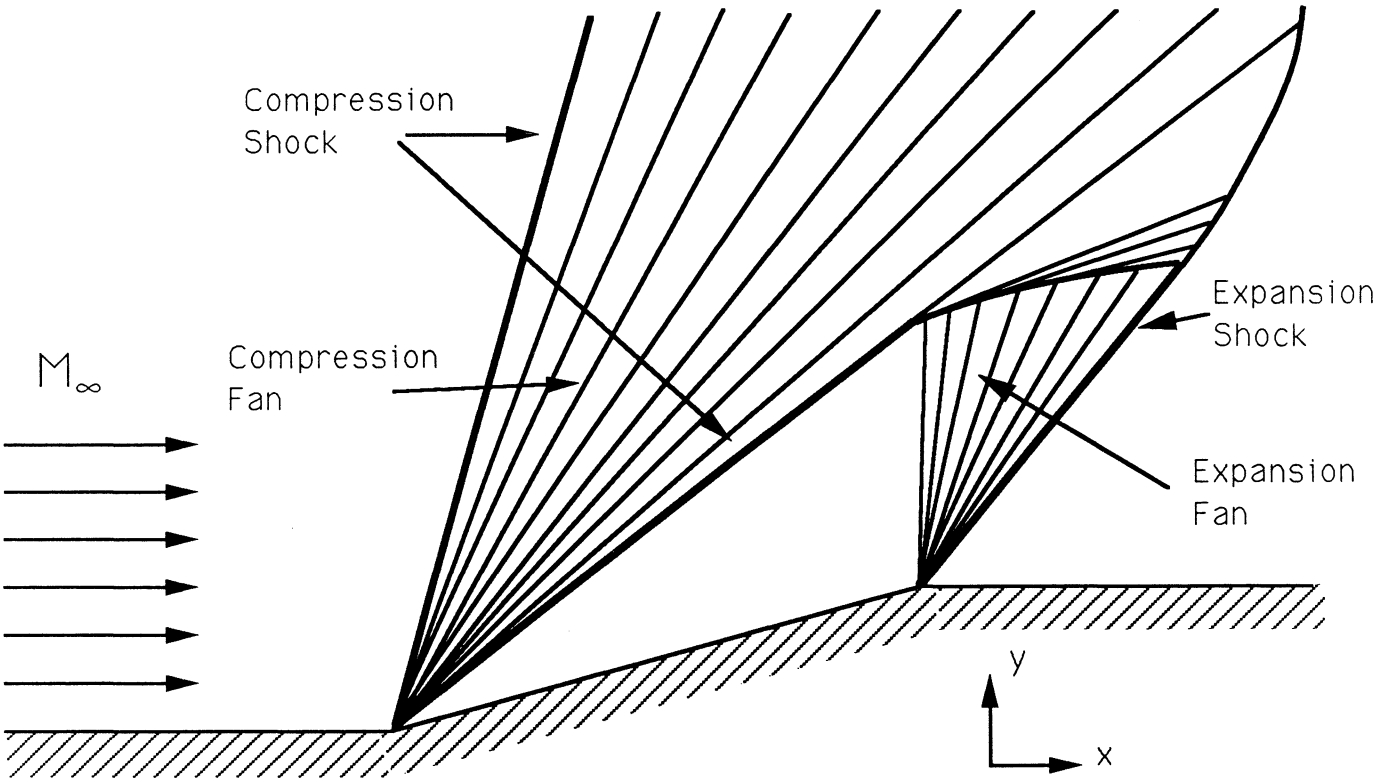

Figure 5.21. Sketch of flow for $\hat{\Gamma}_\infty = 0.8$, $\hat{\Lambda}_\infty = -2.1$, $\Xi_\infty = 1.6$. $M_\infty = 3.3$ over a wedge

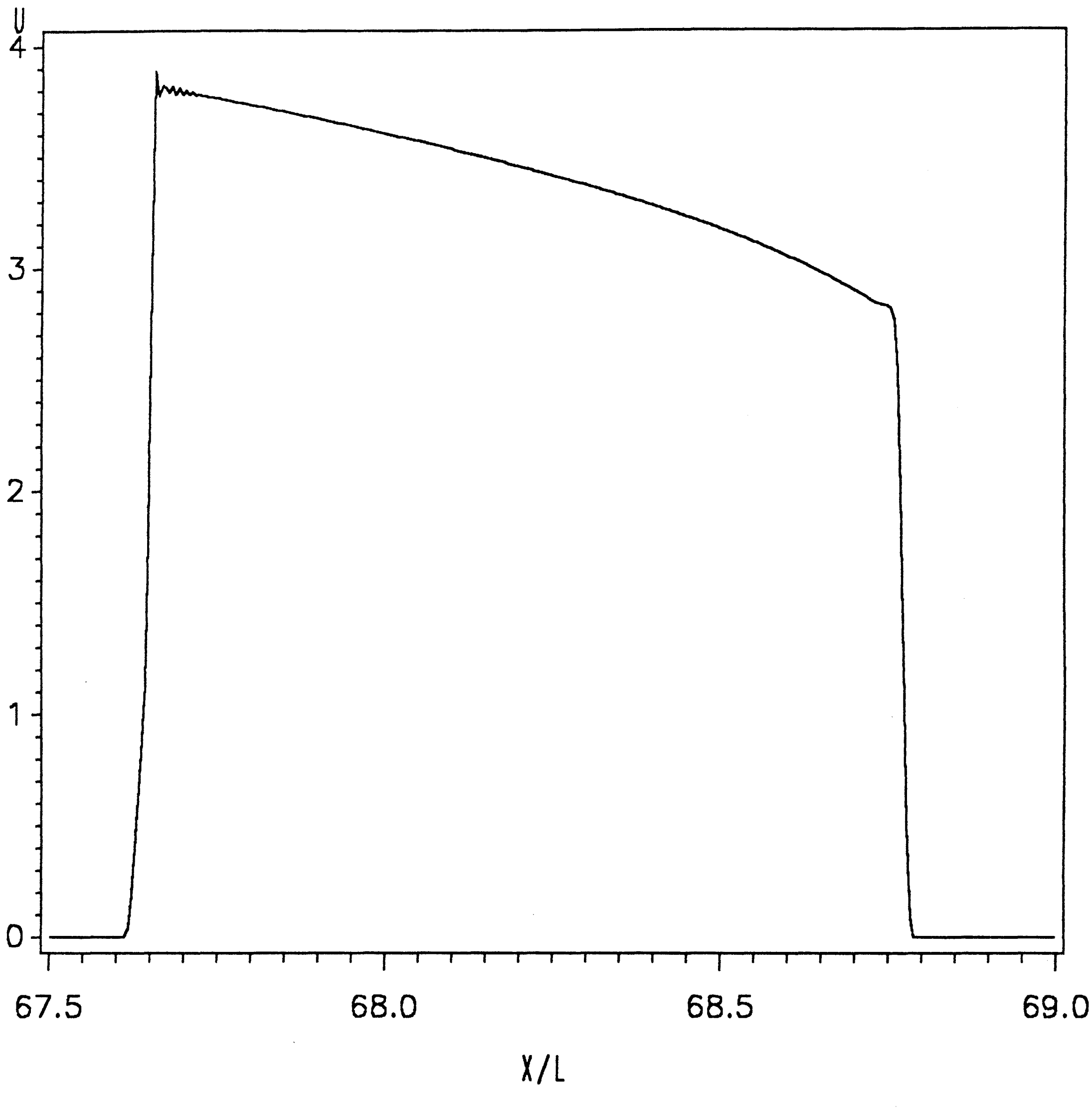

Figure 5.22. x-u plot for $\hat{\Gamma}_\infty = 0.8$, $\hat{\Lambda}_\infty = -2.1$, $\Xi_\infty = 1.6$, $M_\infty = 3.7$ over a wedge at y/L = 19.0

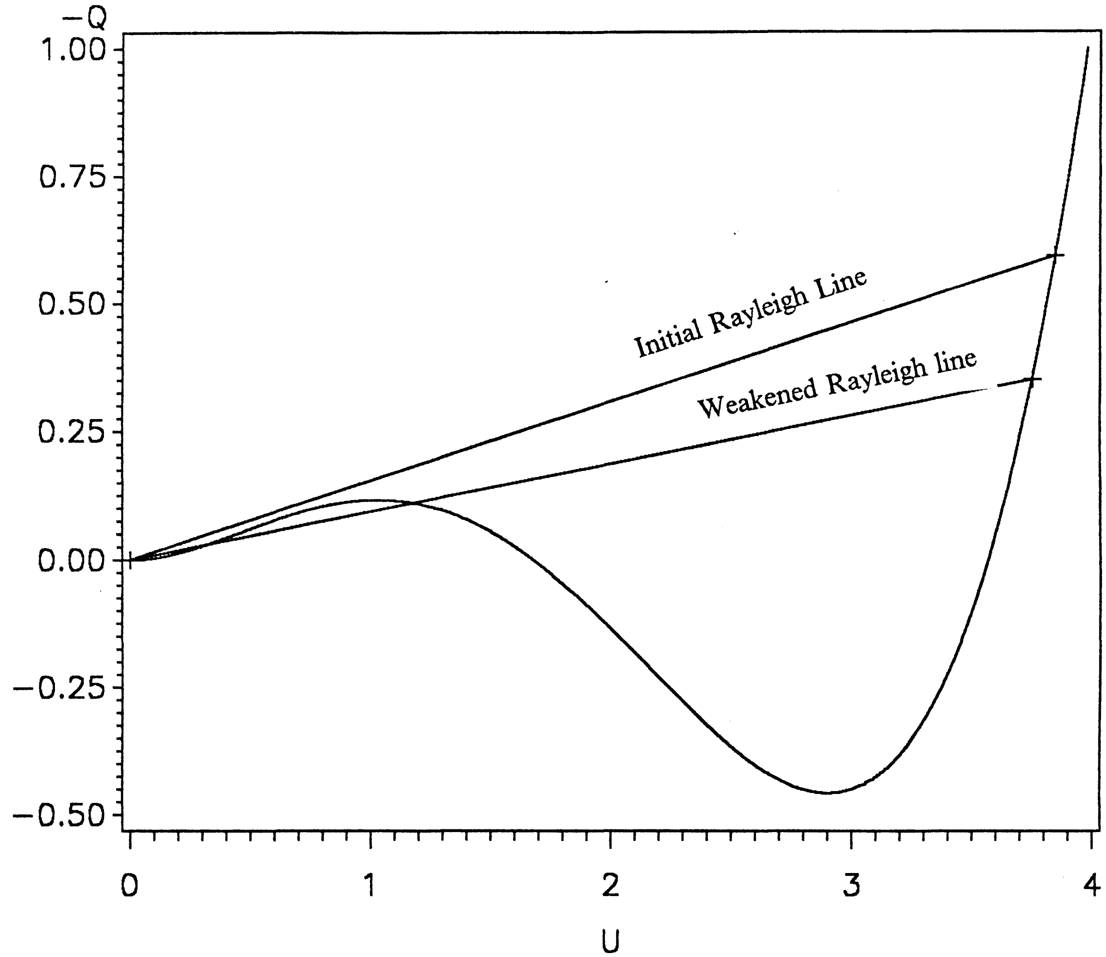

Figure 5.23. Q-curve for $\hat{\Gamma}_\infty = 0.8$, $\hat{\Lambda}_\infty = -2.1$, $\Xi_\infty = 1.6$. $M_\infty = 3.7$

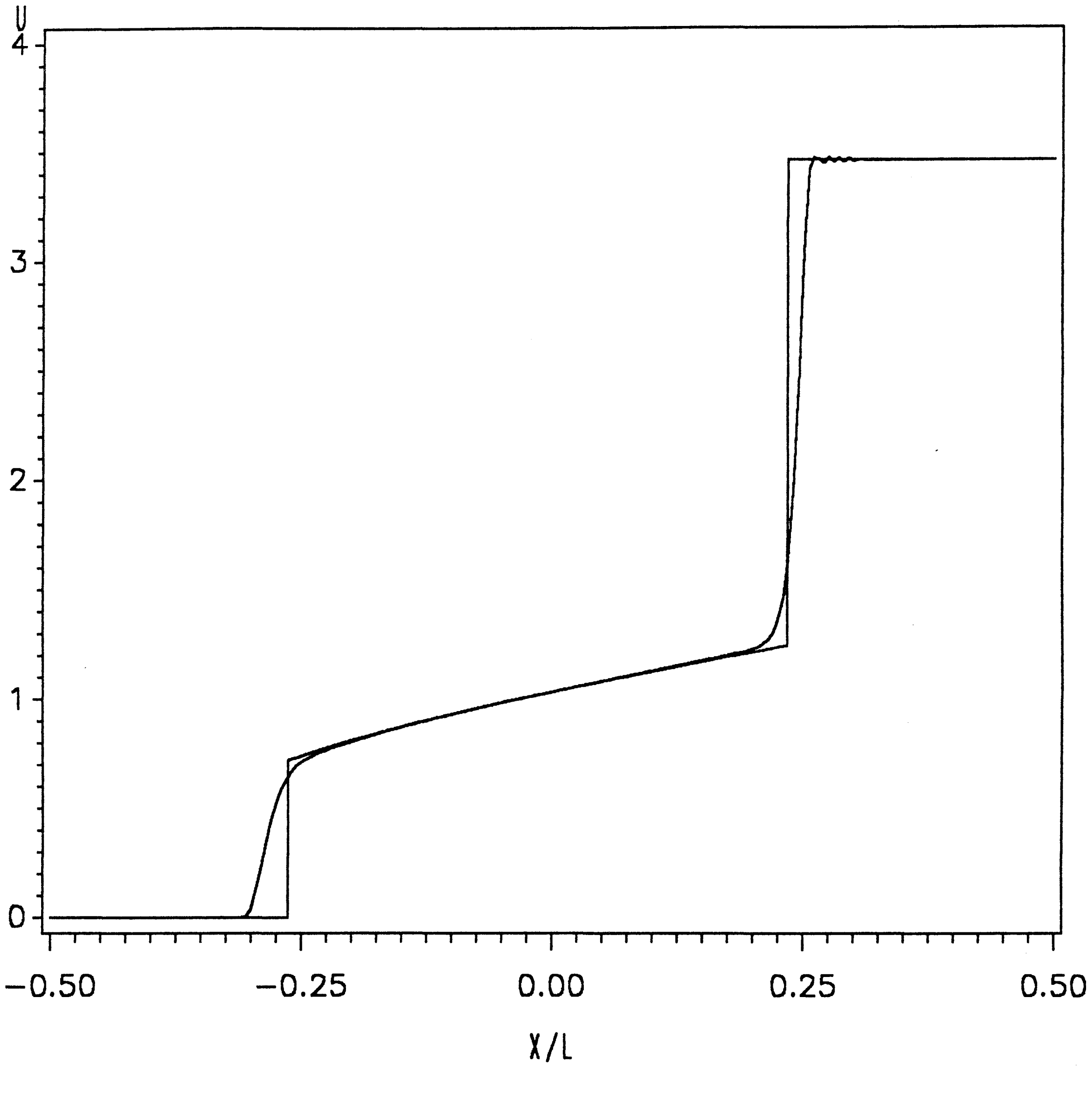

Figure 5.24. Comparison to Appendix A for $\hat{\Gamma}_\infty = 0.8$, $\hat{\Lambda}_\infty = -2.1$, $\Xi_\infty = 1.6.$, $M_\infty = 3.3$ over a wedge at $\bar{y} = 2$

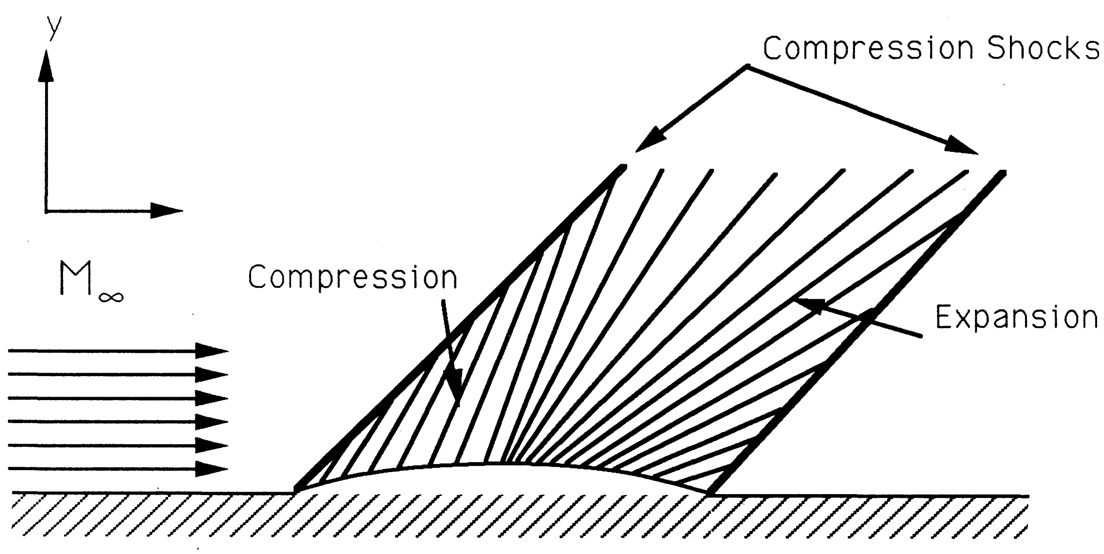

Figure 5.25. Sketch of classical flow over a wing shape.

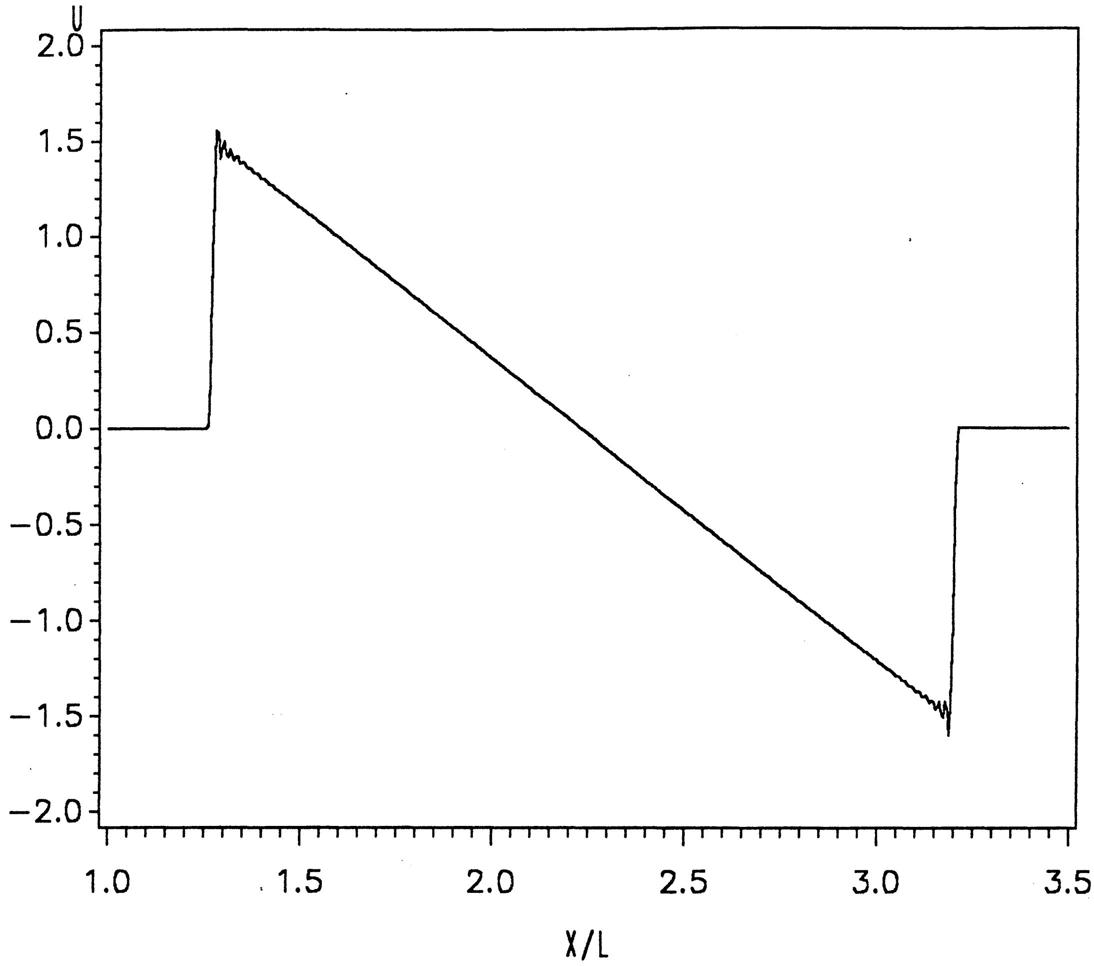

Figure 5.26. x-u plot for $\hat{\Gamma}_\infty = 1.2$, $\hat{\Lambda}_\infty = \Xi_\infty = 0.$, $M_\infty = 2$ over a wing shape at y/L = 0.49

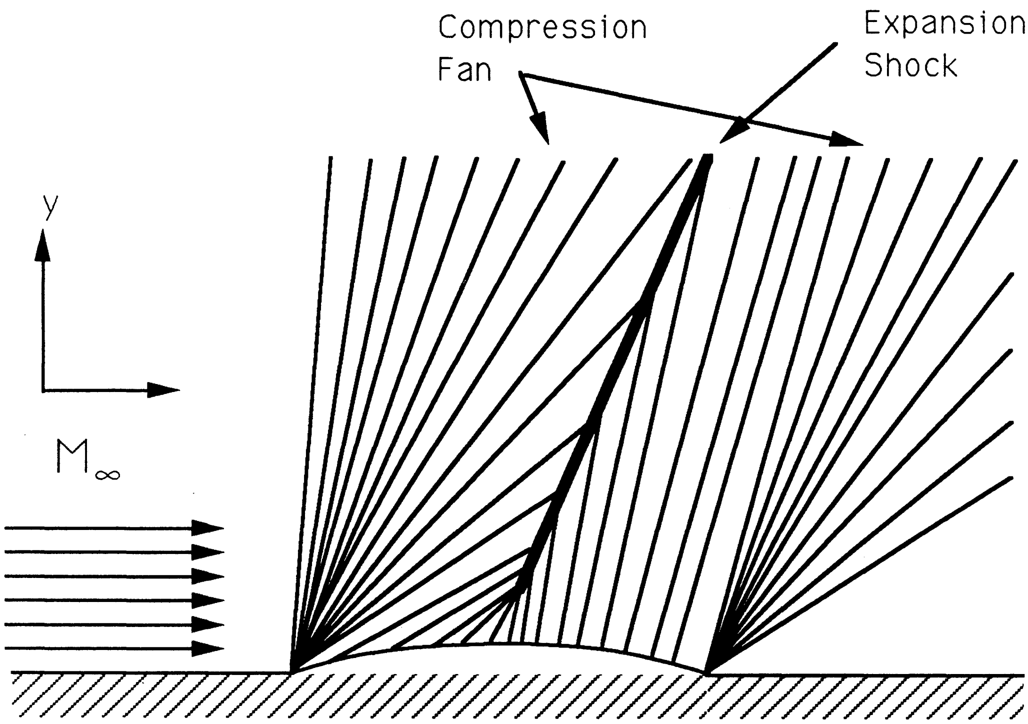

Figure 5.27. Sketch of $\Gamma < 0$ flow over a wing shape.

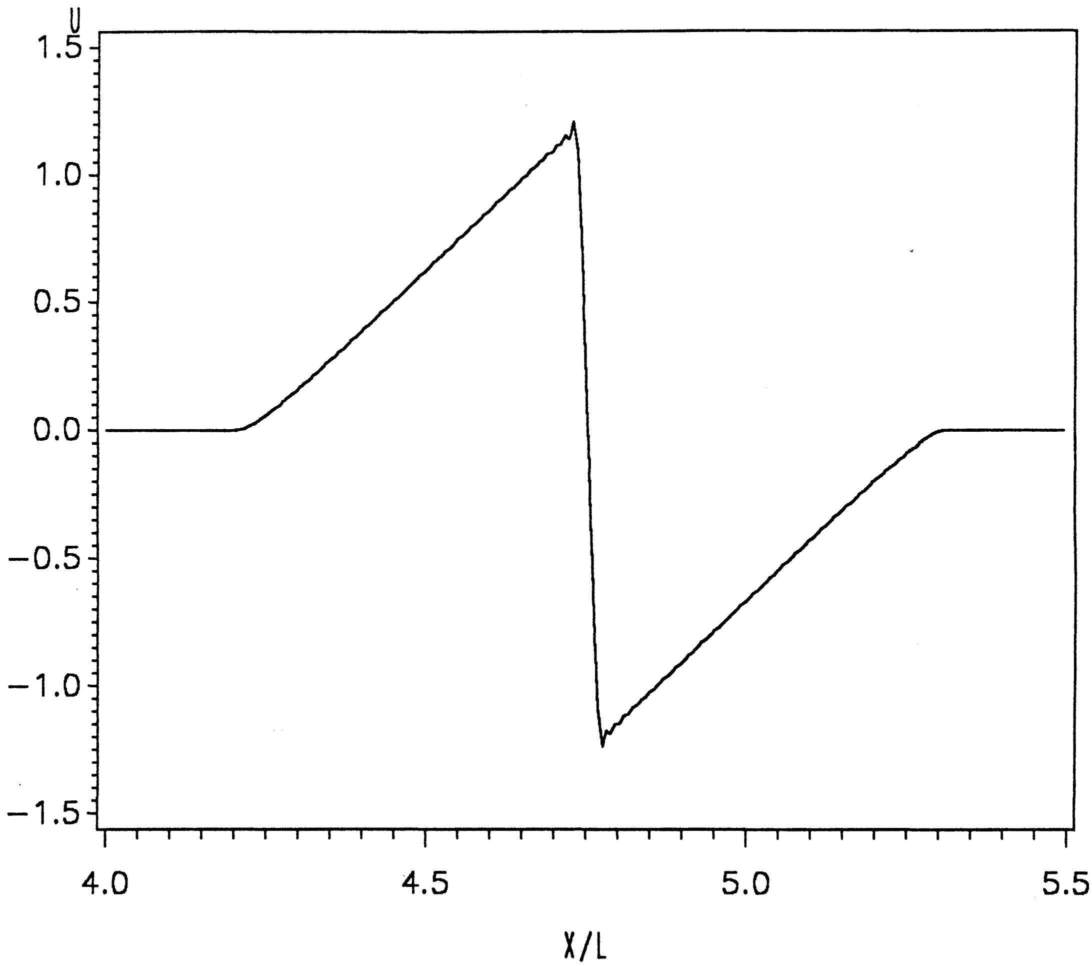

Figure 5.28. x-u plot for $\hat{\Gamma}_\infty = -0.4$, $\hat{\Lambda}_\infty = \Xi_\infty = 0.$, $M_\infty = 2$ over a wing shape at y/L = 2.45

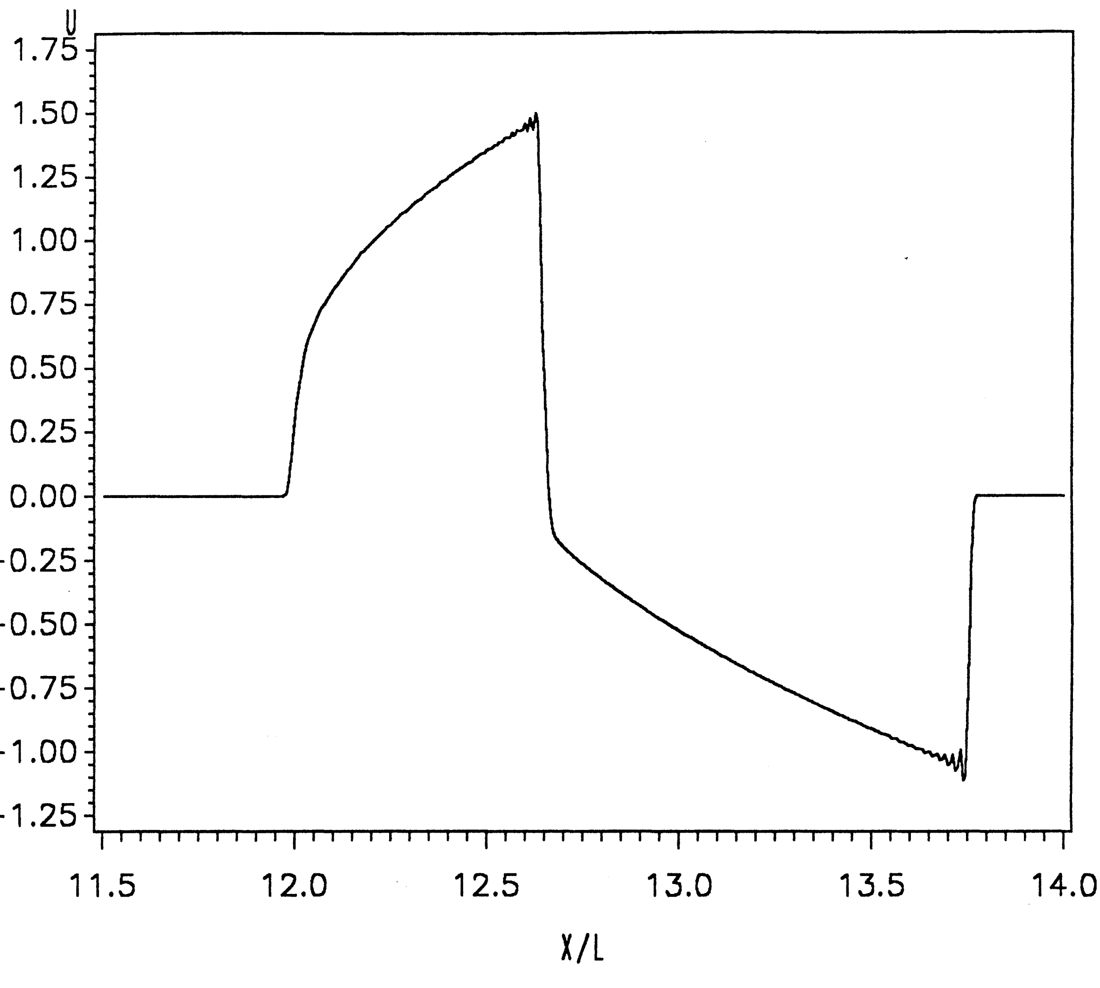

Figure 5.29. x-u plot for $\hat{\Gamma}_{\infty} = 0.8$, $\hat{\Lambda}_{\infty} = -2.1$, $\Xi_{\infty} = 0$, $M_{\infty} = 2$ over a wing at y/L = 6.97

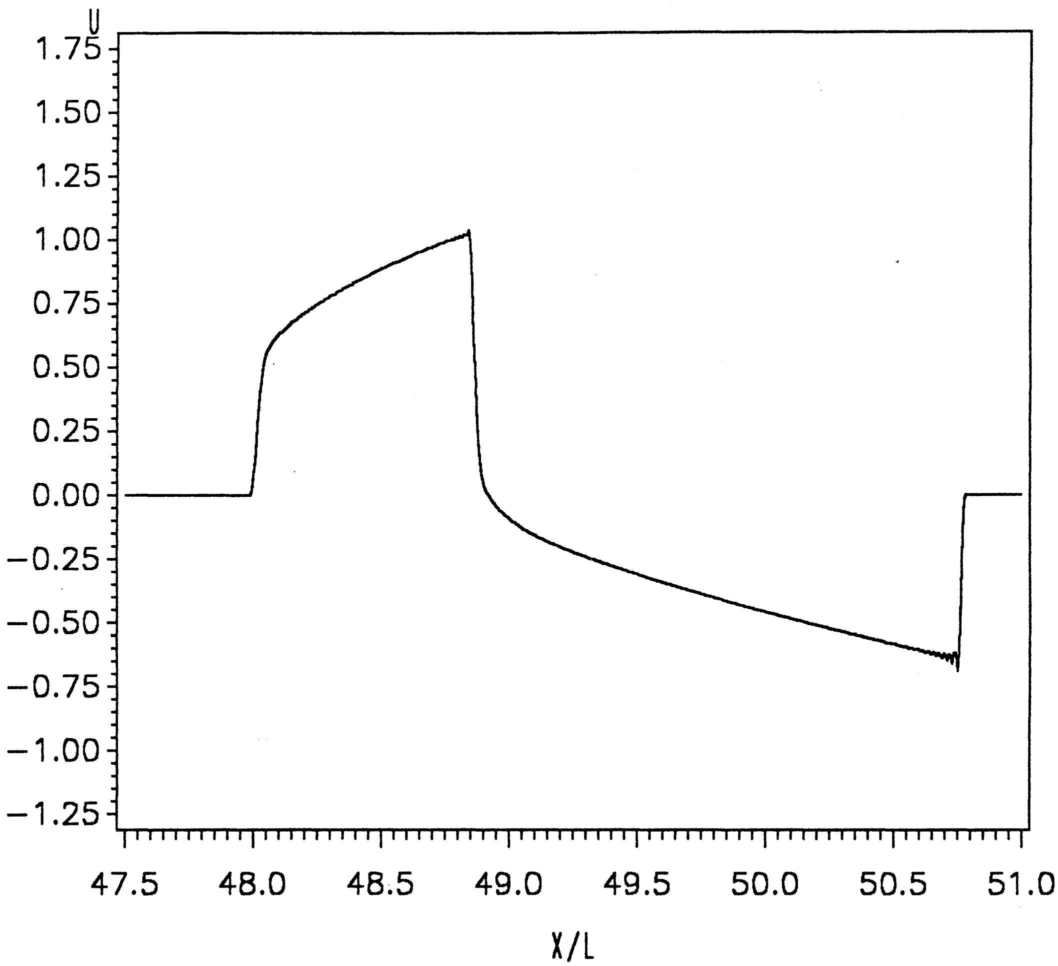

Figure 5.30. x-u plot for $\hat{\Gamma}_\infty = 0.8$, $\hat{\Lambda}_\infty = -2.1$, $\Xi_\infty = 0$, $M_\infty = 2$ over a wing at $y/L = 27.9$

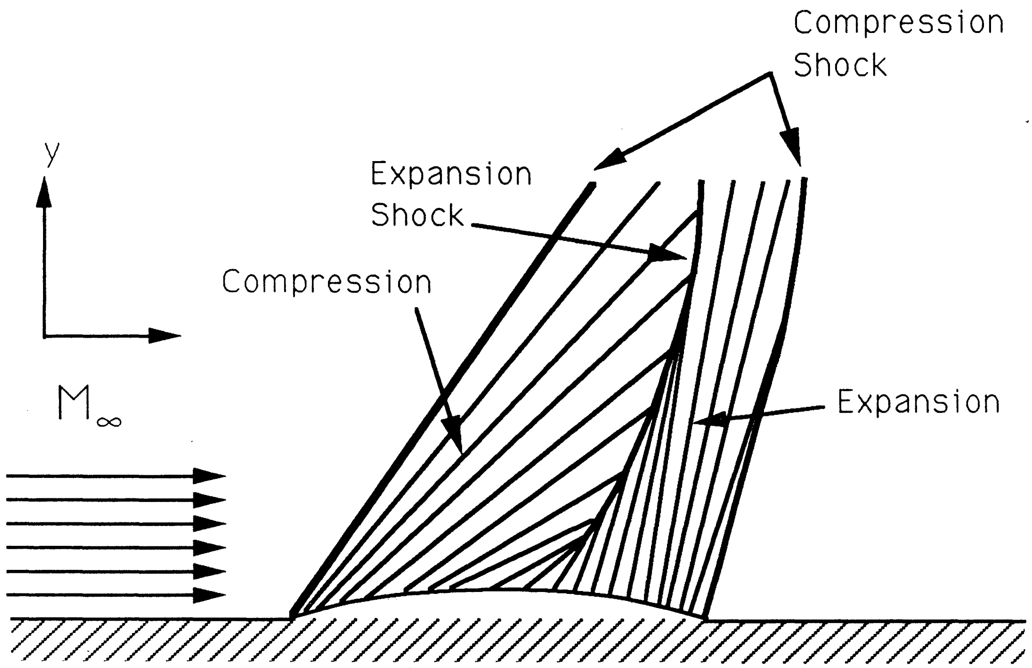

Figure 5.31. Sketch of $\hat{\Gamma}_\infty > 0$ and $\hat{\Lambda}_\infty < 0$ flow over a wing shape

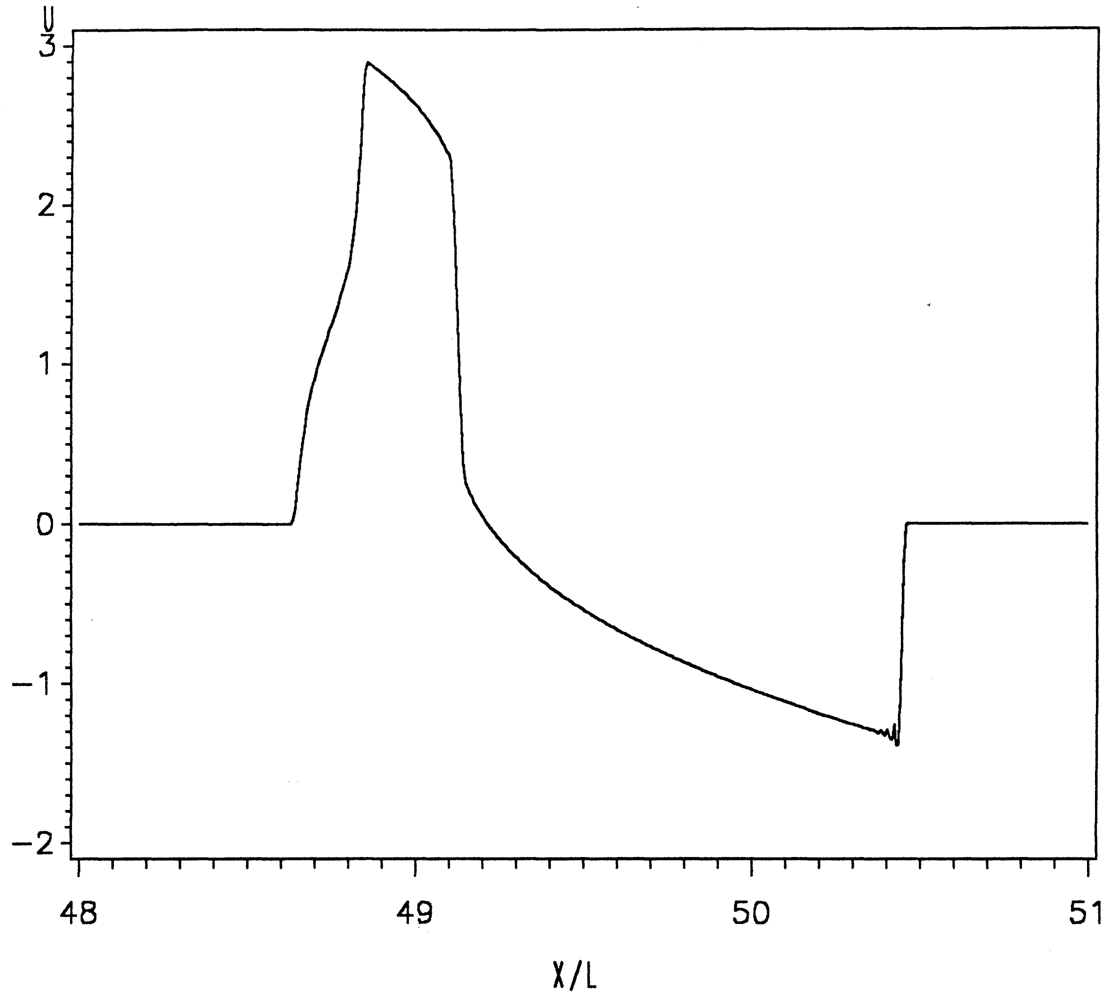

Figure 5.32. x-u plot for $\hat{\Gamma}_\infty = 0.8$, $\hat{\Lambda}_\infty = -2.1$, $\Xi_\infty = 1.6$, $M_\infty = 3.0$ over a wing at y/L = 17.2

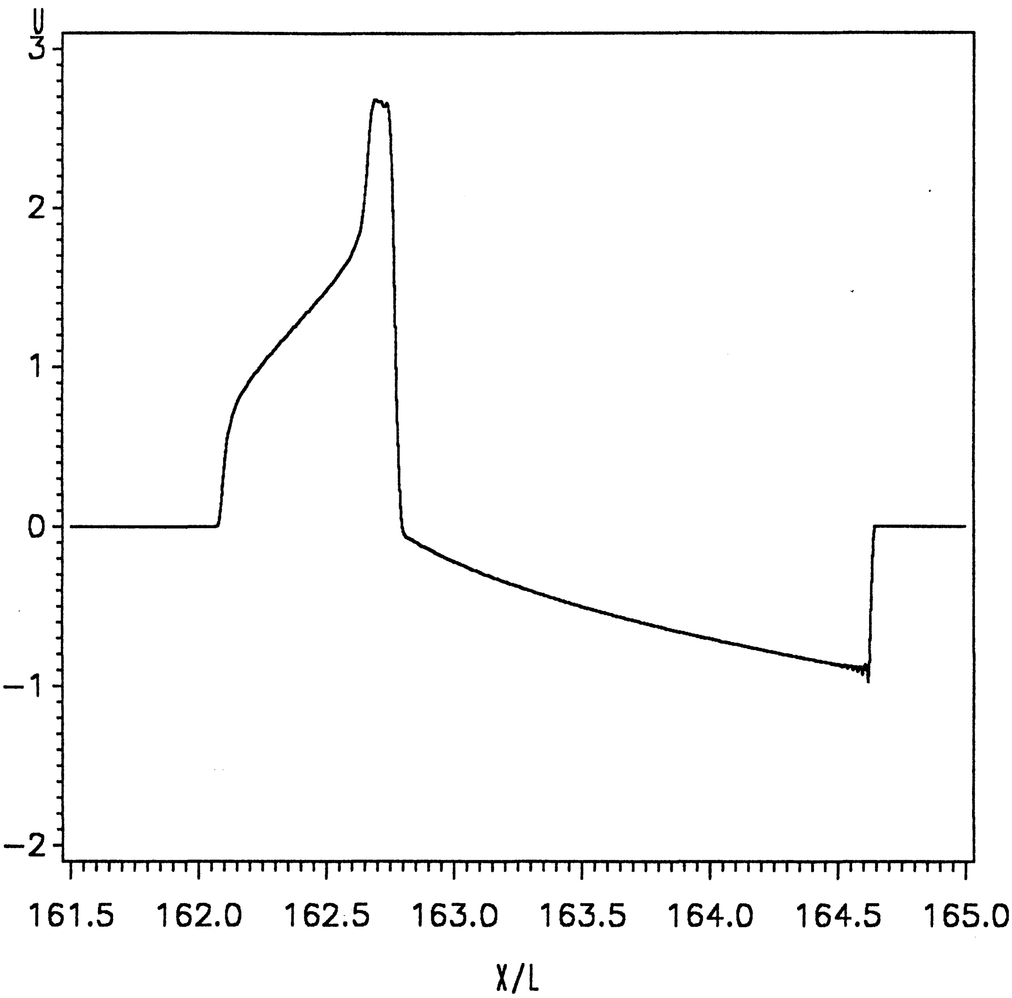

Figure 5.33. x-u plot for $\hat{\Gamma}_\infty = 0.8$, $\hat{\Lambda}_\infty = -2.1$, $\Xi_\infty = 1.6$, $M_\infty = 3.0$ over a wing at y/L = 57.3

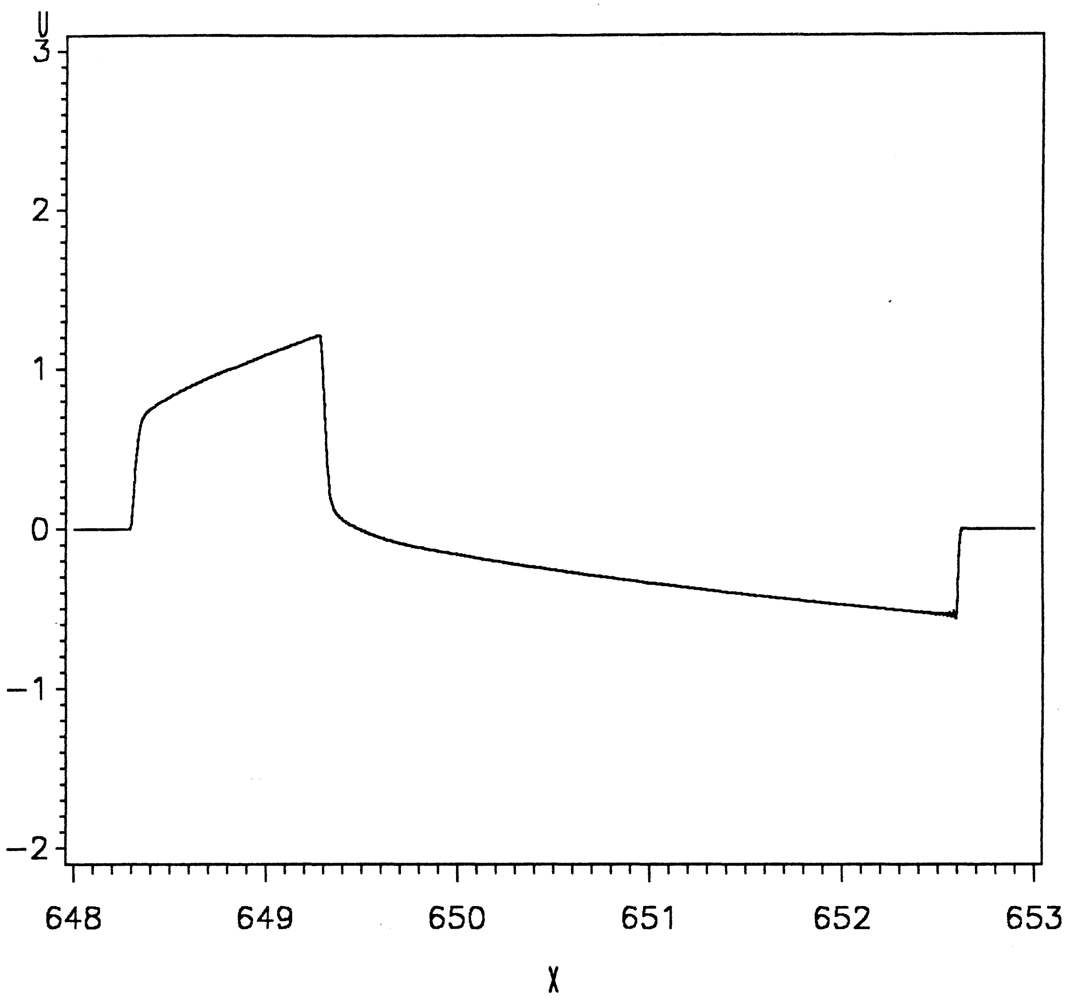

Figure 5.34. x-u plot for $\hat{\Gamma}_\infty = 0.8$, $\hat{\Lambda}_\infty = -2.1$, $\Xi_\infty = 1.6$, $M_\infty = 3.0$ over a wing at y/L = 229

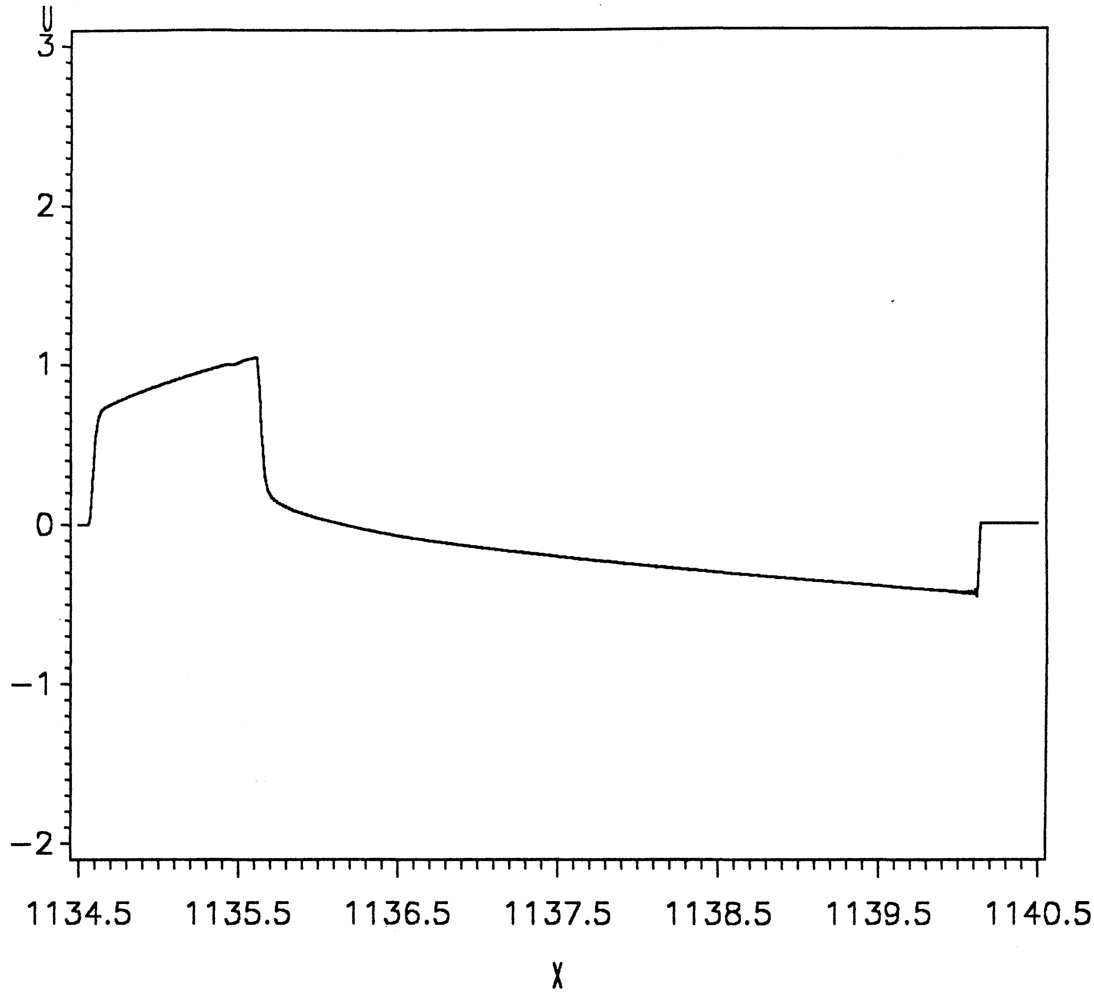

Figure 5.35. x-u plot for $\hat{\Gamma}_\infty = 0.8$, $\hat{\Lambda}_\infty = -2.1$, $\Xi_\infty = 1.6$, $M_\infty = 3.0$ over a wing at y/L = 401

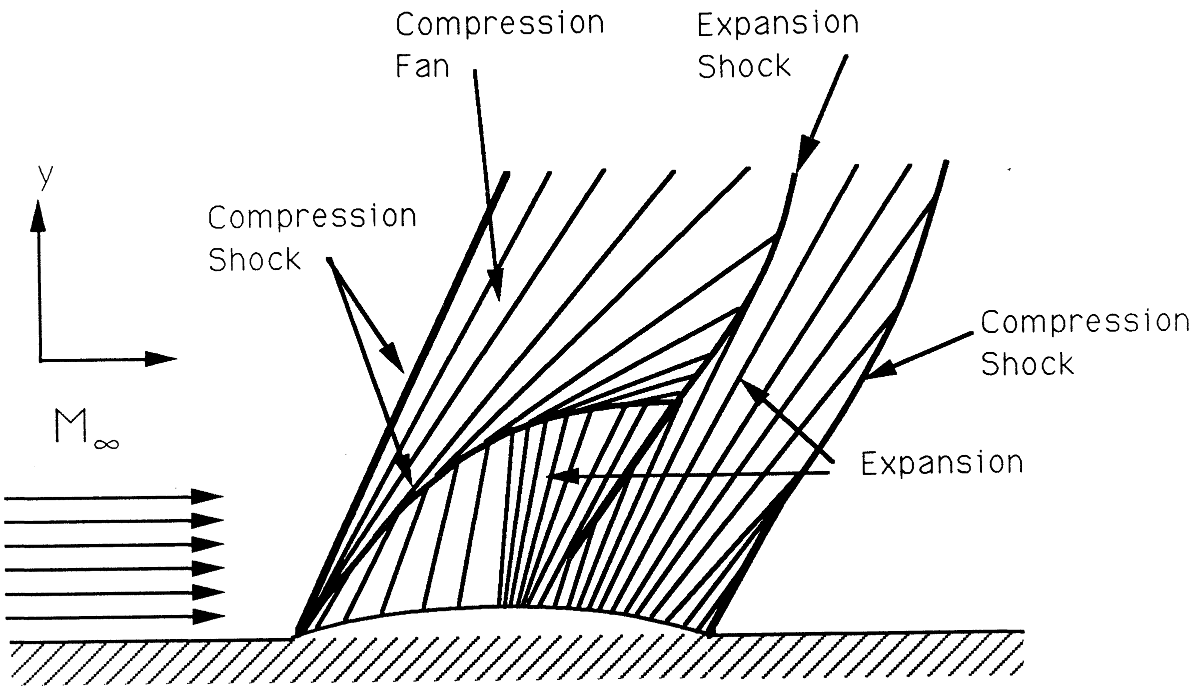

Figure 5.36. Sketch of flow for $\hat{\Gamma}_\infty = 0.8$, $\hat{\Lambda}_\infty = -2.1$, $\Xi_\infty = 1.6$. $M_\infty = 3.6$ over a wing

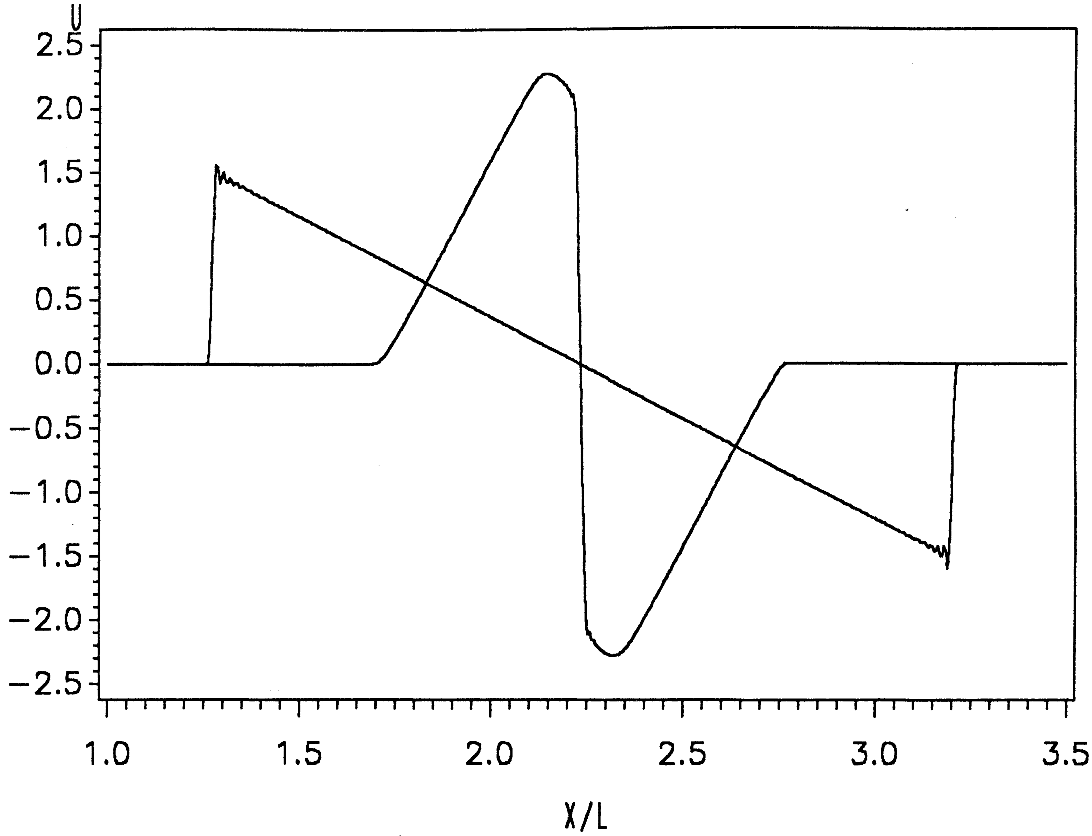

Figure 5.37. Comparison of $\Gamma > 0$ and $\Gamma < 0$ flows over a wing at $M_\infty = 2$, $y/L = 1$

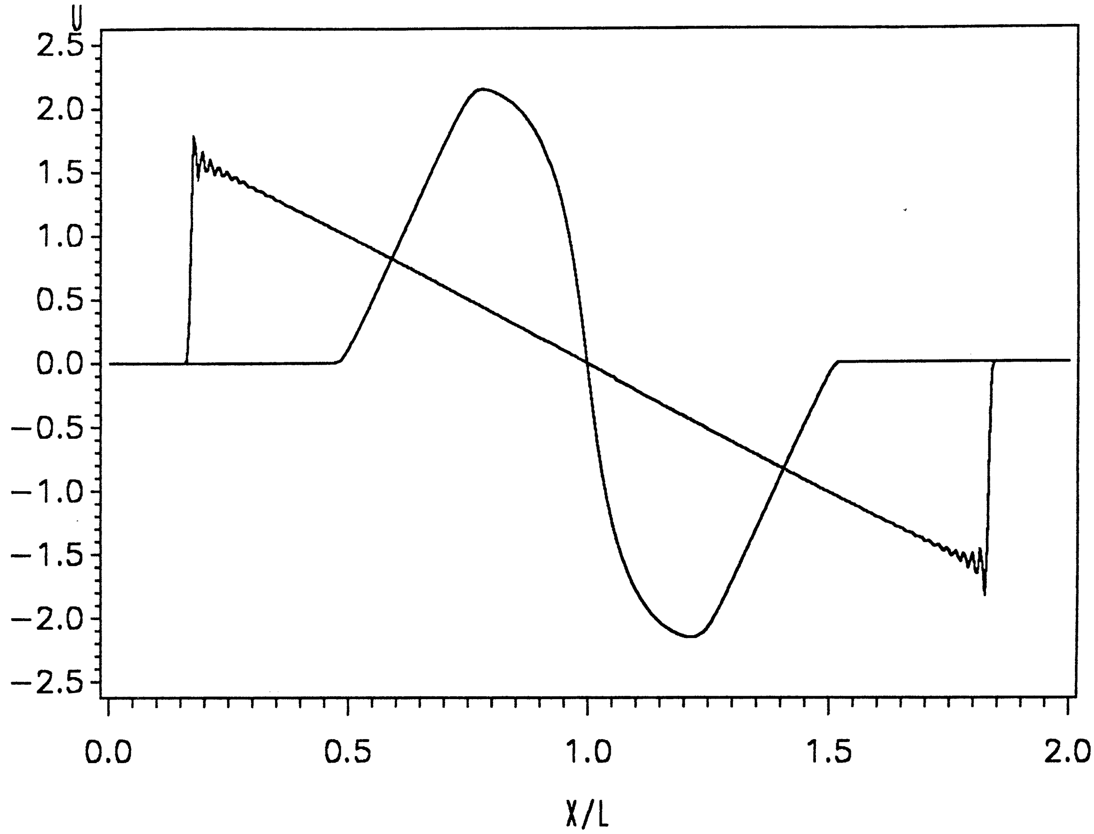

Figure 5.38. Comparison of $\Gamma > 0$ and $\Gamma < 0$ flows over a wing at M_∞ = 1.2, y/L = .75

Appendix A. Exact Solution for Shock Splitting

We will solve the equations [3.51] to exactly, at least to our order of approximation, describe the flow over an infinite wedge. Since this exact solution will include all the constants, $\hat{\Gamma}_\infty$, $\hat{\Lambda}_\infty$, and Ξ_∞, we will be able to describe the flow for any of our cases: compression and expansion shocks, fans, and shock splitting.

We will first find the speed of a shock. This was determined in Section 3.10 by equation [3.76] which is written again here.

$$\frac{d\bar{x}}{d\bar{y}}\Big|_{shock} = \frac{[Q]}{[u]} = -\frac{\hat{\Gamma}_\infty}{2}(u_2 + u_1) - \frac{\hat{\Lambda}_\infty}{6}(u_2^2 + u_1 u_2 + u_1^2). \qquad [A.1]$$

$$-\frac{\Xi_\infty}{24}(u_2^3 + u_1 u_2^2 + u_1^2 u_2 + u_1^3).$$

With this equation we can determine the x position of the shock at any y value. The speed of non-shock disturbances such as fans will be determined by:

$$\frac{d\bar{x}}{d\bar{y}}\Big|_{char.} = Q' = -\hat{\Gamma}_\infty u - \hat{\Lambda}_\infty \frac{u^2}{2} - \Xi_\infty \frac{u^3}{6} \qquad [A.2]$$

The above two expressions will allow us to find the location for any shock or fan in the flow. In order to include shock-splitting in our exact solution, we must be able to determine the strength of the sonic shocks and determine their starting and ending points. We will do this by setting our shock slope [A.1] equal to the slope of the characteristic line, [A.2], and solving for the downstream density u_2 as a function of u_1. We get

$$u_2 = \frac{-\frac{4\hat{\Lambda}_\infty}{3} - \frac{\Xi_\infty u_1}{3} \pm \sqrt{\left(\frac{4\hat{\Lambda}_\infty}{3} + \frac{\Xi_\infty u_1}{3}\right)^2 - 4\Xi_\infty\left(\hat{\Gamma}_\infty + \frac{\hat{\Lambda}_\infty u_1}{3} + \frac{\Xi_\infty u_1^2}{12}\right)}}{\Xi_\infty}. \quad [A.3]$$

which is good for a shock which is sonic at the 2 condition. The results for a shock which is sonic at the 1 condition is obtained by simply interchanging the subscripts 1 and 2 in [A.3] to obtain

$$u_1 = \frac{-\frac{4\hat{\Lambda}_\infty}{3} - \frac{\Xi_\infty u_2}{3} \pm \sqrt{\left(\frac{4\hat{\Lambda}_\infty}{3} + \frac{\Xi_\infty u_2}{3}\right)^2 - 4\Xi_\infty\left(\hat{\Gamma}_\infty + \frac{\hat{\Lambda}_\infty u_2}{3} + \frac{\Xi_\infty u_2^2}{12}\right)}}{\Xi_\infty}. \quad [A.4]$$

We can now use [A.1] - [A.4] to piece together the case of shock splitting, as was done in Figure 5.25. Staring with the upstream flow, u = 0, we use equation [A.3] to get the downstream value for the first sonic shock. We can compute the second sonic shock by using our final downstream u, u_2, in equation [A.4] to get the upstream value for the second shock. We can compute the fan by using the following expression, derived by integrating [A.2], assuming u is constant on the Mach lines

$$\bar{x} = \left(-\hat{\Gamma}_\infty u - \hat{\Lambda}_\infty \frac{u^2}{2} - \Xi_\infty \frac{u^3}{6}\right)\bar{y}. \quad [A.5]$$

Equation [A.5] gives us the fan which will connect the u_2 of the first sonic shock to the u_1 of the second shock. It should be recalled that this solution only holds near the leading edge of a wing.

Appendix B. Determination of Γ and Λ for Real Fluids

The values of $\hat{\Gamma}_\infty$, $\hat{\Lambda}_\infty$, and Ξ_∞ used in our calculations in Chapter 5, with the exception of the classical flow calculations, were approximations of the values for particular fluids. Values for $\overline{\Gamma}$, given by equation [3.42] have been calculated using state of the art equations of state.[17] Since Λ is a function of the derivative of Γ we can estimate Λ, evaluated at the zero of Γ, in the following way

$$\Lambda \simeq \frac{\overline{\Gamma}_2 - \overline{\Gamma}_1}{\rho_2 - \rho_1} \rho_1 - \overline{\Gamma}_1, \qquad [A.6]$$

where $\overline{\Gamma}_1$ is a slightly positive value at ρ_1, and $\overline{\Gamma}_2$ is a slightly negative value at ρ_2. Since Ξ_∞ involves the second derivative of Γ, such a simple formula cannot be obtained for it.

The following chart shows some values of Λ for several fluids of interest. The values were computed by taking an isentrope and using [A.6] at the points where Γ changed sign. Since Γ changes sign at two points, there are two values of Λ produced for each fluid.

Table 1. Values for Λ for some BZT Fluids.

Fluid	Λ_1	$T_1(K)$	$P_1(Atm.)$	Λ_2	$T_2(K)$	$P_2(Atm.)$
FC-70	2.75	609	10.1	-1.14	606	9.1
FC-71	3.53	648	9.3	-1.25	645	8.37
PP-9	1.34	585	15.7	-0.795	581	14.7
PP-10	2.68	632	15.7	-1.15	627	14.2
PP-11	2.81	651	14.3	-1.14	647	12.9
PP-24	4.25	704	15.2	-1.38	699	13.5
PP-25	1.08	689	11.0	-1.07	685	9.83

The vita has been removed from
the scanned document